AD NUMBER

AD891249

NEW LIMITATION CHANGE

TO

Approved for public release, distribution unlimited

FROM

Distribution authorized to U.S. Gov't. agencies only; Test and Evaluation; FEB 1971. Other requests shall be referred to Air Force Armament Lab., Attn: DLGC, Eglin AFB, FL 32542.

AUTHORITY

Air Force Armament Lab ltr dtd 30 May 1978

AFATL-TR-71-28

AD891249

BOATTAIL EFFECTS ON THE DYNAMIC STABILITY OF THE THREE-CALIBER ARMY-NAVY BASIC SPINNER PROJECTILE

DEPARTMENT OF AEROSPACE AND MECHANICAL ENGINEERING
UNIVERSITY OF NOTRE DAME

TECHNICAL REPORT AFATL-TR-71-28

FEBRUARY 1971

AIR FORCE ARMAMENT LABORATORY
AIR FORCE SYSTEMS COMMAND • UNITED STATES AIR FORCE
EGLIN AIR FORCE BASE, FLORIDA

Su 1173

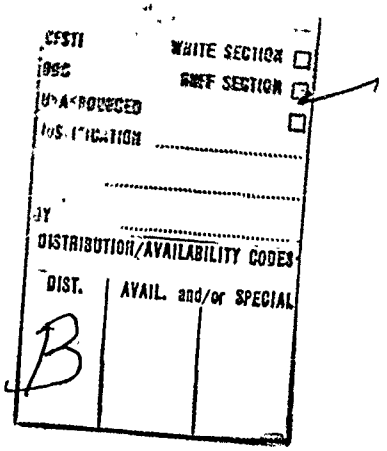
CFSTI
WHITE SECTION
DDC
BUFF SECTION
UNANNOUNCED
JUSTIFICATION
BY
DISTRIBUTION/AVAILABILITY CODES
DIST.
AVAIL. and/or SPECIAL
B

Boattail Effects On The Dynamic Stability Of The Three-Caliber Army-Navy Basic Spinner Projectile

J.D. Nicolaides
C.W. Ingram
T.H. Noethen

FOREWORD

This report documents a study accomplished during the period 15 January 1970 to 14 January 1971 by the Department of Aerospace and Mechanical Engineering, University of Notre Dame, Notre Dame, Indiana 46556, under Contract F08635-70-C-0033 with the Air Force Armament Laboratory, Air Force Systems Command, Eglin Air Force Base, Florida 32542. Program monitor for the Armament Laboratory was Dr. Mark O. Glasgow (DLGR).

This report has been reviewed and is approved.

CHARLES K. ARPKE, Lt Colonel, USAF
Chief, Weapons Effects Division

ABSTRACT

Wind tunnel tests were conducted to study the effects of a boattail on the dynamic stability of the three-caliber Army-Navy basic spinner projectile. Three-degrees-of-freedom angular data was obtained in vertical subsonic wind tunnel tests on one model with no boattail and on one model with a 7.5-degree boattail. Data reduction yielded the restoring, damping, and Magnus moments as functions of time and nonlinear functions of angle of attack for each model. The testing technique employed a low friction jewel bearing model mount and a means for obtaining two-axis data.

(The reverse of this page is blank)

TABLE OF CONTENTS

TABLE OF CONTENTS (Concluded)

LIST OF FIGURES

LIST OF FIGURES (continued)

LIST OF FIGURES (continued)

LIST OF FIGURES (concluded)

LIST OF TABLES

LIST OF ABBREVIATIONS AND SYMBOLS

$C_{m\alpha}$ — pitching moment stability coefficient (1/radian)

$$C_{m\alpha} = \frac{M_{\alpha}\vec{\alpha}}{QSd}$$

$C_{mq}+C_{m\dot{\alpha}}$ — damping moment stability coefficient (1/radian)

$$C_{mq} = \frac{M_q q}{\left(\frac{qd}{2V}\right) QSd} \quad , C_{m\dot{\alpha}} = \frac{M_{\dot{\alpha}}\dot{\vec{\alpha}}}{\left(\frac{\dot{\alpha}d}{2V}\right) QSd}$$

$C_{mp_{\alpha}}$ — Magnus moment stability coefficient (1/rad^2)

$$C_{mp\alpha} = \frac{N_{p\alpha} p\alpha}{\alpha\left(\frac{pd}{2V}\right) QSd}$$

d — reference length, missile diameter (ft)

$I = I_y$ — transverse moment of inertia (slug-ft^2)

I_x — axial moment of inertia (slug-ft^2)

$K_{N,P}$ — nutation and precession arms (degrees)

p, q, r — angular velocity components of missile (rad/sec)

$Q = \frac{1}{2}\rho V^2$ — dynamic pressure (lb/ft)

$S = \frac{\pi d^2}{4}$ — reference area (ft^2)

V — total missile velocity (ft/sec)

α — complex angle of attack (degrees)

$|\vec{\alpha}|$ — mean angle of attack range (degrees)

θ — angle of pitch (degrees)

ψ — angle of yaw (degrees)

$\lambda_{N,P}$ — nutation and precession damping factors (1/second)

$\omega_{N,P}$ — nutation and precession frequencies (radians/second)

K_T — nutation and precession frequencies (radians/second)

SECTION I

INTRODUCTION

The design of small arms projectiles has improved from the classical round shot to the elongated cylinder aft of a pointed nose. A need to obtain greater range and improved accuracy has prompted these configurational changes over the years.

The range of a projectile mainly depends upon two factors: the mass-to-frontal-area ratio and drag.[1] Elongation of a sphere into a cylindrical form greatly decreases the frontal area and also allows the addition of a large amount of mass to the body. Drag is also decreased by virtue of the streamlined shape.

Still less drag and, therefore, greater range can be attained by changing the projectile to the boattail configuration.[2] However, a boattail can be the source of dynamic instability in a projectile and the increase in drag due to the large pitching and yawing motion associated with unstable flight can overcome the advantage. Therefore, it is imperative to determine what aerodynamic effects are caused by a boattail in relation to dynamic stability. This report presents a comparative study of the dynamic stability characteristics of a basic research configuration with and without a boattail.

SECTION II

AEROBALLISTIC THEORY

For constrained center of gravity wind tunnel tests, the normal force contribution is zero. The aerodynamic forces and moments are shown in Figure 1.

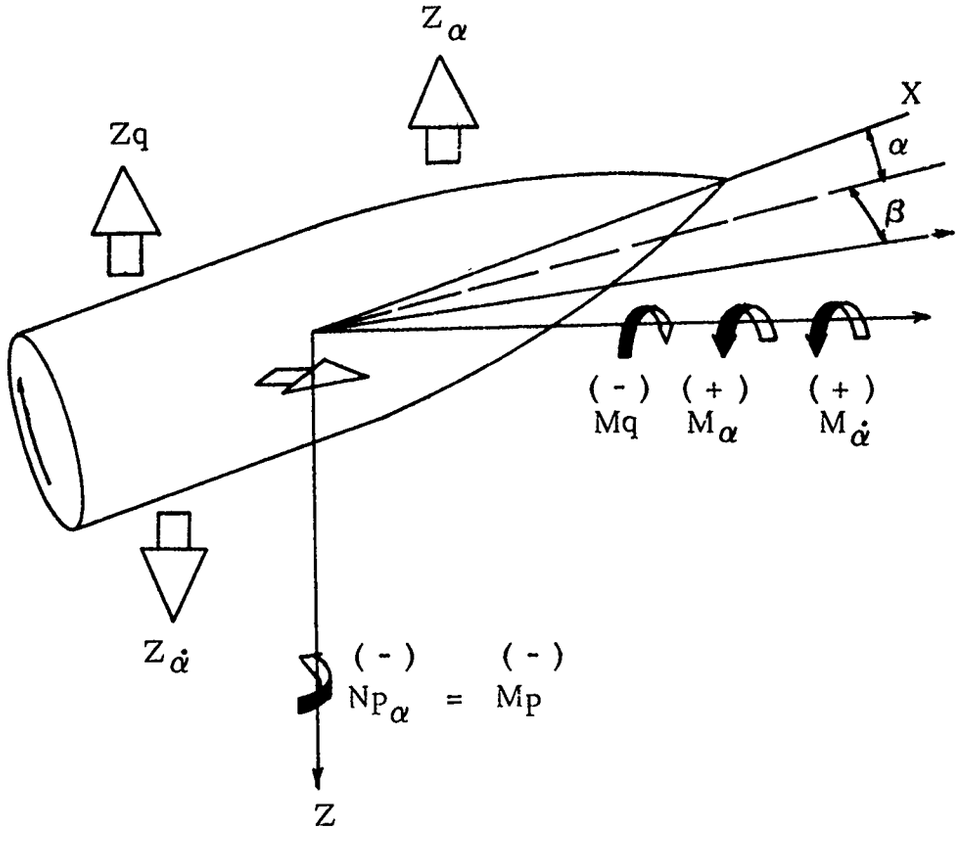

Figure 1. Aerodynamic Forces and Moments

Linear Theory

If linear variations with angle of attack are assumed, the aerodynamic moments can be written as

$$M+iN=-iM_\alpha\alpha + M_q q - iM_{\dot\alpha}\alpha - PM_{p\alpha}\alpha - M_{\delta_\epsilon}\delta_\epsilon e^{ipt} \qquad (1)$$

The resulting complex differential equation of motion is

$$\ddot{\alpha} - \left[i \frac{pI_x}{I} + \frac{M_q + M_{\dot{\alpha}}}{I} \right] \dot{\alpha} - \left[\frac{M_\alpha}{I} + ip \frac{M_{p\alpha}}{I} \right] \alpha = \frac{iM_{\delta_\epsilon} \delta_\epsilon}{I} e^{ipt} \qquad (2)$$

The solution to this equation is found to be

$$\theta = K_N e^{(\lambda_N + \omega_N i)t} + K_P e^{(\lambda_P + i\omega_P)t} + K_T e^{ipt} \qquad (3)$$

where

$$\lambda_{N,P} = \frac{QSd^2}{2V} \left[\frac{C_{m_q} + C_{m_{\dot{\alpha}}}}{2I} (1 \pm \tau) \pm C_{m_{p\alpha}} \frac{\tau}{I_x} \right] \qquad (4)$$

$$\omega_{N,P} = \frac{pI_x}{2I} \left(1 \pm \frac{1}{\tau}\right) \qquad (5)$$

$$\tau = \frac{1}{(1-1/S)^{1/2}} \qquad (6)$$

$$S = \frac{(Ixp)^2}{4\, IC_{m_\alpha} QSd} \qquad (7)$$

$$K_T = \frac{C_{m_{\delta_\epsilon}} \; QSd}{I\,[\,i(p-\omega_N)-\lambda_N]\;[\,i(p-\omega_P)-\lambda_P} \qquad (8)$$

Nonlinear Theory[3,4]

If the aerodynamic moments are assumed to be nonlinear functions of the complex angle of attack,

$$-i(M+iN) = M_\alpha(|\vec{\alpha}|)\vec{\alpha} + M_q(|\vec{\alpha}|)\dot{\vec{\alpha}} + M_{\dot{\alpha}}(|\vec{\alpha}|)\vec{\alpha} + M_{p\alpha}(|\vec{\alpha}|)\, p\, \vec{\alpha} \qquad (9)$$

where

$$M_\alpha(|\vec{\alpha}|) = M_{\alpha_o} + M_{\alpha_2} |\vec{\alpha}|^2 \qquad (10)$$

$$M_q(|\vec{\alpha}|) = M_{q_o} + M_{q_2} |\vec{\alpha}|^2 \qquad (11)$$

$$M_{\dot{\alpha}}(|\vec{\alpha}|) = M_{\dot{\alpha}_o} + M_{\dot{\alpha}_2} |\vec{\alpha}|^2 \qquad (12)$$

$$M_{p\alpha}(|\alpha|) = M_{p\alpha_o} + M_{p\alpha_2} |\alpha|^2 \tag{13}$$

(The Nonlinear Theory used assumes an approximate solution of the same form as the Linear Theory; however, the stability parameter now reflects the nonlinearity in the stability coefficients.)

The solution for the complex angle of attack is given by[5]

$$\vec{\theta} = K_N e^{i\phi_N t} + K_P e^{i\phi t} \tag{14}$$

$$\vec{\theta} = \theta + i\psi \tag{15}$$

$$K_N = K_{N_o} e^{\lambda^*_N t} \quad , \quad K_P = K_{P_o} e^{\lambda^* P t} \tag{16}$$

$$\lambda^*_{N,P} = \lambda_{N,P} + \lambda^V_{N,P} \tag{17}$$

$$\lambda^V_{N,P} = \frac{QSd^2}{2V} \left[\frac{2IV}{d(pI_x)^2} C_{m_{\alpha_2}} \tau^2_{N,P} \left(K_{N,P} \dot{K}_{N,P} + 2K_{P,N} \dot{K}_{P,N} \right) \right] \tag{18}$$

$$\lambda_{N,P} = \frac{QSd^2}{2V} \Bigg\{ \frac{\left[C_{mq} + C_{m_{\dot{\alpha}}} \right]_o}{2I} (1 + \quad_{N,P}) + \frac{\left[C_{m_o} + C_{m_{\dot{\alpha}}} \right]_2}{2I}$$

$$\left[\left[K^2_{N,P} + K^2_{P,N} \right] (1 \pm \quad_{N,P}) + K^2_{P,N} \tau_{N,P} \left(\frac{-1}{P,N} \pm 1 \right) \right]$$

$$\pm \; C_{mp_{\alpha_o}} + C_{mp_{\alpha_2}} \delta_\epsilon{}^2_{N,P} \; \frac{\tau_{N,P}}{I_x} \Bigg\} \tag{19}$$

$$\phi_{N,P} = \frac{pI_x}{2I} \left(1 \pm \frac{1}{\tau_{N,P}} \right) t + \phi_{N_o,P_o} \tag{20}$$

$$\omega_{N,P} \equiv \phi_{N,P} = \frac{pI_x}{2I} \left(1 \pm \frac{1}{\tau_{N,P}} \right) \tag{21}$$

$$r_{N,P} = \left(1 - \frac{1}{S_{N,P}}\right)^{-1/2} \tag{22}$$

$$S_{N,P} = \frac{(P I_x)^2}{4I\,(Cm_{\alpha_o} + Cm_{\alpha_2}\delta^2_{N,P})\;QSd} \tag{23}$$

$$\delta^2_{\epsilon_{N,P}} = K^2_{N,P} + 2K^2_{P,N} \tag{24}$$

A frequency variation, resulting from a nonlinear restoring moment, or changes in the density, velocity or roll rate, or any combination of the above will cause the model amplitudes to vary in the following manner.[1, 3, 6]

$$K_{N,P}(t) = \left(\frac{\omega_{N,P}(o)}{\omega_{N,P}(t)}\right)^{+1/2} K_{N,P}(o) \tag{25}$$

SECTION III

COMPUTATION OF AERODYNAMIC STABILITY COEFFICIENTS

To obtain aerodynamic stability coefficients from the angular data obtained from the wind tunnel tests, the Aeroballistic Theory is fitted to the angular orientation data, θ, ψ . This is done through the use of the "Wobble" computer program.[6] This program fits the theory to short segments of the data in overlapping sections so that the stability parameters, $K_{N,P}$, $\lambda_{N,P}$, $\omega_{N,P}$, are determined as functions of time. Since the Nonlinear Theory assumes an approximate solution of the same form as the Linear Theory, the "Wobble" program can be applied to both.

Computation of Linear Coefficients

Using $\lambda_{N,P}$ and $\omega_{N,P}$, along with the velocity, dynamic pressure, roll rate, and physical parameters of the projectile, the aerodynamic stability coefficients, $C_{m\alpha}$, $C_{mq} + C_{m\dot{\alpha}}$, and $C_{mp\alpha}$, were computed as functions of time from the following equations:

$$C_{m_\alpha} = \frac{\omega_N \omega_P \, 8I}{\pi \rho d^3 V^2} \tag{26}$$

$$C_{m_q} + C_{m_{\dot{\alpha}}} = \frac{2IV}{QSd^2} (\lambda_N + \lambda_P) \tag{27}$$

$$C_{mp\alpha} = \pm \frac{I_x}{I} \left[\frac{2V}{QSd^2} (\lambda_N \lambda_P) - \frac{1}{2I} (C_{mq} + C_{m\dot{\alpha}})(1 \pm r) \right] \tag{28}$$

Computation of Nonlinear Coefficients

The nonlinear aerodynamic stability coefficients, $C_{m_{\vec{\alpha}}}(\vec{\alpha})$, $C_{mq}(\vec{\alpha}) + C_{m\dot{\alpha}}(\vec{\alpha})$, and $C_{mp\alpha}(\vec{\alpha})$ were computed as polynomial functions of the complex angle of attack as follows:

$$\omega_N \omega_P = \left[\frac{C_{m_\alpha}}{I}_0 + \frac{C_{m_\alpha}}{I}_2 \delta_\alpha^2 \right] QSd \tag{29}$$

where

$$\delta_\alpha^2 = K_N^2 + K_P^2 + \frac{K_N^2 \omega_N - K_P^2 \omega_P}{\omega_N - \omega_P} \tag{30}$$

Using a least squares technique to fit a straight line to $\omega_N \omega_P$ versus δ_α^2 yields $C_{m\alpha_o}$ as the intercept and $C_{m\alpha_2}$ as the slope.

Correcting λ_N^* and λ_P^* by determining λ_N^v and λ_P^v from a logarithmic technique developed in Reference 6, the actual damping rates λ_N and λ_P are fitted simultaneously with a least squares procedure to yield $(C_{mq} + C_{m\dot{\alpha}})_o$, $(C_{mq} + C_{m\dot{\alpha}})_2$, $C_{m_{p\alpha_o}}$, and $C_{m_{p\alpha_2}}$.

SECTION IV

THREE-DEGREES-OF-FREEDOM

WIND TUNNEL TESTING TECHNIQUE [7]

A unique technique was developed for obtaining three-degrees-of-freedom angular data for the Army-Navy basic spinner in a subsonic vertical wind tunnel. The test model was mounted on a sting with a needle point set into an inverted jewel cup bearing which allows roll, pitch, and yaw with a minimum of friction[8]. An optical reference system which introduces absolutely no air flow interference was also used.

Motion pictures of the angular motion of the model were taken with a constant frame rate camera positioned almost vertically above the model. The departure of the line-of-sight from the vertical was accounted for in the data reduction process. The data, obtained from the films through the use of an optical comparator, was converted to Euler angles and fitted with the "Wobble" fitting program.

Moment of Inertia

The axial and transverse moments of inertia were found with the use of a torsional pendulum.

The axial moment of inertia was theoretically computed for a cylindrical mass of known density and dimensions. The mass was then suspended from a stiff wire and given an initial angular displacement. The period of the oscillation was measured, using a photo-diode. Dividing the period of oscillation by the theoretical moment of inertia yields the torsional spring constant.

Knowing the torsional spring constant, the moment of inertia for the model was then determined by suspending the model from the mass and again measuring the period of oscillation with the photo-diode. The total moment of inertia minus the theoretical moment of inertia yields the moment of inertia for the model. This was done to find both the axial and transverse moments of inertia.

Data Acquisition

The tests were performed in a vertical subsonic wind tunnel which allows the use of a low friction jewel type bearing.

The jewel bearing is positioned securely inside the model on its axis of symmetry and coincident with its center of gravity. The model is placed on a needle tipped sting of sufficient thickness to limit vibrations which, in turn, is positioned in a holder mounted inside the wind tunnel. The model has a tiny white dot painted on the nose for reference.

With the model in place, a high speed camera which operates at a constant 128 frames per second is positioned outside the wind tunnel and above the model (Figure 2). (The ideal situation would be to have the camera looking straight down at the nose of the model; however, the angle of the camera with respect to the flow is taken into account when reducing the data.) The movie camera is then focused on the white dot on the nose of the model. The camera is equipped with a lens having a focal length of 20 mm. The short focal length is needed to insure a large depth of field since the nose of the model travels slightly above and below the plane of focus during the test.

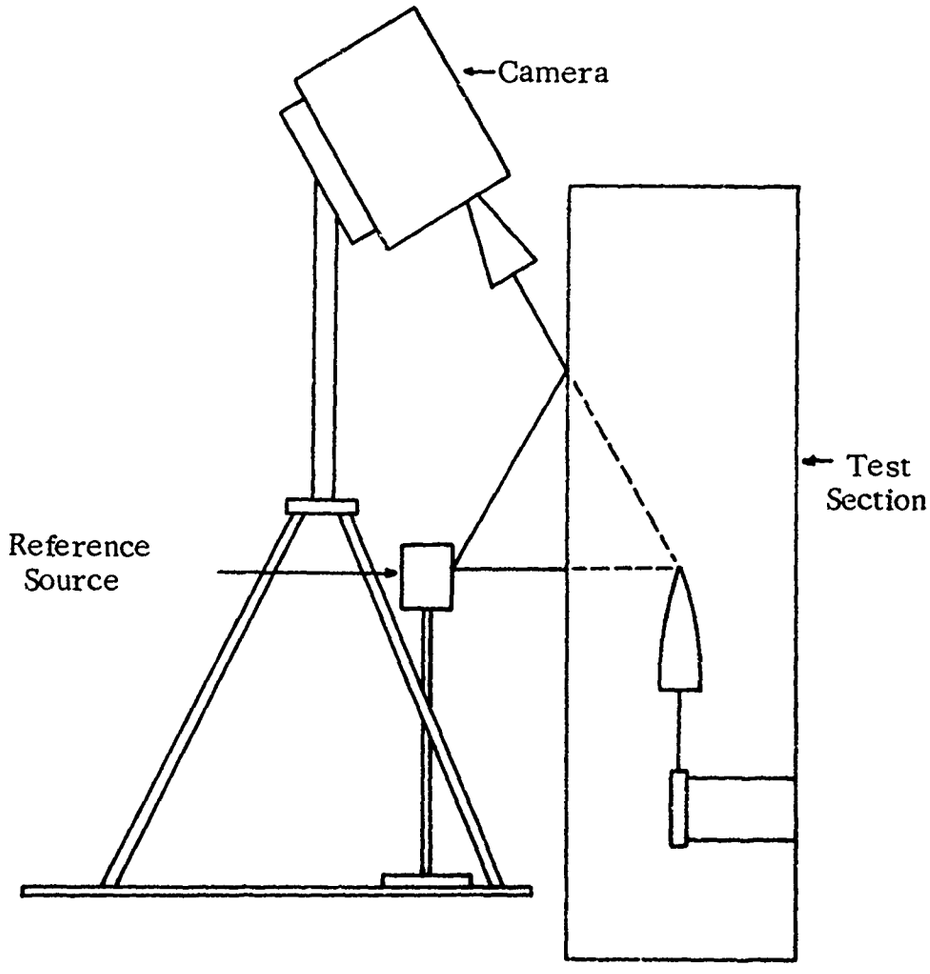

Figure 2. Position of Test Equipment.

A reference system is employed which causes no flow obstruction whatsoever. To obtain the true motion of the test model, it is important that nothing be placed in the flow so as to alter the aerodynamics.

A black box with two pinholes 0.035 inch in diameter and with a light source inside is positioned outside the wind tunnel. The wind tunnel glass reflects the light emitted by the pinholes into the lens of the camera. This gives the appearance of two dots of light seemingly suspended in the test section (Figure 2). Fine adjustment of the position of the box must be made so that both dots are in focus and do not interfere with the dot on the nose of the model.

Measurements taken include the angle of the camera with respect to the flow, the x,y, and z coordinates of the dots with respect to a fixed point (usually the position of the nose of the model at zero angle of attack), and the distance from the nose of the model to the jewel bearing.

With the camera and reference dots in place, the model is given a rolling velocity by tangentially directing a stream of compressed air on its side. The model is held in place by means of a rod with a roller bearing attached to the end which fits over the nose. A variable frequency strobe light is used to indicate when the desired initial roll rate is obtained. The model is then disturbed and allowed to pitch, yaw, and roll while the motion is recorded by the camera.

Data Reduction[7]

A digital computer program was developed to convert the numerical information provided by the comparator readings of the test films into Euler angles. No small angle assumptions are made; therefore,the accuracy of the test data is increased.

Considering the kinematic relationships of the test set-up with modified Euler angles as conventionally defined for aeroballistic axes, the geometry of the motion of the model is shown in Figure 3.

The following quantities are defined as:

R = distance from the pivot point to the nose of the model

y_c, z_c = coordinates of nose of model projected on horizontal plane

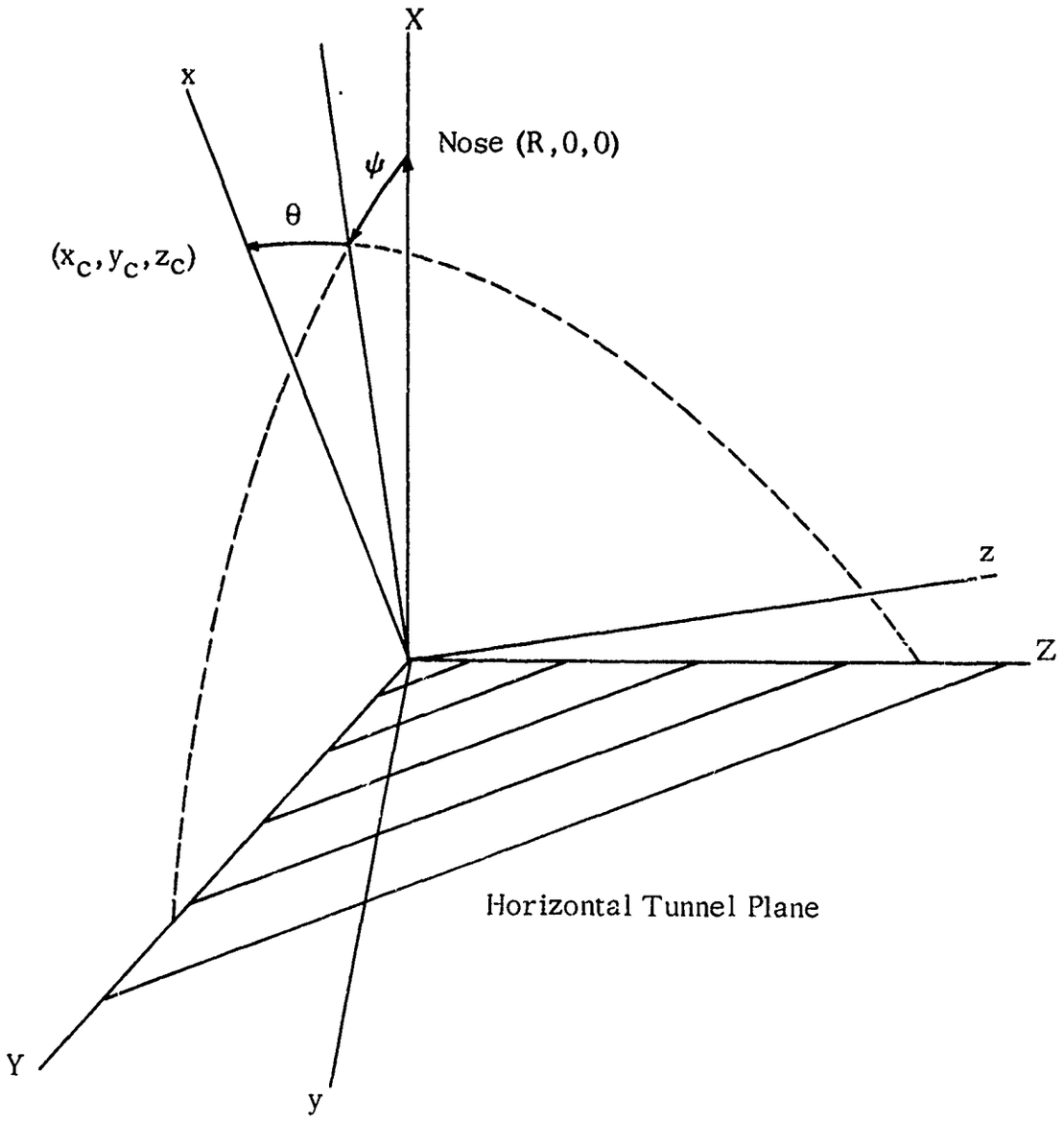

Figure 3. Aeroballistic Axis System and Euler Angles.

y_c', z_c' = coordinates of nose of model on viewing plane of camera

γ = inclination of line-of-sight of camera below horizontal

The fixed (inertial) axis system, X,Y,Z, is positioned with the origin at the pivot, the X-axis vertically upward opposite the direction of

the air flow in the wind tunnel, and the Y,Z plane parallel to the horizontal plane of the wind tunnel. As the model yaws and pitches, the aeroballistic axes, x,y,z, which are fixed to the body but do not roll with it, move through the yaw angle, ψ, and the pitch angle, θ. A point in the fixed axis system can be transformed to the aeroballistic axis system through the matrix equation

$$\begin{bmatrix} x \\ y \\ z \end{bmatrix} = T \begin{bmatrix} X \\ Y \\ Z \end{bmatrix} \tag{31}$$

where

$$T = \begin{pmatrix} \cos\theta\cos\psi & \cos\theta\sin\psi & -\sin\theta \\ -\sin\psi & \cos\psi & 0 \\ \sin\theta\cos\psi & \sin\theta\sin\psi & \cos\theta \end{pmatrix} \tag{32}$$

Therefore, the coordinates of the nose of the model, which are (R,0,0) in the aeroballistic axis system, are expressed by Equations (31) and (32) as

$$\begin{aligned} x_c &= R\cos\theta\cos\psi \\ y_c &= R\sin\psi\cos\theta \\ z_c &= -R\sin\theta \end{aligned} \tag{33}$$

The Euler angles can then be found from equations to be:

$$\theta = \sin^{-1}\left(\frac{z_c}{R}\right) \tag{34}$$

$$\psi = \sin^{-1}\left(\frac{y_c}{R\cos\theta}\right) \tag{35}$$

Next, the relevant camera angle relationships are derived. As shown in Figure 4, the effect of the camera inclination angle, γ, is to rotate the Y,Z plane about the Y-axis through the angle $\gamma' = 90-\gamma$. Since the choice of where the viewing plane lies is arbitrary, it was chosen to coincide with the plane which passes through the origin and the Y-axis and is inclined at the angle γ' to the Z-axis.

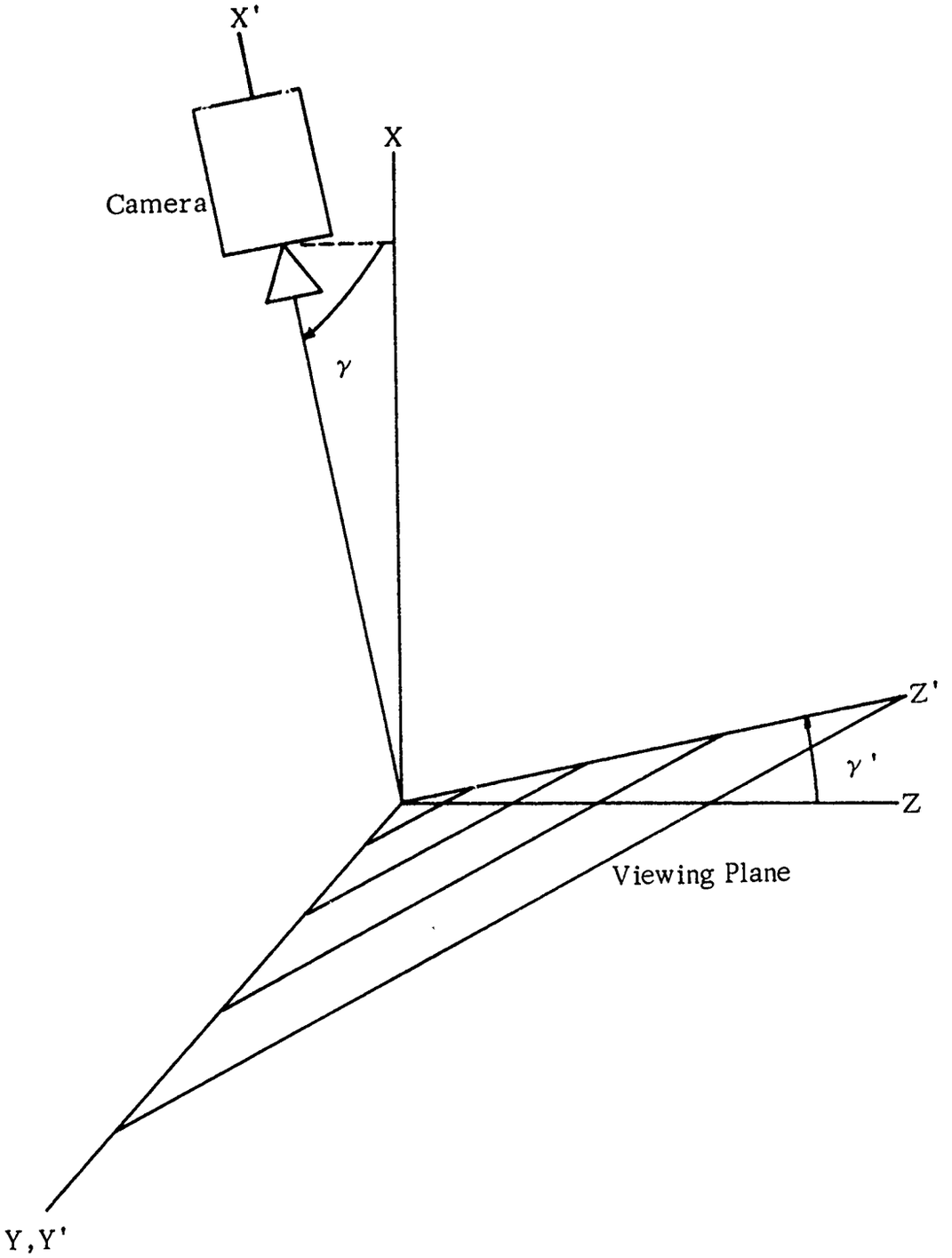

Figure 4. Angle of Camera Relative to Inertial Axis System.

Thus, a point in the fixed axis system is transformed to the tipped axis system of the camera through the matrix equation

$$\begin{bmatrix} X' \\ Y' \\ Z' \end{bmatrix} = T_\gamma \begin{bmatrix} X \\ Y \\ Z \end{bmatrix} \tag{36}$$

where the orthogonal transformation

$$T_\gamma = \begin{pmatrix} \sin\gamma & 0 & -\cos\gamma \\ 0 & 1 & 0 \\ \cos\gamma & 0 & \sin\gamma \end{pmatrix} \tag{37}$$

Therefore, the coordinates measured from the film frame, y'_c, z'_c can be transformed back to the wind tunnel plane through the inverse of Equation (37):

$$y_c = y'_c \tag{38}$$

$$z_c = z'_c/\sin\gamma \tag{39}$$

These are the coordinates necessary to determine the Euler angles from Equations (34) and (35).

It is necessary to derive the relationship governing the data on the film frame and unite them with previous relationships.

Chances are that the plane of the film frame in the camera and the viewing plane containing the reference dots do not coincide. They may be assumed parallel due to the large depth of focus of the lens; however, a relative translation and/or rotation can be present due to movement of the camera during a test. Consequently, account must be taken to eliminate this possibility of error.

If the axes of the viewing plane are defined as y', z', and the reference points are R_1 and R_2, then

$$R_1 = (y'_1, z'_1) \tag{40}$$

$$R_2 = (y'_2, z'_2) \tag{41}$$

and the angle of rotation is

$$\epsilon_1 = \tan^{-1} \frac{z'_2 - z'_1}{y'_2 - y'_1} \tag{42}$$

If the axes of the film plane are defined as y_f, z_f, then

$$R_1 = (y_{f1}, z_{f1}) \tag{43}$$

$$R_2 = (y_{f2}, z_{f2}) \tag{44}$$

Projection of the film plane onto the comparator yields numerical quantities for R_1, R_2, and the nose dot, N, in terms of the comparator system

$$R_1 = (n_1, n_2) \tag{45}$$

$$R_2 = (n_3, n_4) \tag{46}$$

$$N = (n_5, n_6) \tag{47}$$

The result is a conversion factor, C, from comparator units of measurement to the actual wind tunnel units:

$$C = \frac{\sqrt{(n_1 - n_3)^2 + (n_2 - n_4)^2}}{D} \tag{48}$$

where D is the measured distance between the reference points.

In order to eliminate comparator bias and the effect of a translation by the camera during the test, the comparator origin is moved to the left hand (arbitrarily) reference point by letting

$$R_1 = (u_1, v_1) = (0, 0) \tag{49}$$

$$R_2 = (u_2, v_2) = (y_{f1} - y_{f2}, z_{f2} - z_{f1}) \tag{50}$$

$$N = (u_3, v_3) = (y_{f1} - y_{f3}, z_{f3} - z_{f1}) \tag{51}$$

The angle of rotation of the projection of the film with respect to the comparator can now be computed as

$$\epsilon_2 = \tan^{-1} \left(\frac{v_2}{u_2} \right) \tag{52}$$

Therefore, the net rotation to be considered is

$$\epsilon = \epsilon_2 - \epsilon_1 \tag{53}$$

The comparator coordinates can now be transformed to the wind tunnel reference system by a rotation through the angle ϵ:

$$\begin{bmatrix} u' \\ v' \end{bmatrix} = \begin{pmatrix} \cos\epsilon & \sin\epsilon \\ -\sin\epsilon & \cos\epsilon \end{pmatrix} \begin{bmatrix} u \\ v \end{bmatrix} \tag{54}$$

where u' and v' are the desired rotated coordinates.

Finally, these coordinates must be transformed to viewing plane coordinates. Since the position of the origin of the wind tunnel system is the position of the model nose at zero angle of attack, the coordinates of the origin with respect to the reference points can be computed by averaging the measured relative displacement to each reference point. Letting Q_y and Q_z be these coordinates, then

$$y'_c = u'_3 - Q_y \tag{55}$$

$$z'_c = v'_3 - Q_z \tag{56}$$

Substitution of these quantities into Equations (38) and (39) and the results into Equations (34) and (35) will yield the desired Euler angles.

Wind Tunnel Facility and Models

All tests were conducted in contractor's vertical subsonic wind tunnel which is equipped with anti-turbulence screens and a 16.625-by 16.625-inch test section. The maximum wind velocity is 150 feet per second; however, all tests were run at approximately 45 feet per second. Employment of the vertical wind tunnel facilitated the use of a low friction, three-degrees-of-freedom, jewel bearing model mount. The model is shown mounted in the wind tunnel in Figure 5.

Two configurations of the three caliber Army-Navy Basic Spinner Rocket were tested: one with a zero-degree boattail and one with a 7.5-degree boattail. Both models were 2.5 inches in diameter, constructed from aluminum, and had a center of gravity positioned 2.0 calibers from the nose. The 7.5-degree boattail was 0.40 caliber in length. Model exteriors are shown in Figures 6 and 7 and other physical parameters are listed in Table I.

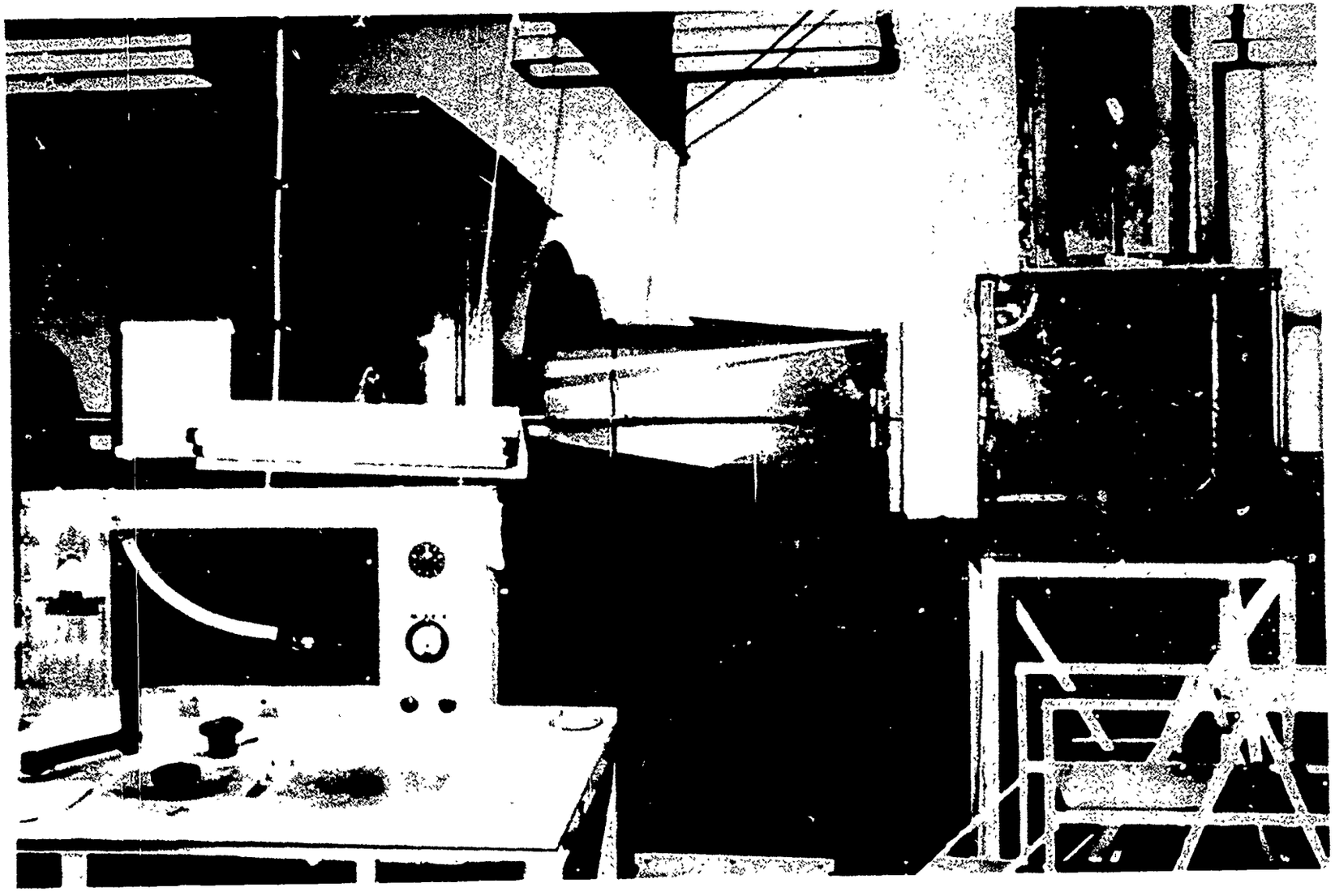

Figure 5. Model Mounted in Wind Tunnel Test Section.

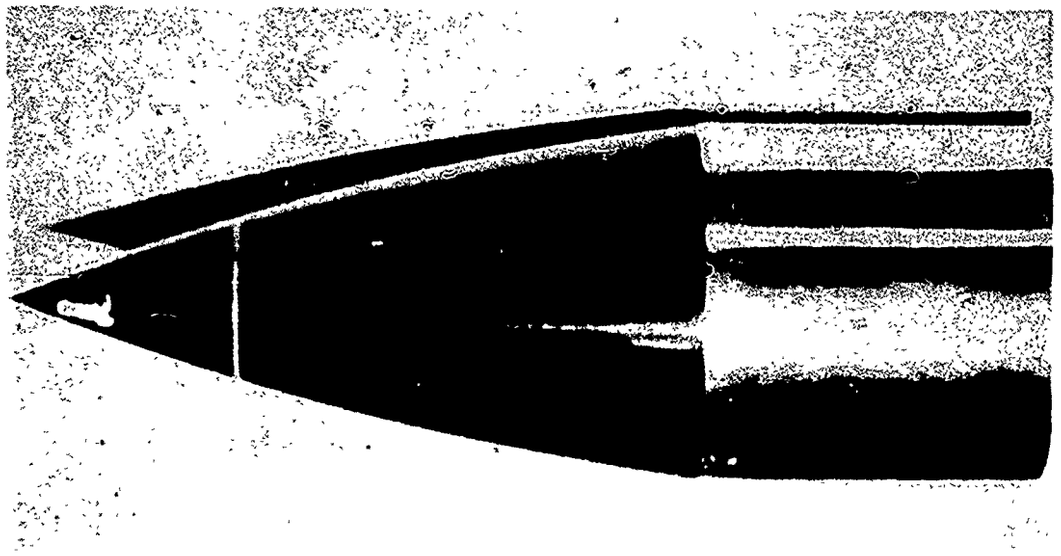

Figure 6. A-N Basic Spinner with Zero-Degree Boattail.

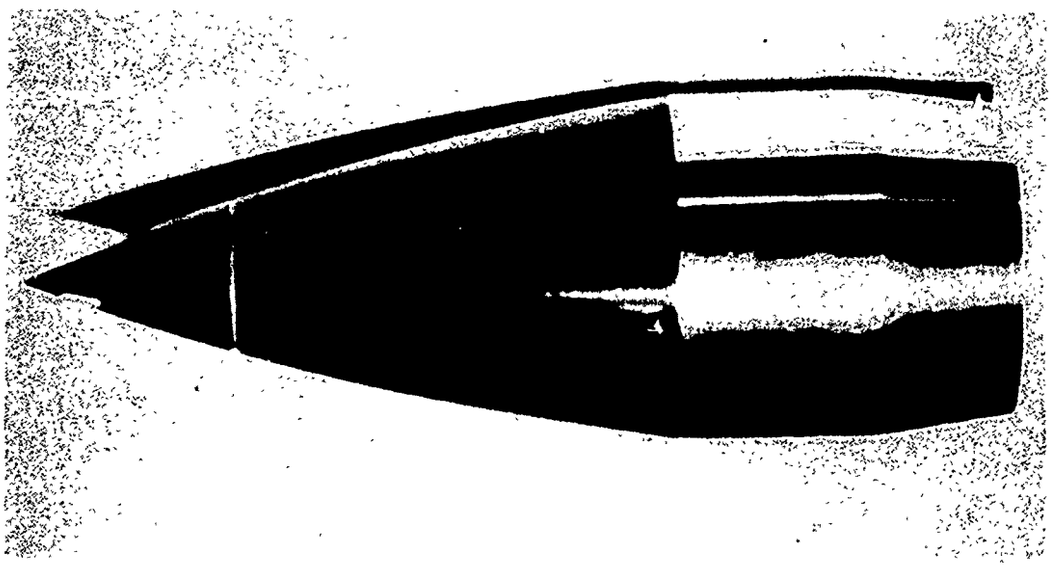

Figure 7. A-N Basic Spinner with 7.5-Degree Boattail.

Before testing,the models were balanced in still air to eliminate the effects of a moment due to their own weight. An adjustable jewel bearing mount and weight ring allowed movement of both the center of gravity and bearing (Figure 8).

When spinning in still air the model is a gyroscopic pendulum. A center of gravity positioned above the point of rotation and non-zero angle of attack causes a precessional motion in the same direction as the rolling velocity. Conversely, a center of gravity positioned below the point of rotation causes precessional motion opposite the rolling velocity. If the two coincide, the model is neutrally stable and no precessional motion is caused. Adjustment of the weight ring and bearing position was made until

TABLE I. PHYSICAL PARAMETERS OF TEST MODELS

	Mass (Slugs)	I_x(Slug-Ft^2)	I_y(Slug-Ft^2)	CG Position (Inches from Nose)
Zero-degree Boattail	0.02384	0.0001707	0.0004706	5.0
7.5-degree Boattail	0.02248	0.0001606	0.0004554	5.0

the last condition persisted. The jewel bearing was positioned exactly the same distance from the nose for the 7.5-degree boattail model as it was for the zero-degree boattail model. Only the weight ring was moved in balancing so that the center of gravity positions of the two models were identical.

Friction Analysis

Frictional effects were first noticed when an attempt was made to coincide the center of gravity of the model with the position of the jewel bearing. Adjustments had been made so that no angular velocity resulted over a time span of 15 seconds (at least twice the duration of an aerodynamic test); however, it was noticed that an angular displacement decreased in amplitude, that is, when displaced the model tended to right itself. This way theorized to be a frictional effect since the equations of motion for a gyroscopic pendulum predict zero damping.[1] Neglecting this phenomenon could possibly cause serious inaccuracies in the dynamic damping factors.

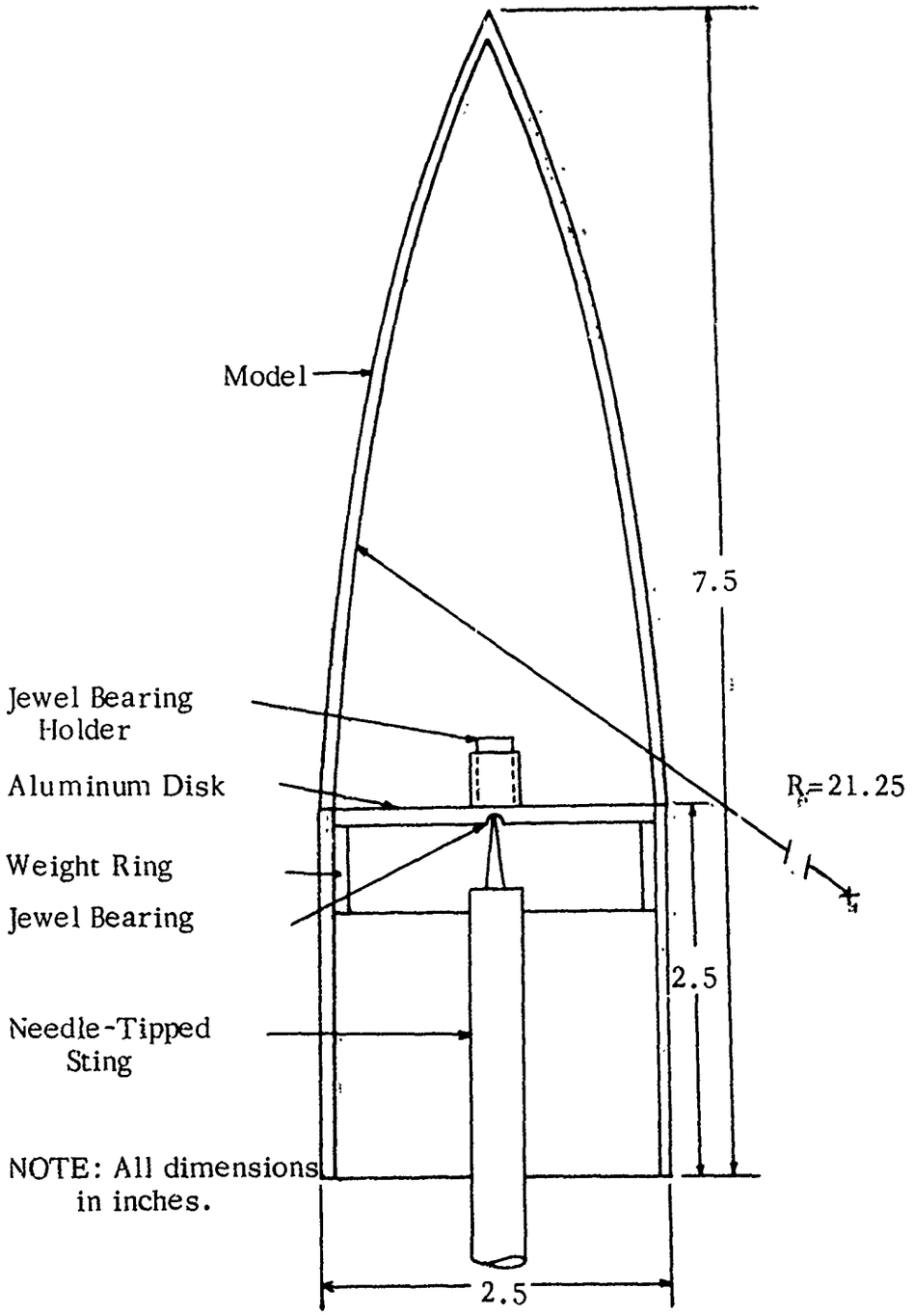

Figure 8. Model Interior and Dimensions.

Several mathematical models were conceived to handle the problem; however, none actually gave a true representation of what was qualitatively observed. Consequently, compensation for the frictional effects was made by an approximation. Three-degrees-of-freedom data was taken of the model in still air. The data was then reduced to obtain the damping factors due to friction (aerodynamic forces were assumed negligible). The damping factors obtained from the aerodynamic tests were then corrected through the following equation:

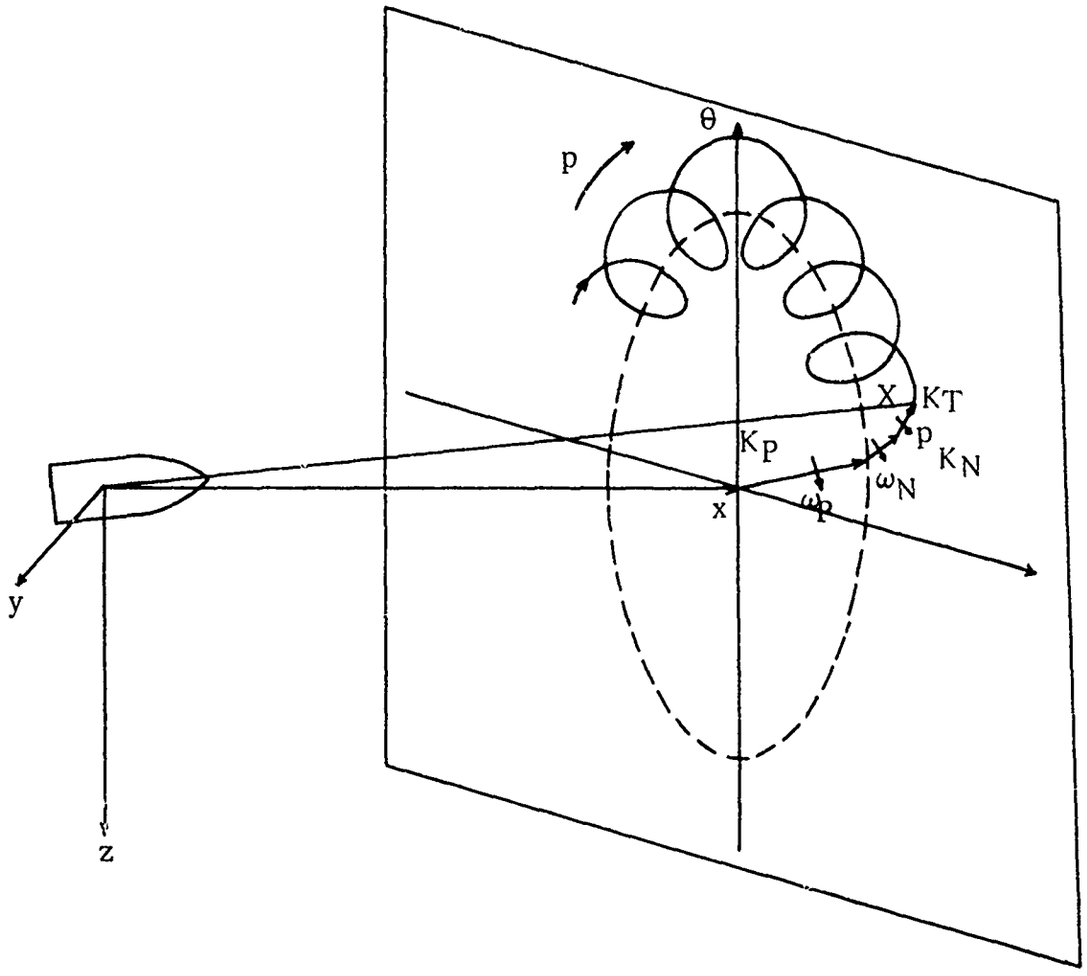

Figure 9. Arms of Tri-Cyclic Motion.

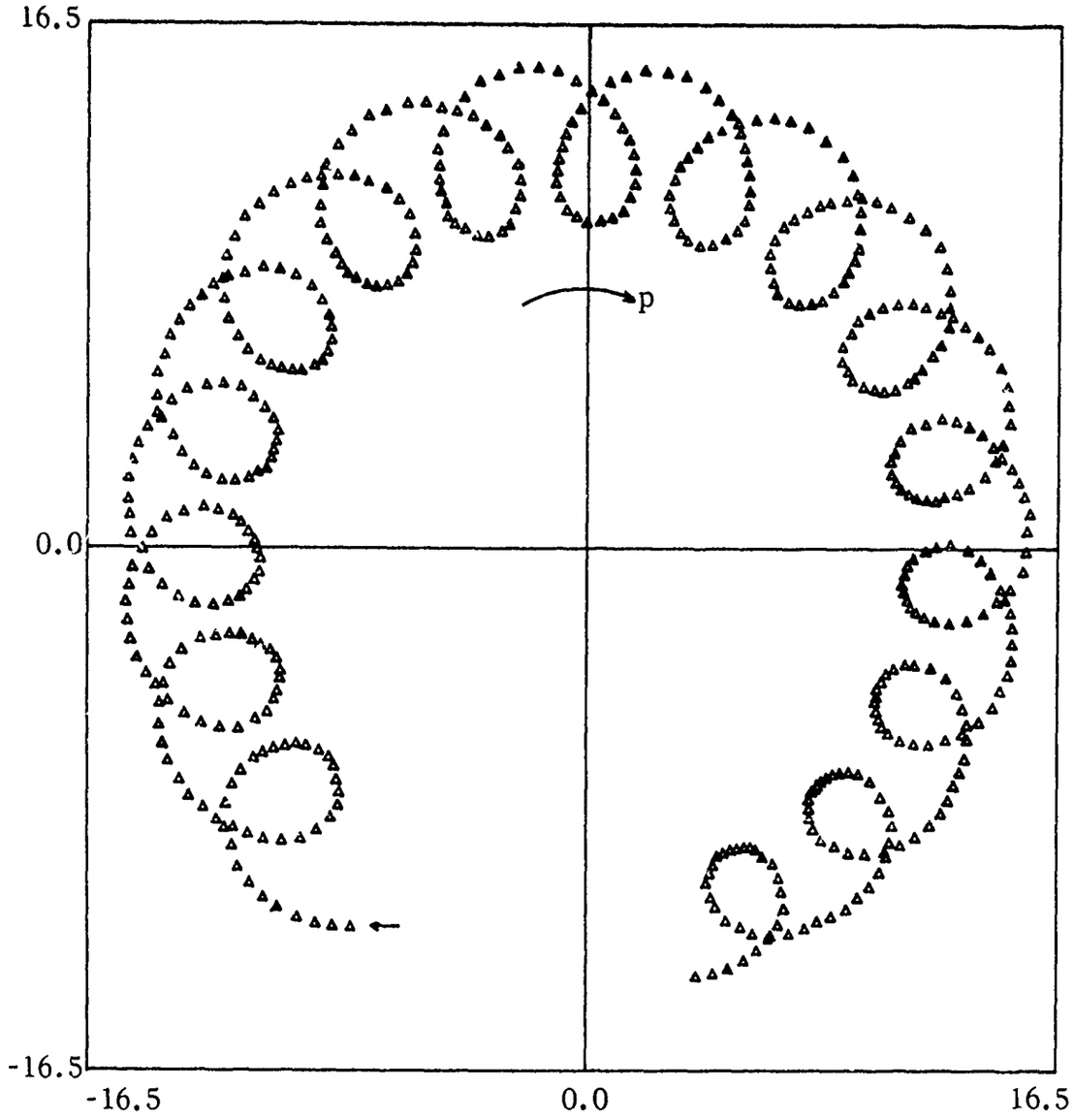

Figure 10. Sample Three-Degrees-of-Freedom Motion for Zero-Degree Boattail Model.

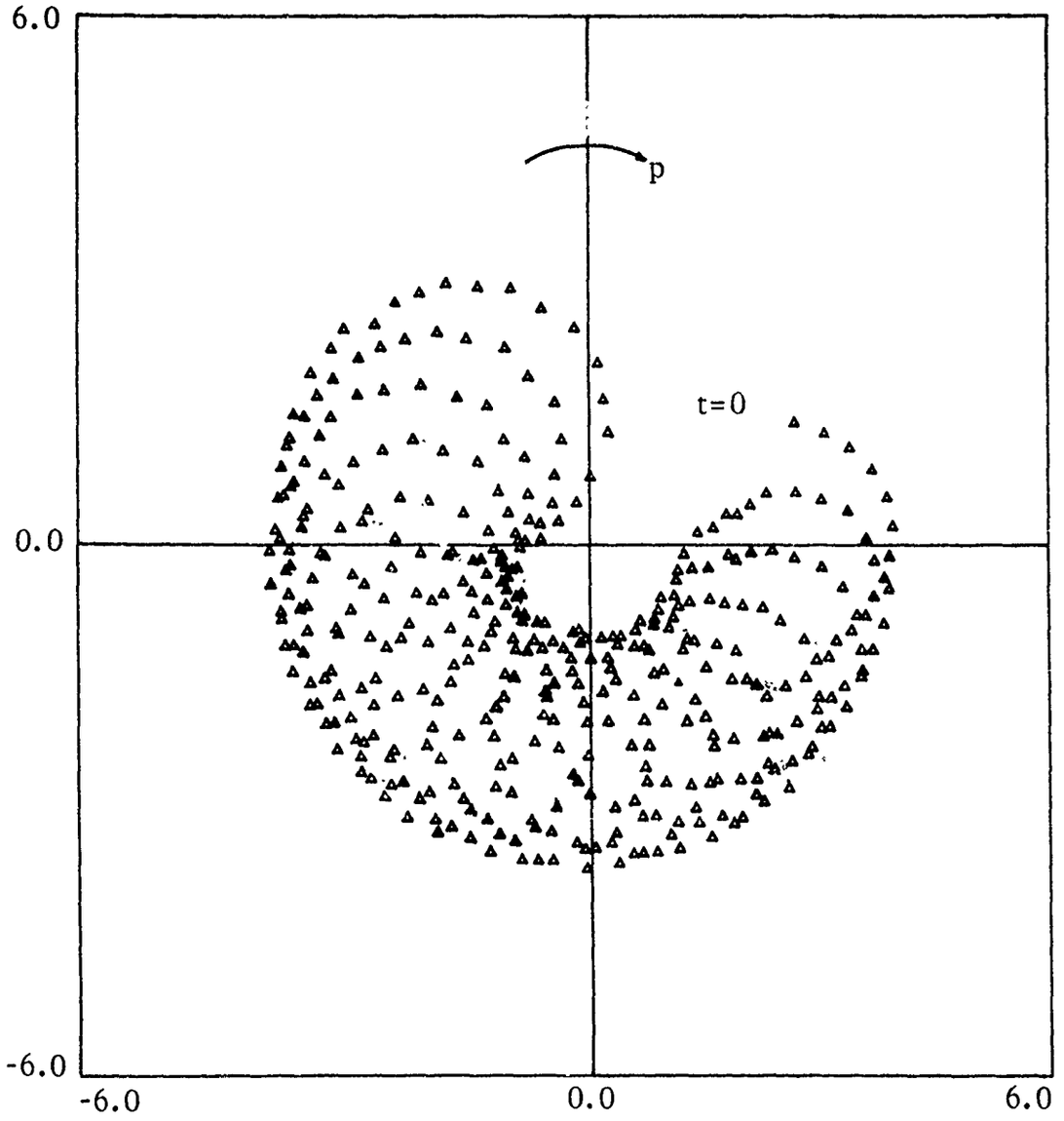

Figure 11. Sample Three-Degrees-of-Freedom Motion for 7.5-Degree Boattail Model.

SECTION V

EXPERIMENTAL RESULTS

Data

The data acquisition technique provided two-axis Euler angles. Figure 9 shows the arms of tri-cyclic motion and their angular rates. No small angle assumptions were used in computing the θ, ψ angles and they, therefore, contain a higher degree of accuracy. Samples of the three-degrees-of-freedom angular data are shown in Figures 10 and 11 for the zero-degree and 7.5-degree boattail models, respectively.

Inspection of Figure 10 shows the smaller, faster nutation arm rotating in a clockwise direction (the same direction as the roll rate). A large difference can be seen between the nutation and precession frequencies.

Comparison of Figures 10 and 11 shows a difference in the relative sizes of the nutation and precession arms of the two models. The frequency ratio, however, is approximately the same for both.

Friction

Reduction of the data films taken on the three-degrees-of-freedom motion of the models in still air yielded the damping characteristics due to friction alone. Results indicate that the precession arm was strongly affected while negligible effect was contributed to the nutation arm. The still air damping factors were small but of the same order of magnitude as the dynamic precession damping factors for both models. The damping factors for the nutation arm were two orders of magnitude smaller than the dynamic nutation damping factors; hence, they were neglected.

The value of λ_{Pf} was -0.023 for the zero-degree boattail and -0.056 for the 7.5-degree boattail. Corrections were made in the dynamic precession damping factors using these quantities.

Zero-Degree Boattail Analysis

A series of qualitative wind tunnel tests were conducted as the initial step in the testing procedure. These provided an estimate of the aerodynamic characteristics of the model and helped establish an orderly quantitative testing procedure.

Initially the model was spun up to approximately 900 rpm (this was

close to the maximum roll rate attainable before the model would separate itself from the sting due to vibrations). The model was then disturbed to excite both the nutation and precession modes. The resulting motion was comprised of a low frequency precession arm having an amplitude of about nine degrees and a high frequency nutation arm.

The precession amplitude increased very slightly with time, indicating a weak instability. On the other hand, the nutation amplitude usually decreased to zero before the completion of three precession cycles. Also, at 900 rpm it was virtually impossible to disturb the model in such a way that a large nutation amplitude could be attained. Consequently, it was judged that the nutation arm was highly stable and the precession arm was slightly unstable at this roll rate.

Qualitative observations were also made at a lower roll rate to determine possible effects of roll rate on the dynamic stability. The initial value was about 650 rpm. No lower values were used; this insured that the model possessed adequate gyroscopic stability throughout the test.

At 650 rpm an initial disturbance resulted in a larger total motion. The initial nutation and precession amplitudes were greater with a large change in the size of the nutation arm. The nutation amplitude still damped to zero but much more slowly than at the higher roll rate.

A significant change was noted in the precession mode at 650 rpm. Insteady of the slight undamping that was present at 900 rpm, the amplitude slowly decreased. The only other noticeable difference was an increased precession frequency and a decreased nutation frequency.

The performance of the model at the lower roll rate and higher angle of attack indicated the presence of a roll rate dependence and a possible nonlinear Magnus moment.

Since the purpose of the test program was to determine the effects of a boattail on the dynamic stability of the model, an attempt to determine roll rate effects was not pursued. However, two of the six quantitative tests of the zero-degree boattail were conducted at a lower roll rate than the other four. This was done primarily to obtain the broadest possible range of complex angles of attack in an effort to sensibly obtain the aerodynamic coefficients as nonlinear functions of angle of attack.

The linear quantitative test results were broken up into two sets of three each - the three lowest and the three highest amplitude runs. All three of the lower amplitude runs [1(A), 1(B), and 1(C)] exhibited a stable nutation mode and an unstable precession mode. The higher amplitude runs [2(A), 2(B), and 2(C)] were all stable in both modes. The stability parameters are shown in Figures 12 through 18 for runs 1, and in Figures 19

through 25 for runs 2. The accuracy of the stability parameters is indicated by the small probable errors-of-fit plotted versus time in Figures 12 and 19. The figures also include the nutation and precession arms, damping factors, and frequencies plotted versus time.

Friction caused a slight roll rate decay over the duration of a test. The effect of the roll rate decay was time varying frequencies. Because of this the dynamic damping factors were corrected on the basis of Equation (25).

Inspection of the numerical values for the dynamic precession damping factors for runs 2 showed them to be of lesser magnitude than the friction damping factors. Consequently, correcting the damping factors for friction resulted in positive values. This indicated that at the higher angles of attack the friction was overcoming the weak precession instability.Therefore, Figures 20 and 21, which show decreasing precession arms and positive damping factors for runs 2, are misleading. The precession arms determined by the fitting routine were not corrected for friction before plotting, whereas the damping factors were.

Linear aerodynamic coefficients were calculated from Equations (26), (27), and (28), using the stability parameters obtained from the "Wobble" program. The coefficients are plotted versus time in Figures 26 through 28 for runs 1 and Figures 29 through 31 for runs 2. The average values are listed in Table II.

TABLE II. LINEAR COEFFICIENTS (AVERAGE VALUES)

Run	$C_{m\alpha}$ (1/Rad)	C_{mq} (1/Rad)	$C_{mp\alpha}$ (1/Rad^2)
Zero-degree Boattail			
1(A)	1.0996	-0.3472	-0.1795
1(B)	1.1140	-0.5913	-0.1391
1(C)	1.1051	-0.8252	-0.1333
2(A)	1.1299	-1.1059	-0.0957
2(B)	1.1768	-0.6422	-0.0489
2(C)	1.1262	-0.2497	-0.0440
7.5-degree Boattail			
3(A)	1.1126	1.2498	0.2150
3(B)	1.0682	1.3094	0.2279
3(C)	1.0838	1.4225	0.0181
3(D)	1.1194	1.0500	0.2492

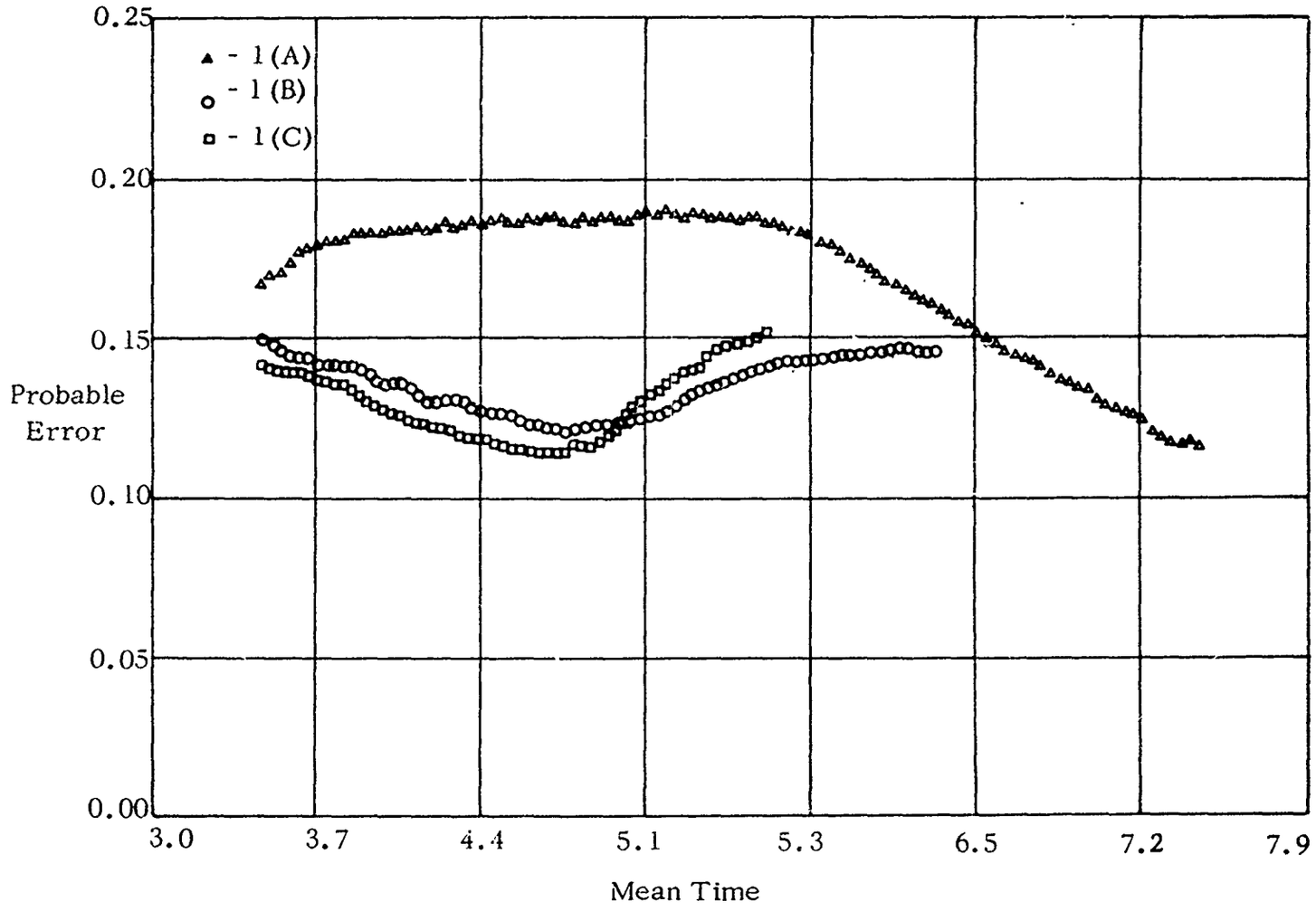

Figure 12. Probable Error-of-Fit (Degrees) versus Mean Time (Seconds)[Runs 1(A), 1(B) and 1(C)] .

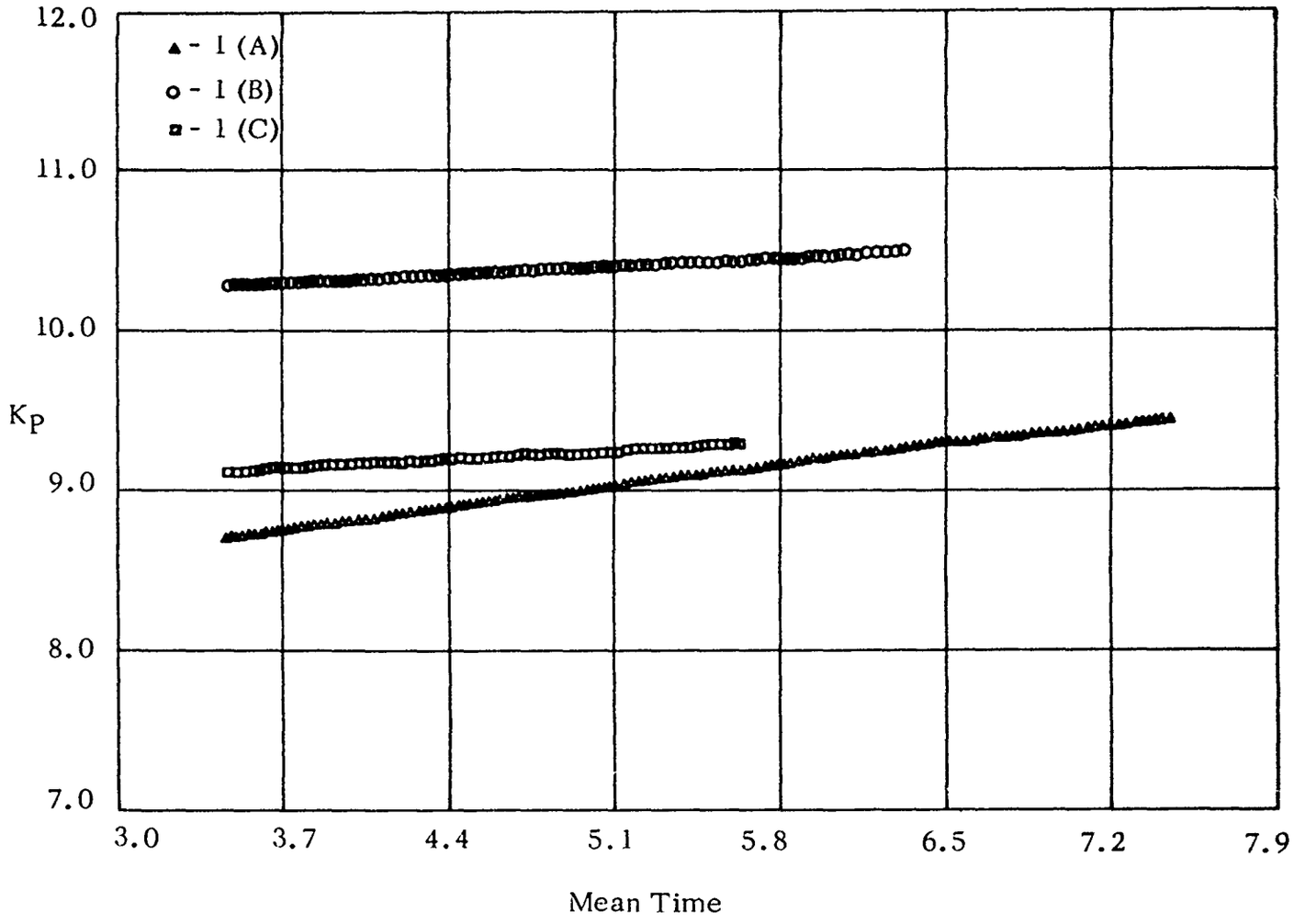

Figure 13. Precession Arm (Degrees) versus Mean Time (Seconds) [Runs 1(A), 1(B), 1(C)] .

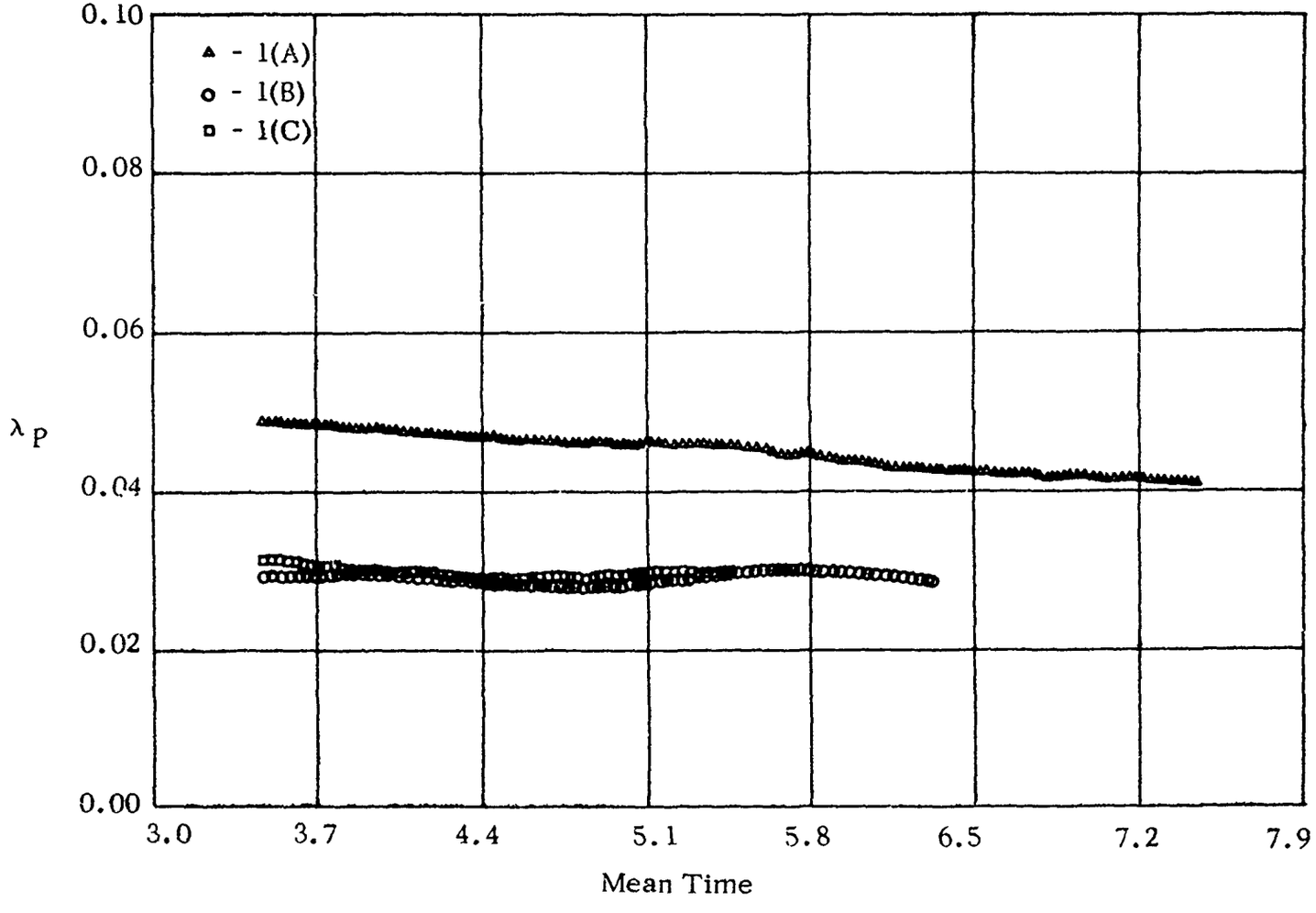

Figure 14. Dynamic Precession Damping Factor (One Per Second) versus Mean Time (Seconds) [Runs 1(A), 1(B), 1(C)] .

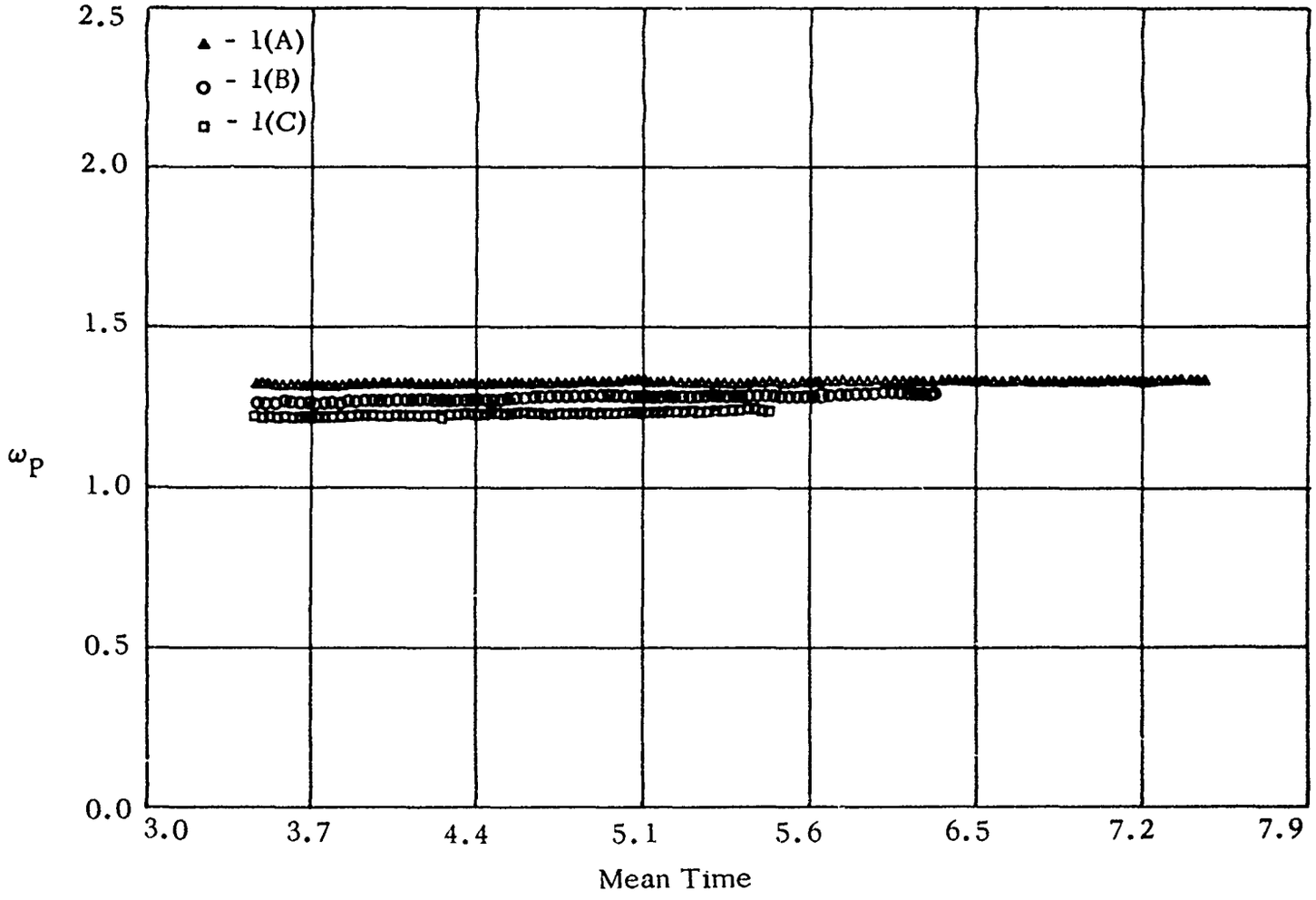

Figure 15. Precession Frequency (Radians/Second) versus Mean Time (Second)[Runs 1(A), 1(B), 1(C)] ..

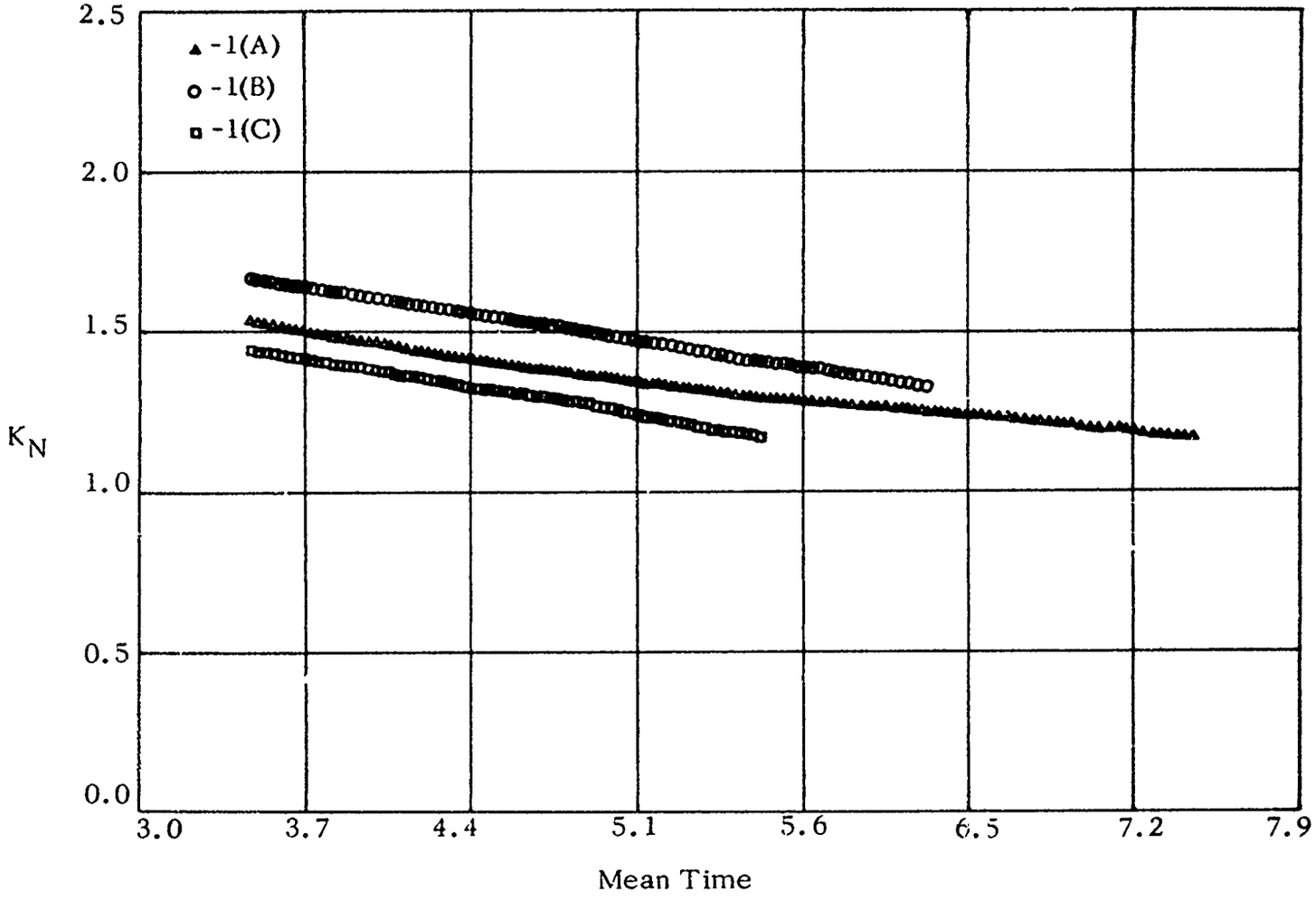

Figure 16. Nutation Arm (Degree) versus Mean Time (Seconds) [Runs 1(A), 1(B), 1(C)].

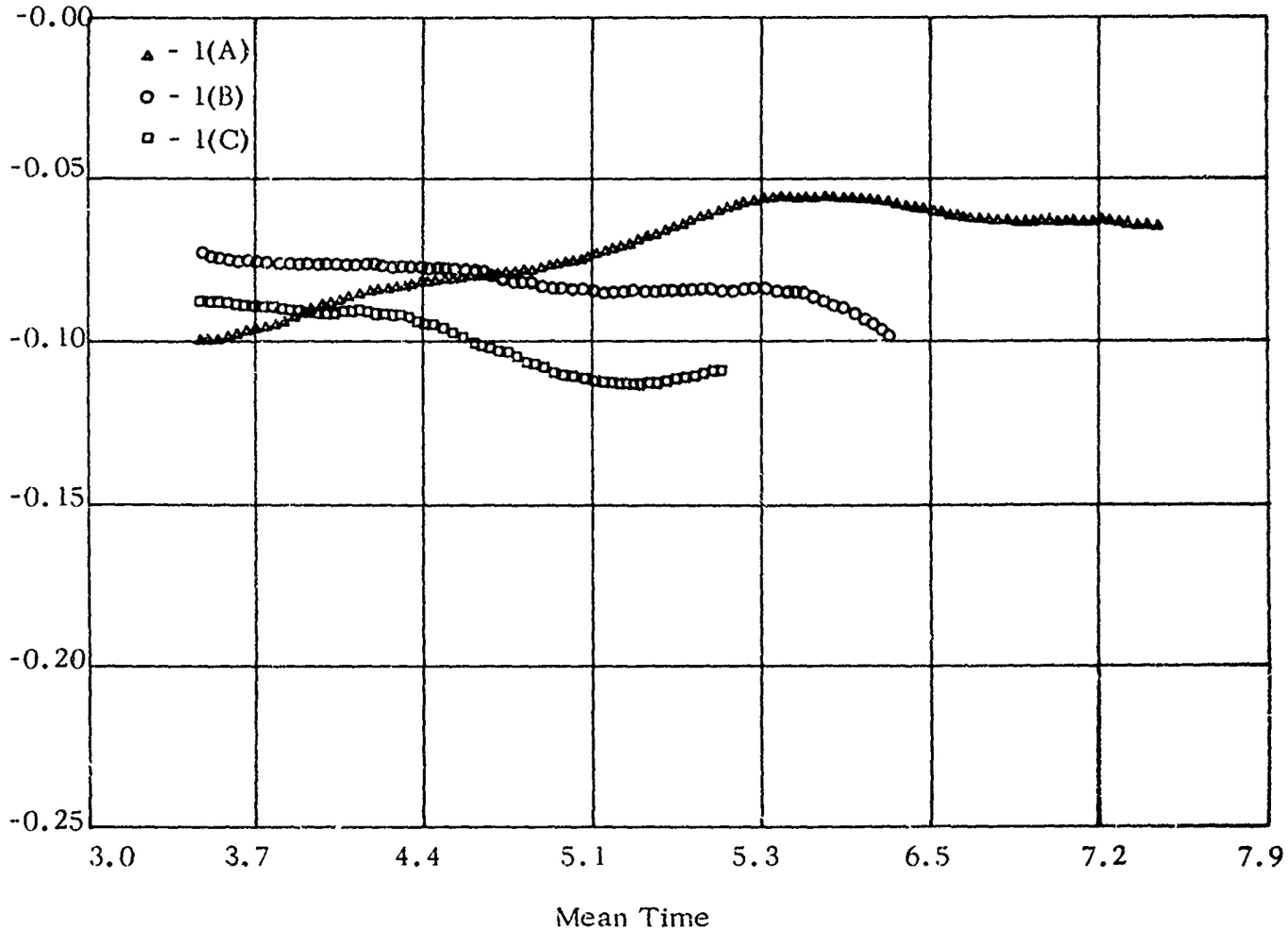

Figure 17. Dynamic Nutation Damping Factor (One/Second) versus Mean Time (Seconds) [Runs 1(A), 1(B), 1(C)].

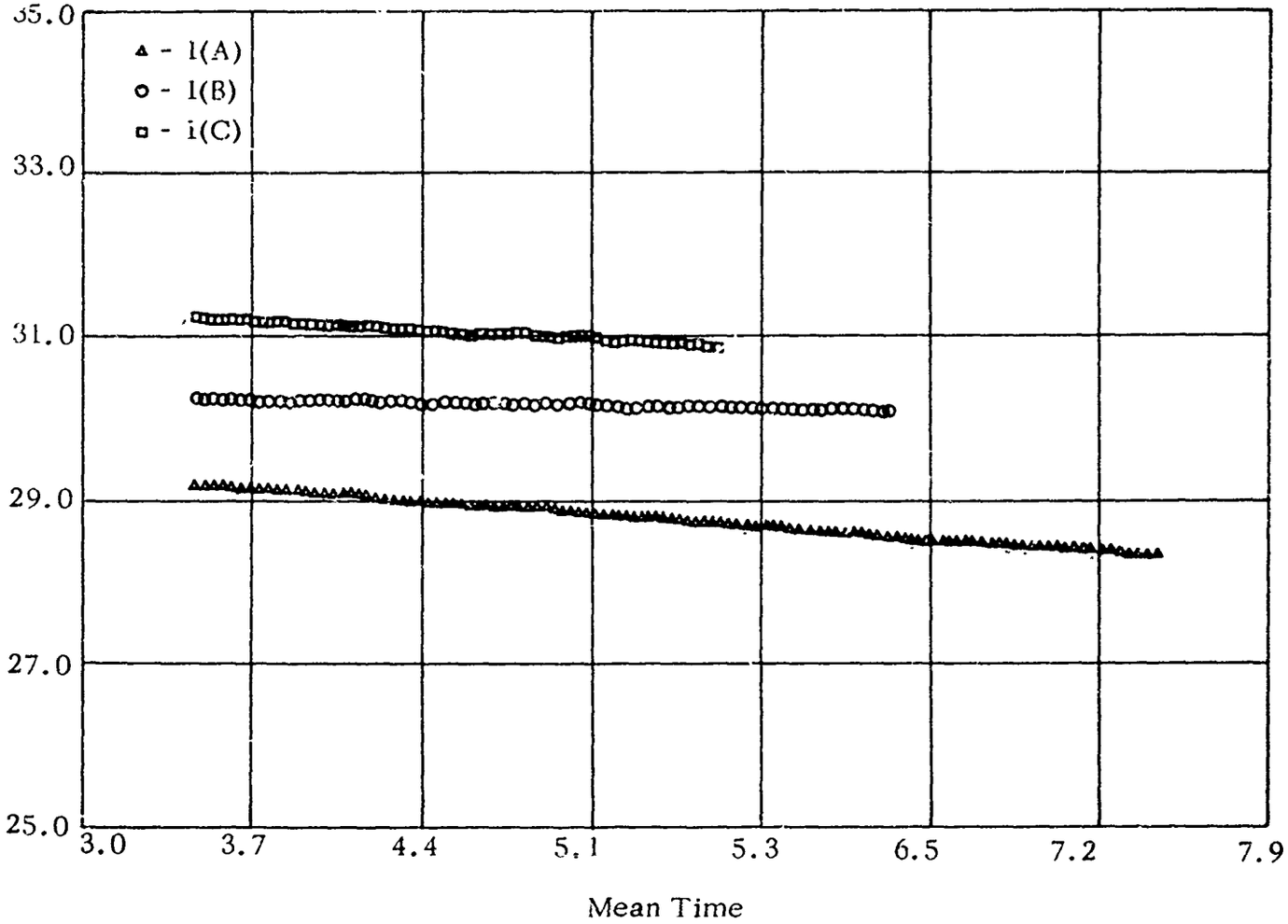

ω_z

Figure 18. Nutation Frequency (Radians/Second) versus Mean Time (Second)[Runs 1(A), 1(B), 1(C)].

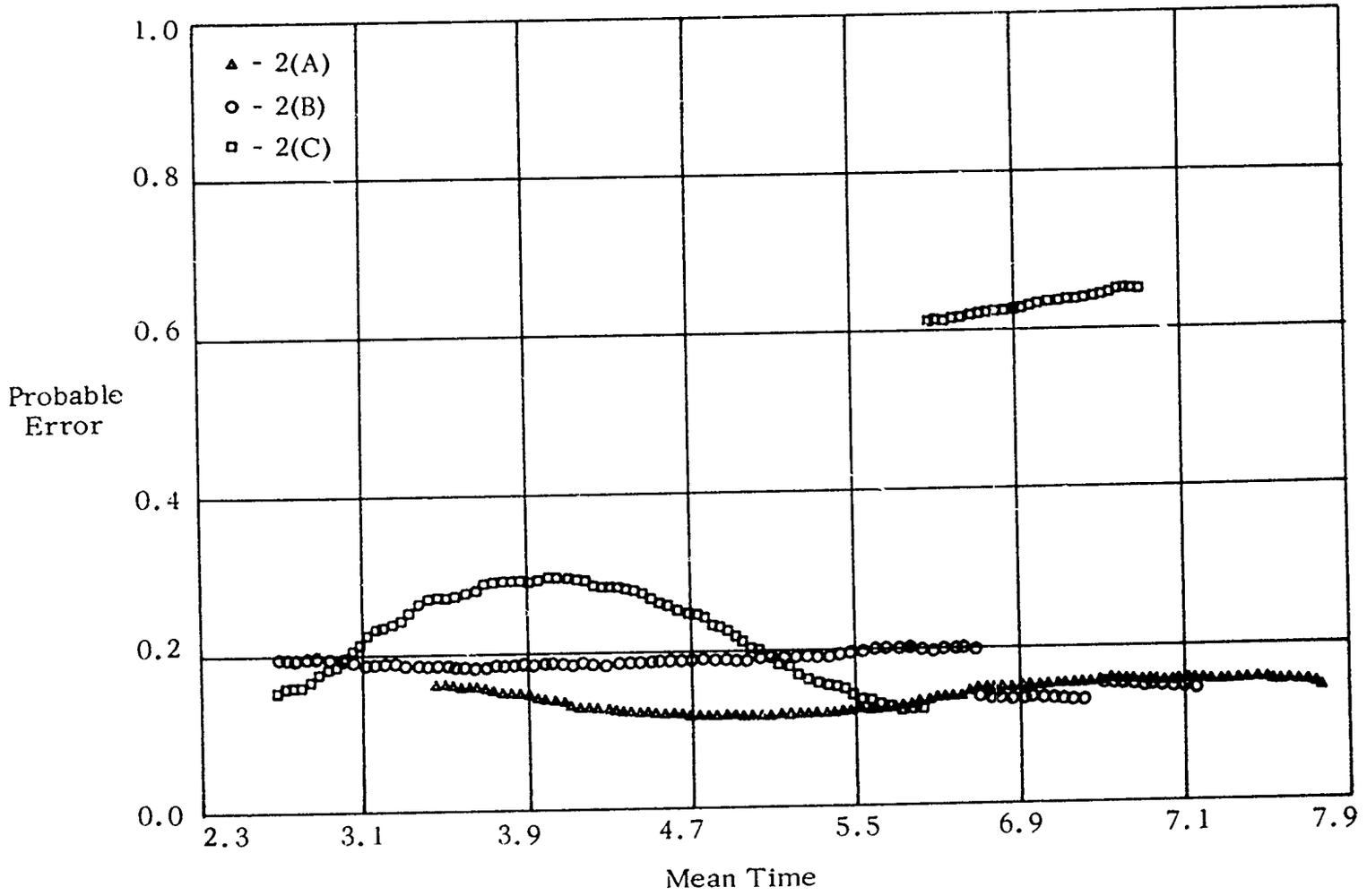

Figure 19. Probable Error-of-Fit (Degrees) versus Mean Time (Seconds) [Runs 2(A), 2(B), 2(C)] .

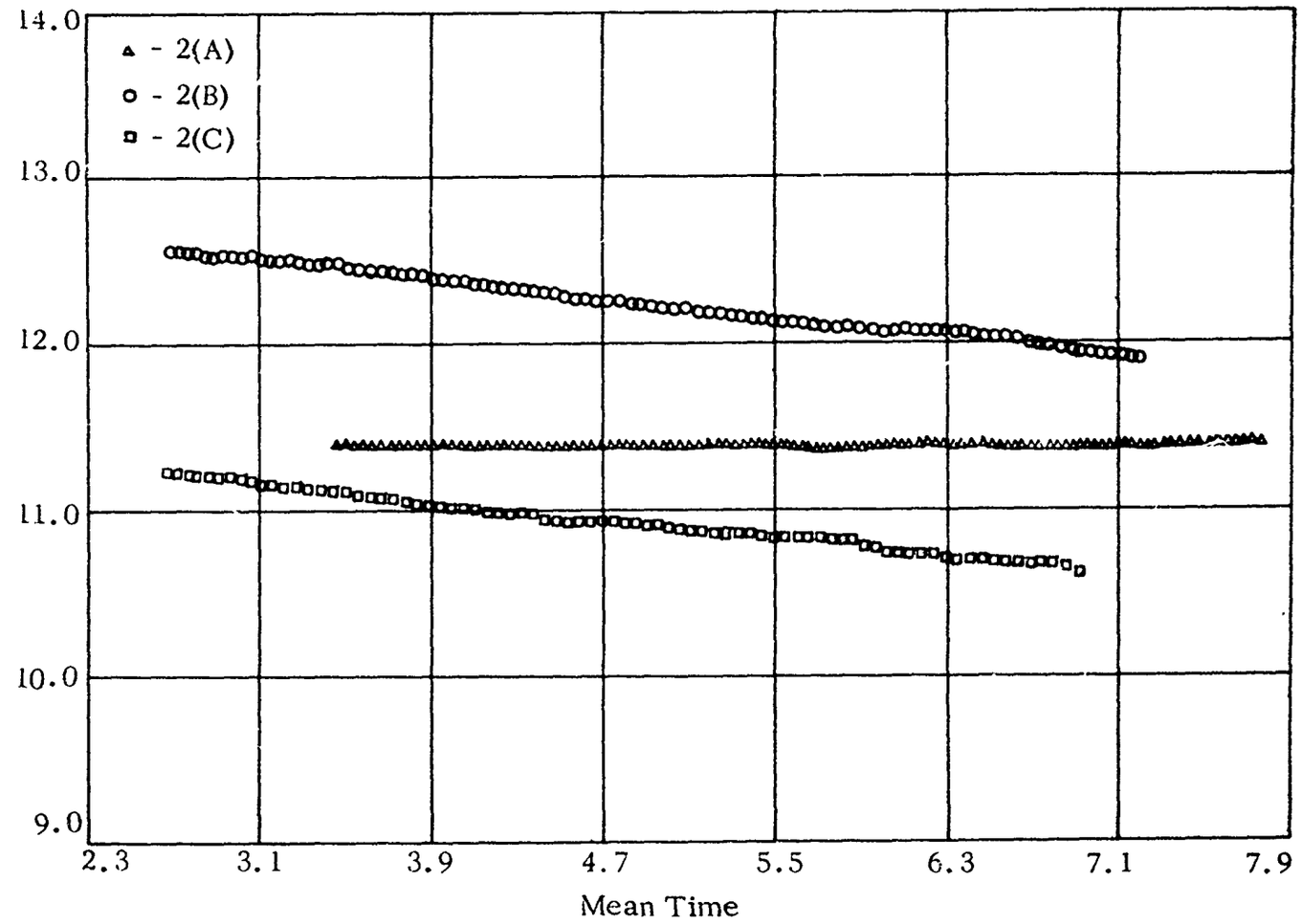

Figure 20. Precession Arm (Degrees) versus Mean Time (Seconds) [Runs 2(A), 2(B), 2(C)] .

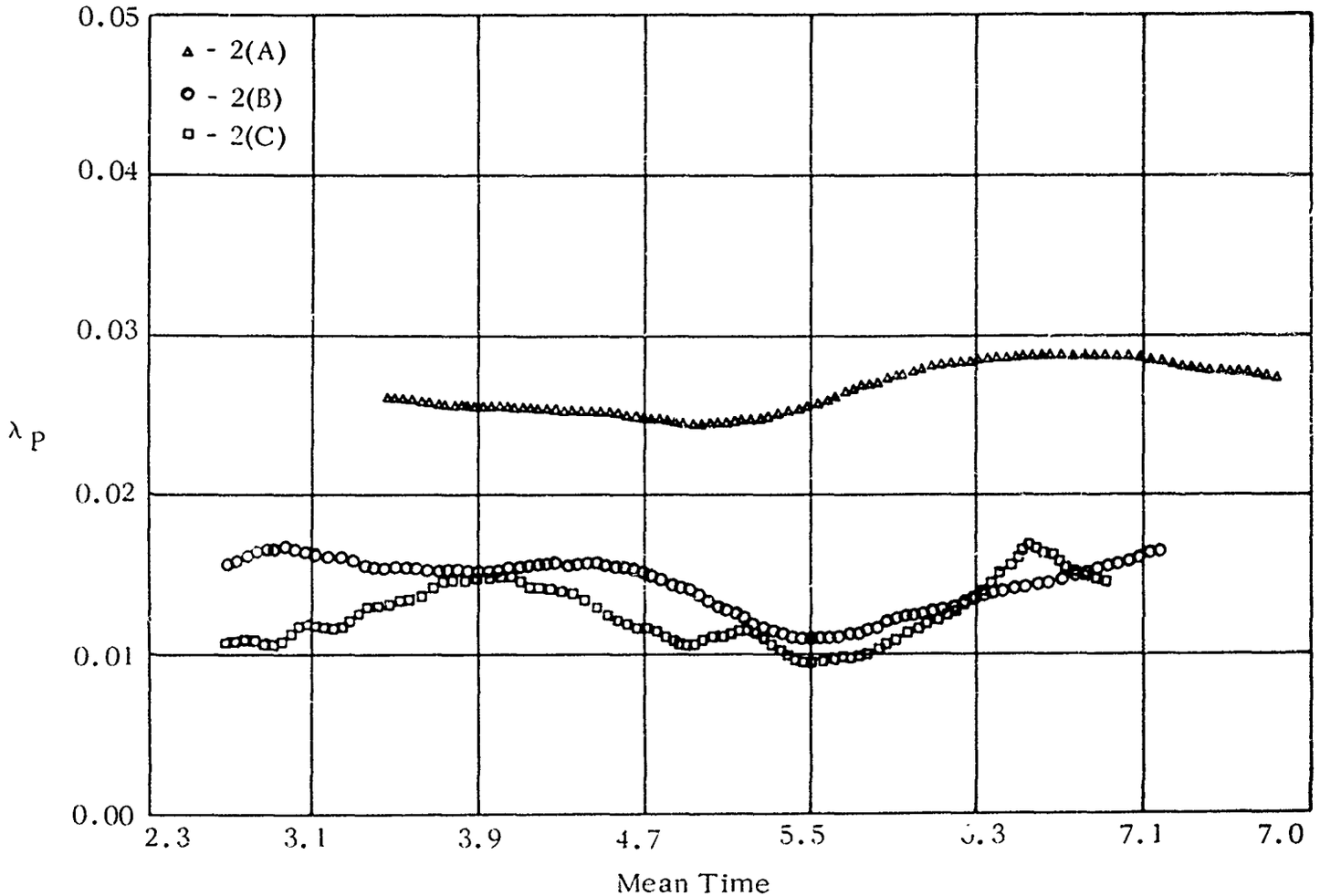

Figure 21. Dynamic Precession Damping Factor (One/Second) versus Mean Time (Second) [Runs 2(A), 2(B), 2(C)].

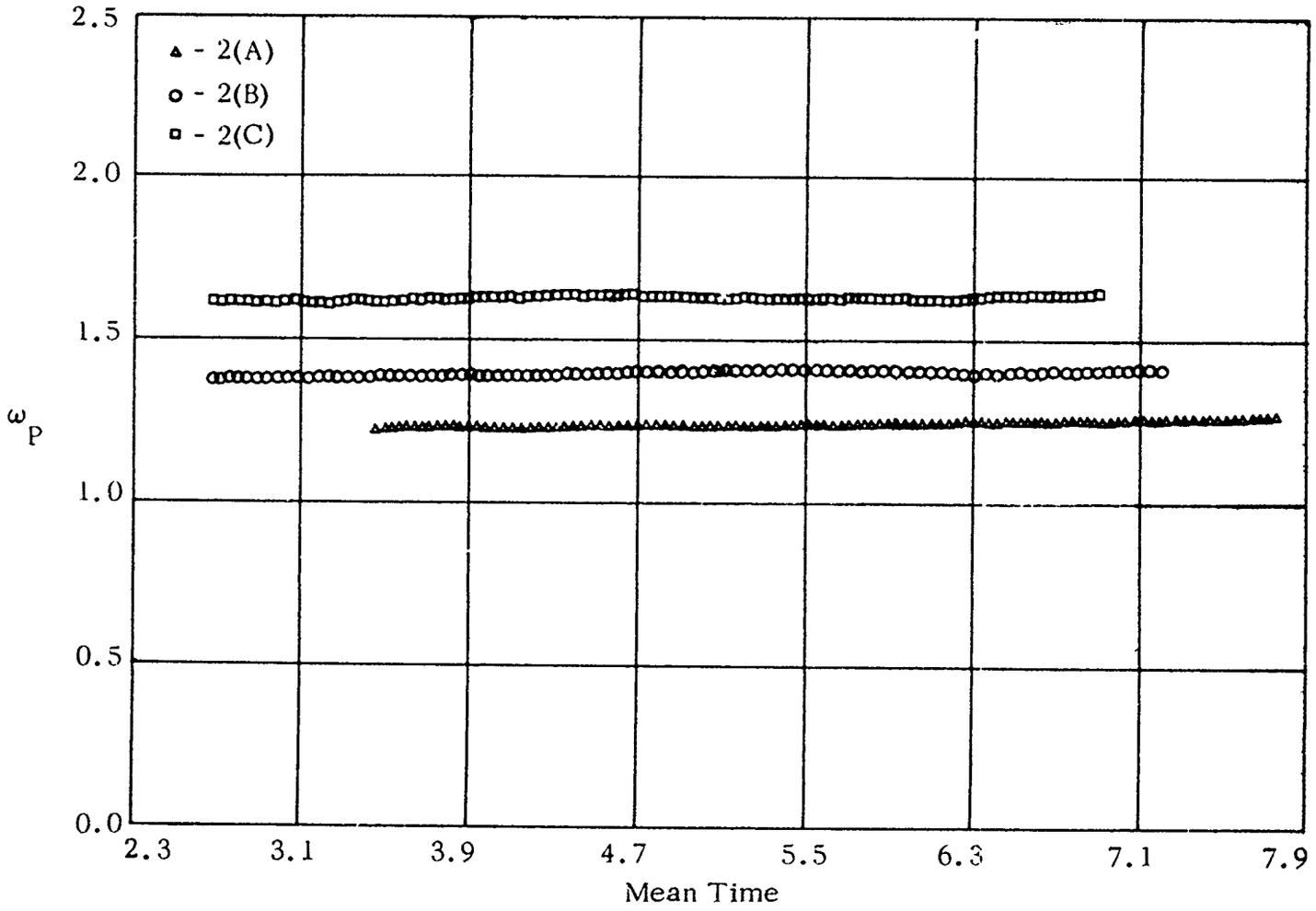

Figure 22. Precession Frequency (Radians/Second) versus Mean Time (Seconds) [Runs 2(A), 2(B), 2(C)].

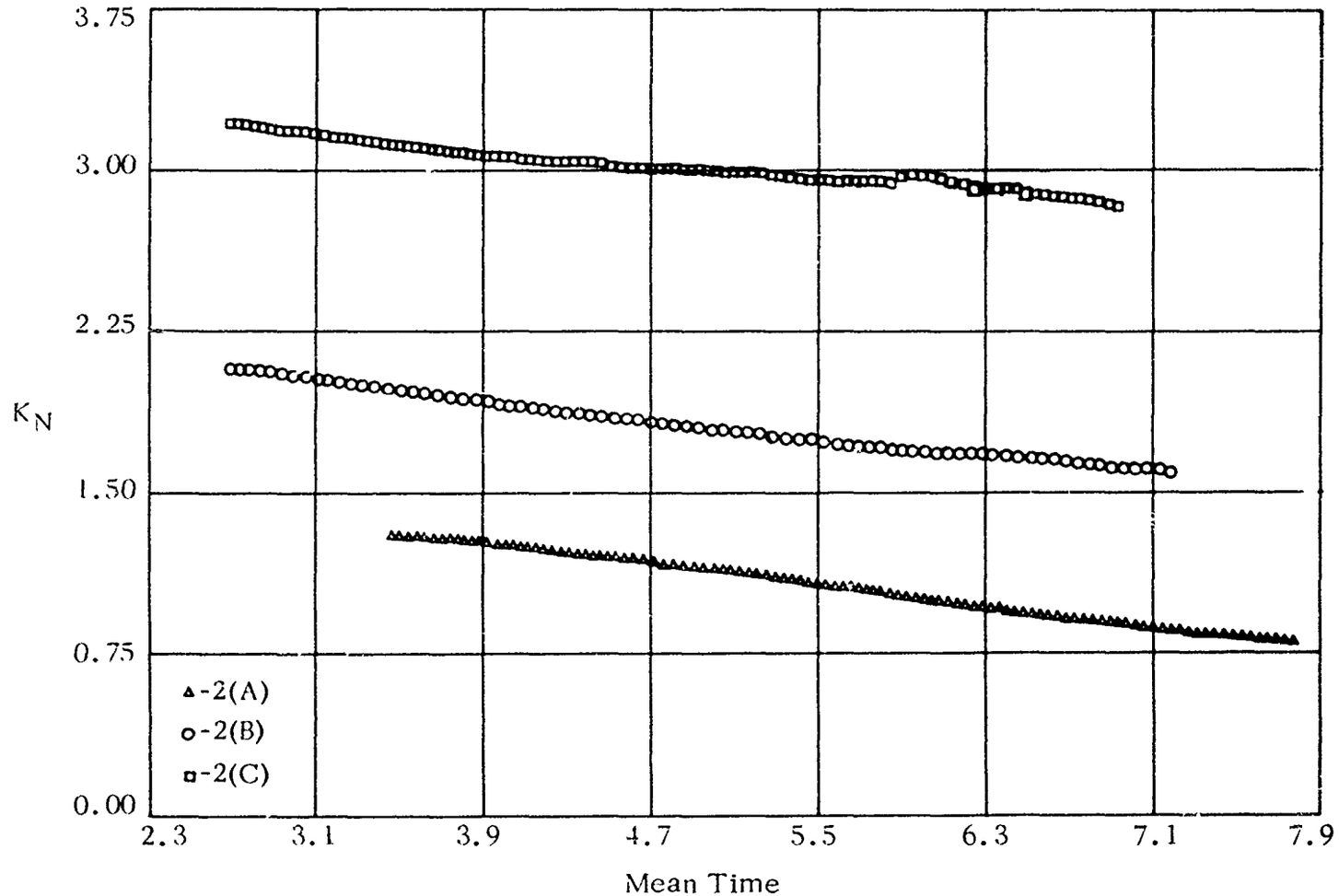

Figure 23. Nutation Arm (Degree) versus Mean Time (Seconds)[Runs 2(A), 2(B), 2(C)] .

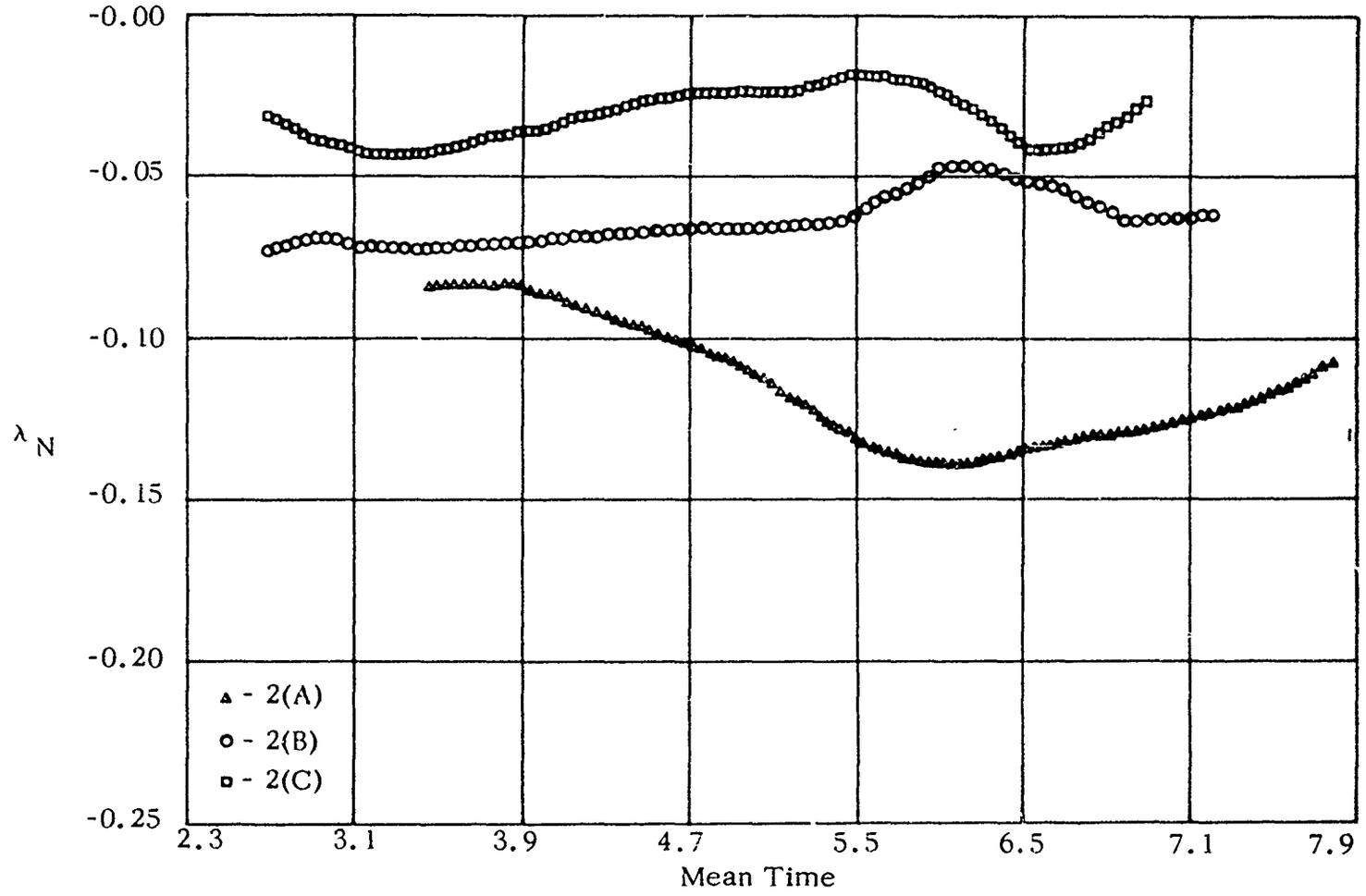

Figure 24. Dynamic Nutation Damping Factor (One/Second) versus Mean Time (Seconds) [Runs 2(A), 2(B), 2(C)].

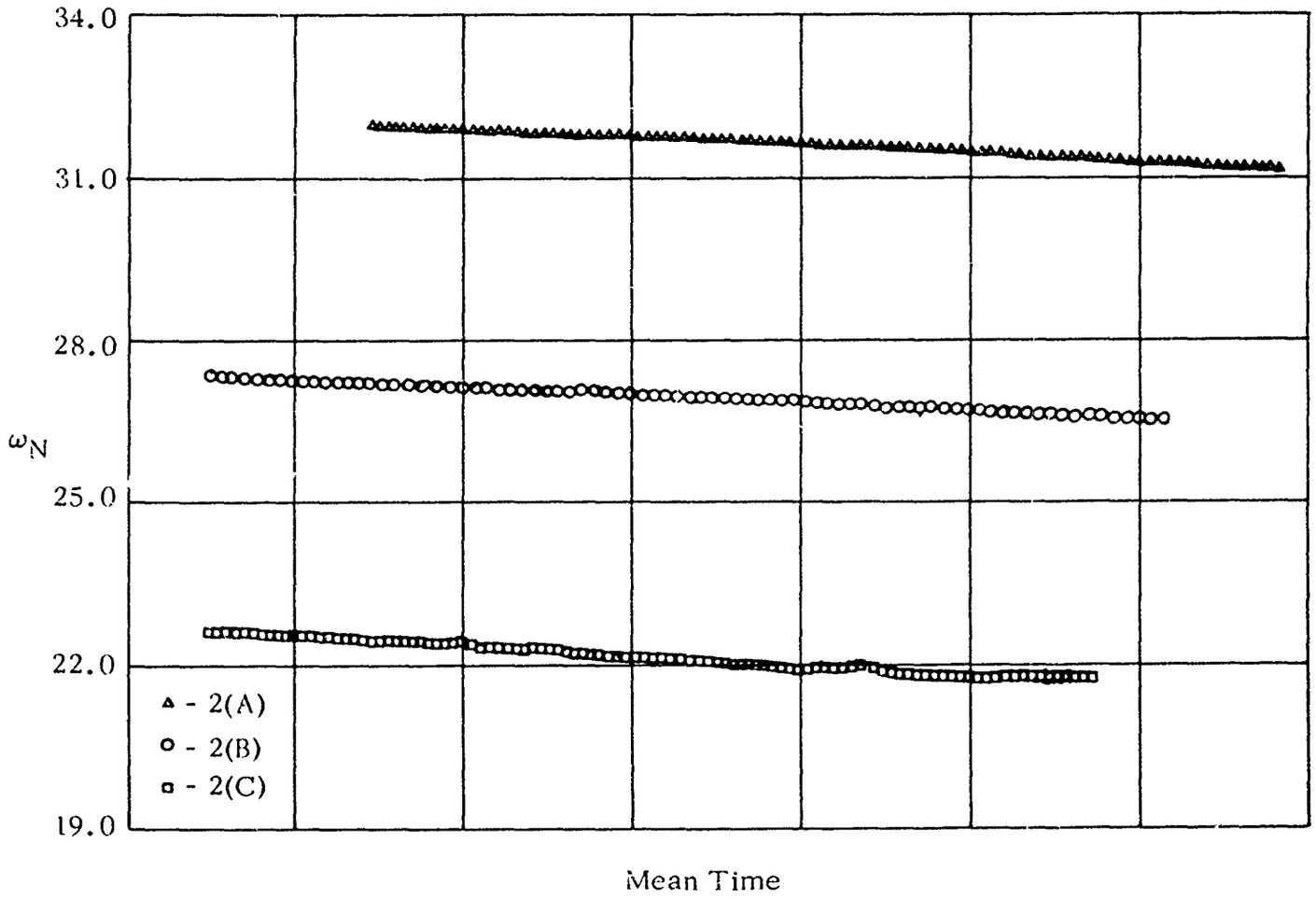

Figure 25. Nutation Frequency (Radians/Second) versus Mean Time (Seconds) [Runs 2(A), 2(B), 2(C)].

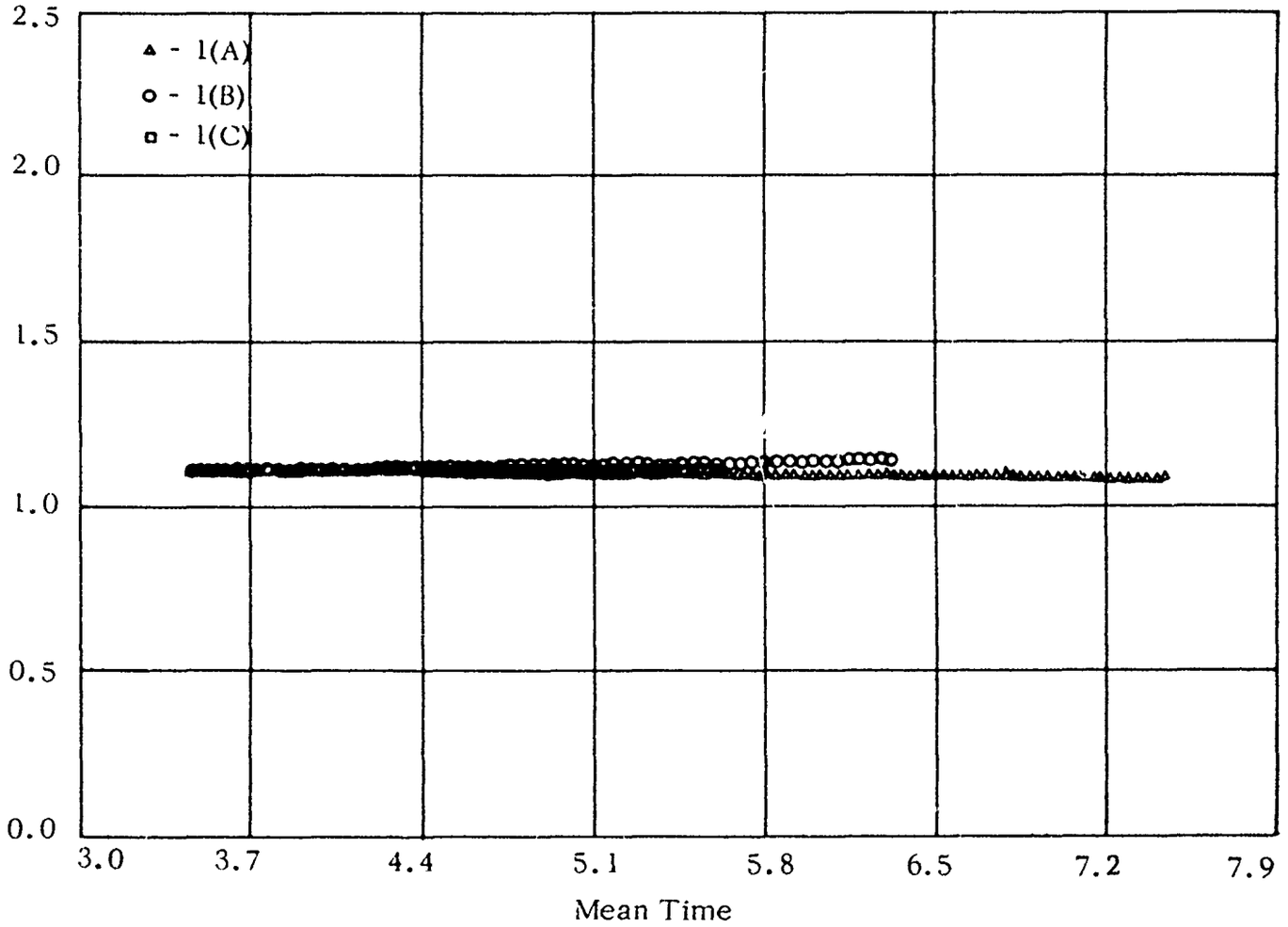

Figure 26. Restoring Moment Coefficient (One/Radian) versus Mean Time (Second) [Runs 1(A), 1(B), 1(C)].

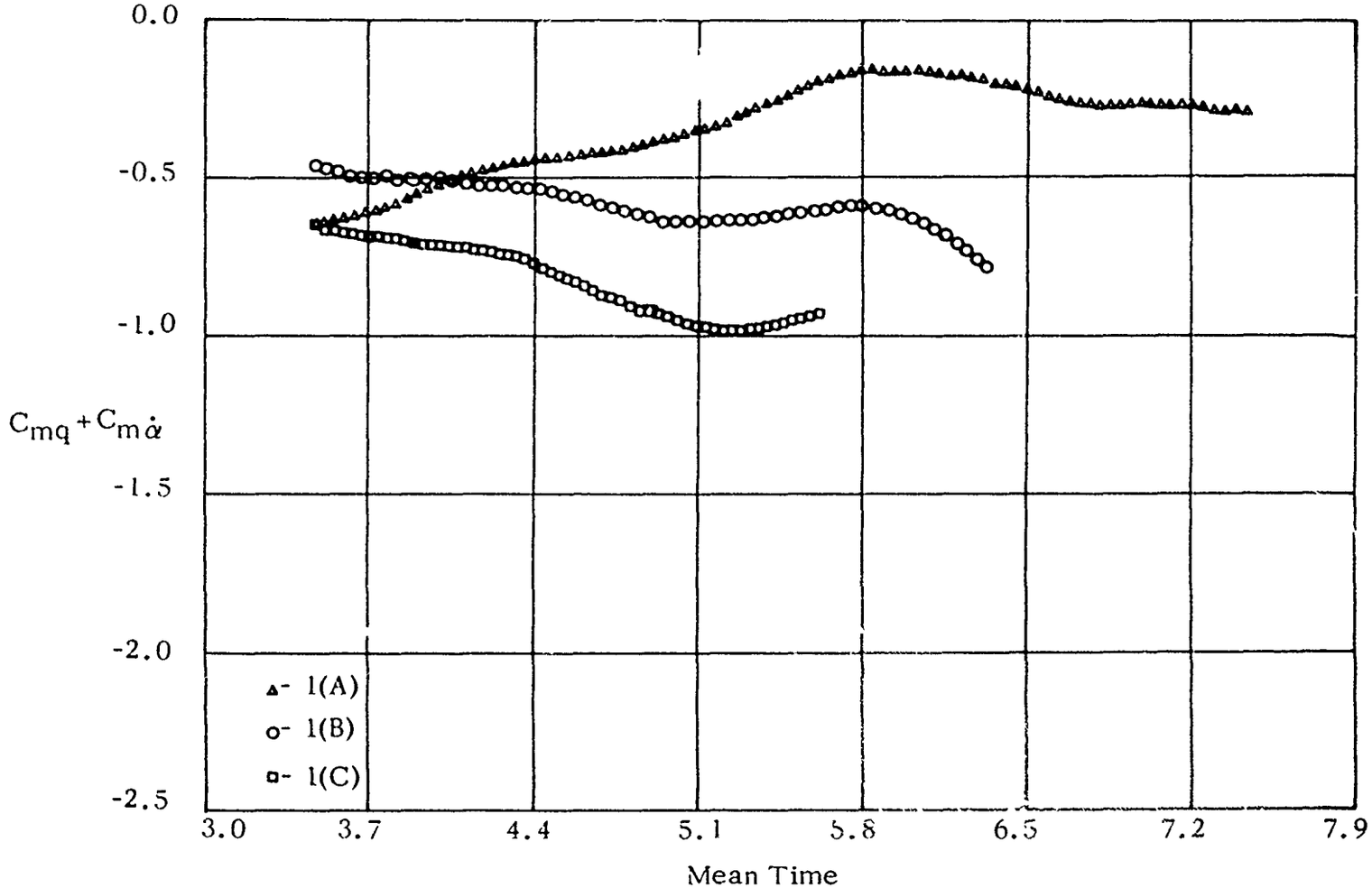

Figure 27. Damping Moment Coefficient (One/Radian) versus Mean Time (Second) [Runs 1(A), 1(B), 1(C)].

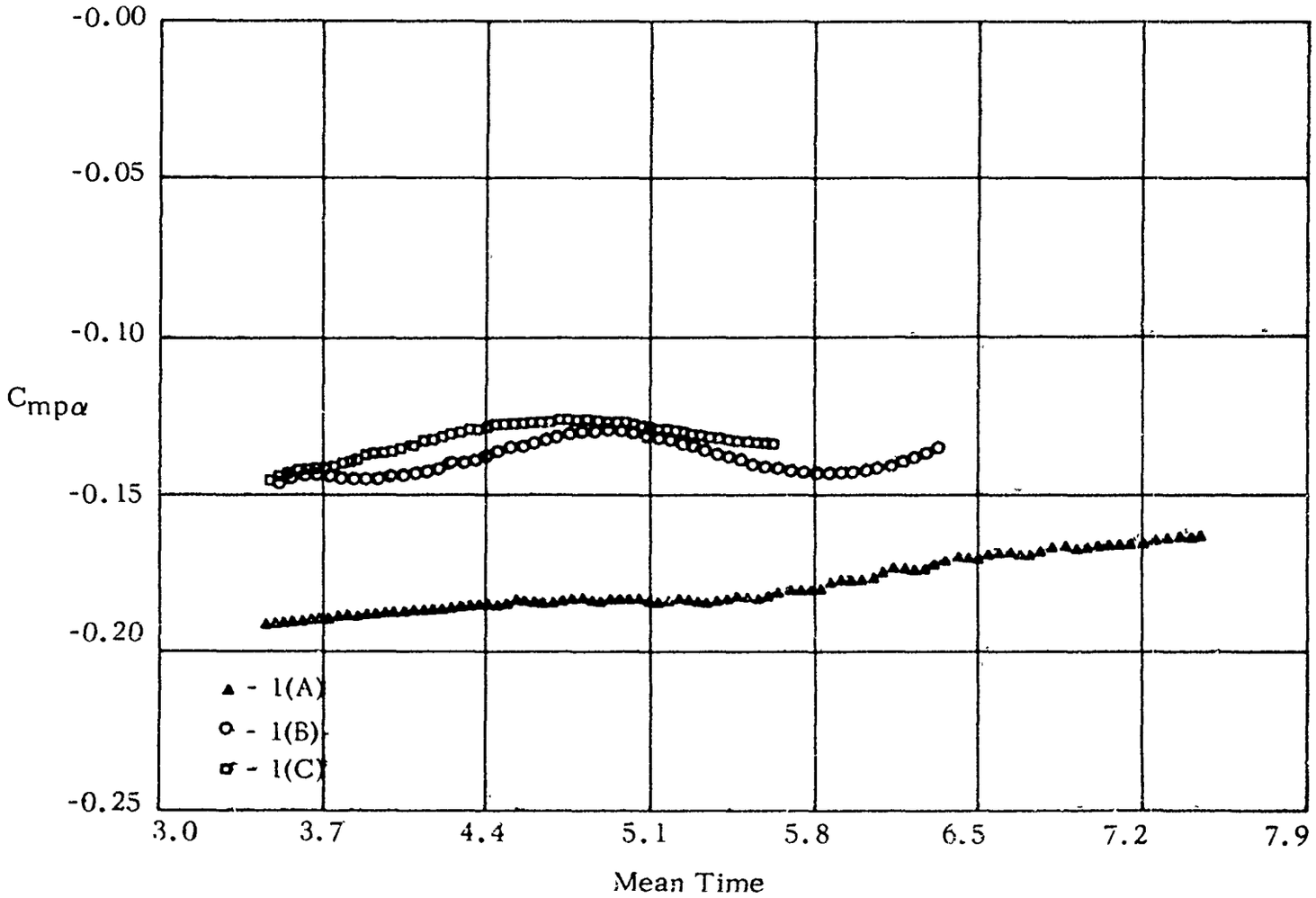

Figure 28. Magnus Moment Coefficient (One/Radian^2) versus Mean Time (Second) [Runs 1(A), 1(B), 1(C)] .

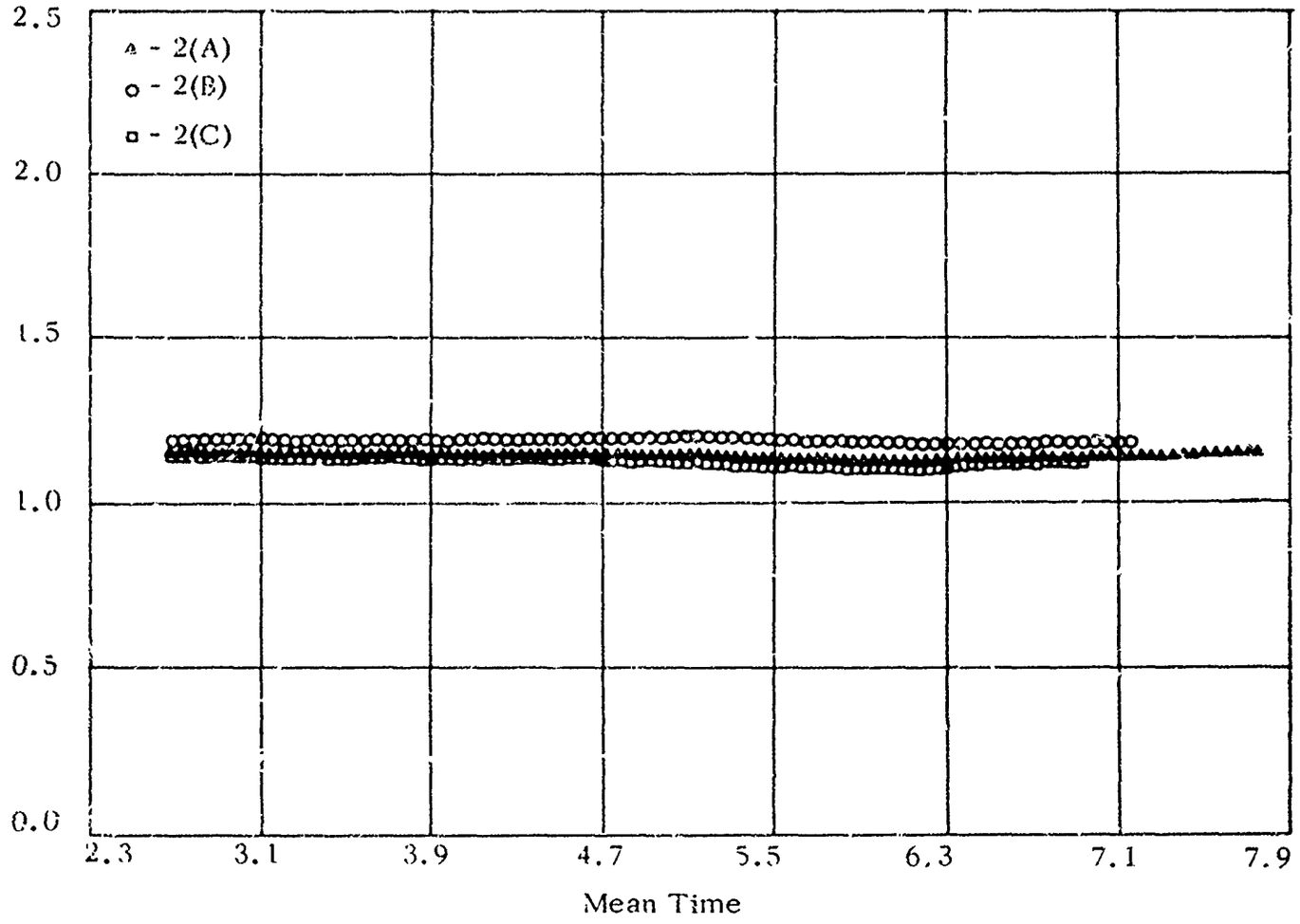

Figure 29. Restoring Moment Coefficient (One/Radian) versus Mean Time (Second) [Runs 2(A), 2(B), 2(C)] .

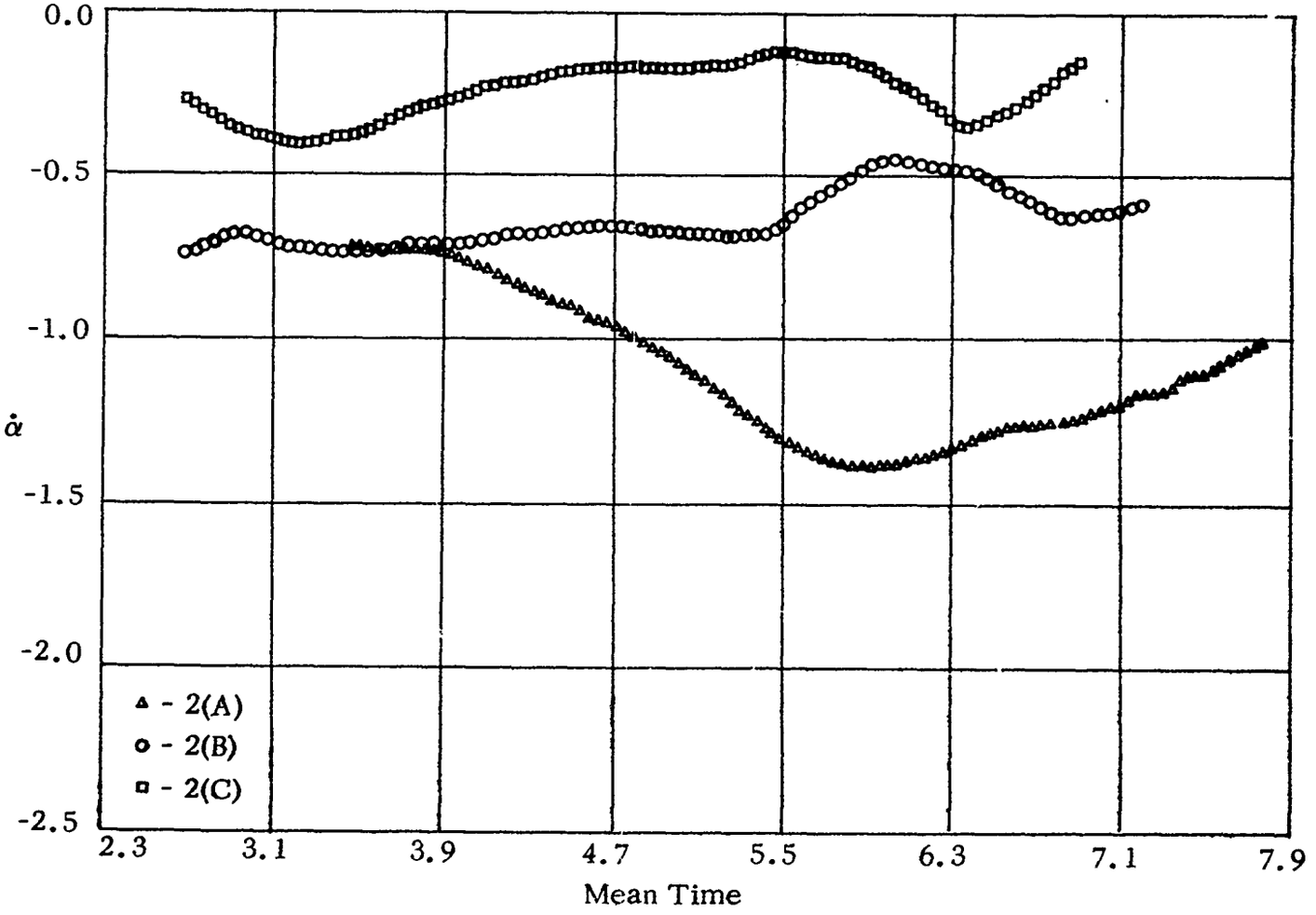

Figure 30. Damping Moment Coefficient (One/Radian) versus Mean Time (Second) [Runs 2(A), 2(B), 2(C)] .

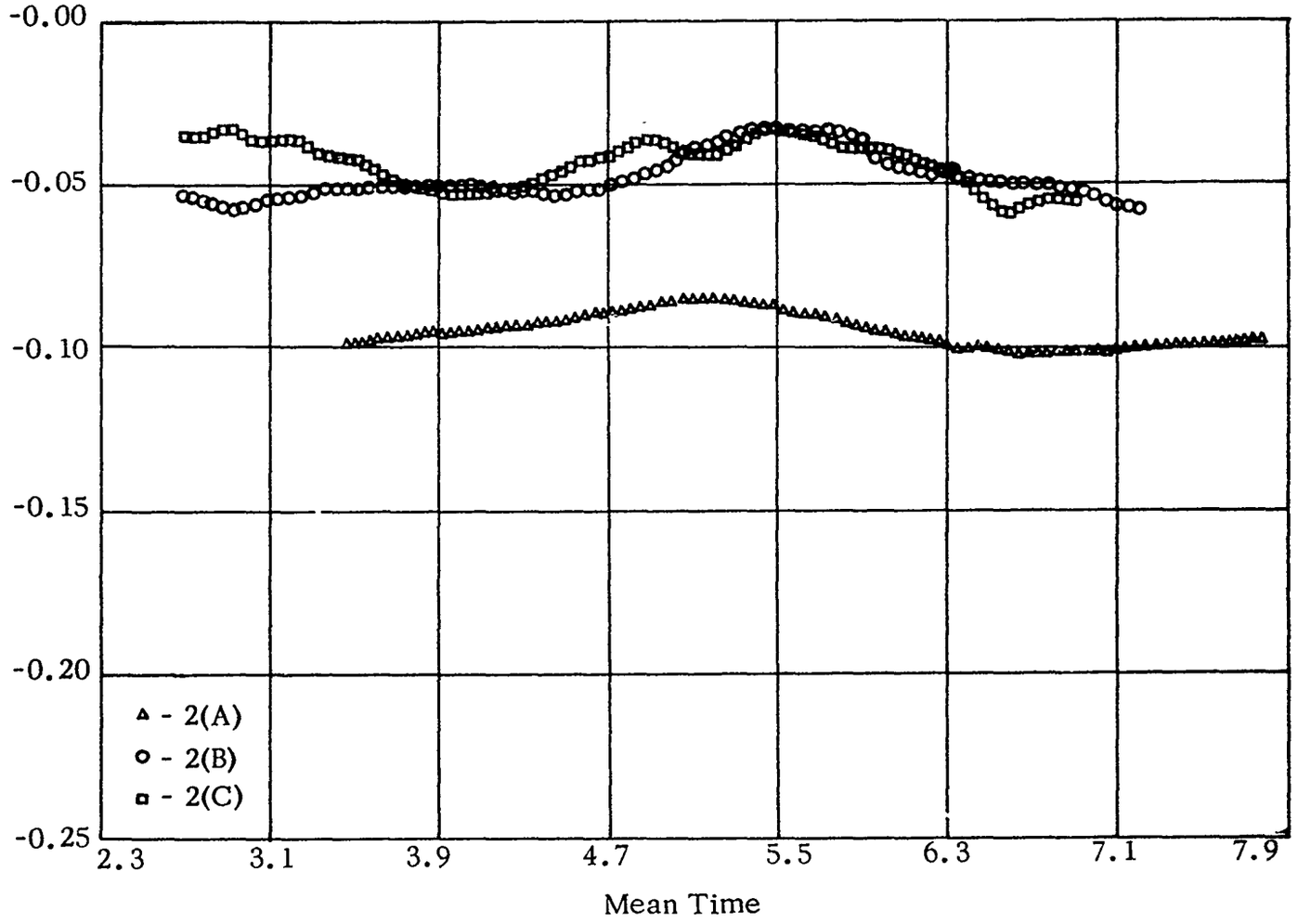

Figure 31. Magnus Moment Coefficient (One/Radian^2) versus Mean Time (Second) [Runs 2(A), 2(B), 2(C)] .

Of primary importance is the near constant value of the restoring moment coefficient for any particular run. One of two possible conclusions can be drawn: either the angle of attack range is small so that the nonlinear effect is not seen, or, the nonlinearity itself is small enough to be neglected. In either case, the constant $C_{m\alpha}$ allows the roll rate to be calculated as a function of time from the nutation and precession frequencies and the moments of inertia (Equation 5). This parameter is needed for the nonlinear analysis.

The linear Magnus moment coefficients, $C_{m_{p\alpha}}$, are all less than zero. From the Linear Theory, a negative $C_{m_{p\alpha}}$ will have a stabilizing effect on the nutation arm and a destabilizing effect on the precession arm.

The damping moment coefficients, $C_{mq} + C_{m\dot{\alpha}}$, are all also less than zero. The effects of a negative sign are to stabilize the nutation arm and slightly destabilize the precession arm. Combining the effects of the damping moment coefficients and Magnus moment coefficients predict a highly stable nutation arm and an unstable precession arm. The test results support this.

$C_{mp\alpha}$ and $C_{mq} + C_{m\dot{\alpha}}$ were not as constant over a given run as $C_{m\alpha}$. Indications are that these two coefficients are much more nonlinear than $C_{m\alpha}$.

Nonlinear coefficients were determined, using the procedure outlined in Section III. All of the stability parameters from the six test runs were evaluated together to include the entire angle of attack range covered by the tests, thereby giving a better representation of the nonlinear characteristics of the coefficients. The nonlinear coefficients are plotted versus angle of attack in Figures 32 through 34 and listed in Table III. The angle of attack range and corresponding range of linear coefficients for each run are superimposed on these plots to show how well the linear and nonlinear results compare.

The nonlinear coefficient results are in good agreement with the qualitative observations. Both the damping and restoring moment coefficients exhibited hard spring characteristics while the Magnus moment coefficient was a soft spring nonlinearity.

As expected, the nonlinear term in $C_{m\alpha}$ was small. This verifies the prior assumption which allowed the roll rate to be calculated. Virtually no effect was felt by the nonlinearity over the angle of attack range tested.

$C_{mq} + C_{m\dot{\alpha}}$ was quite nonlinear and, being less than zero, contributed greatly to the stability of the nutation arm and to the instability of the precession arm. These effects increase with angle of attack.

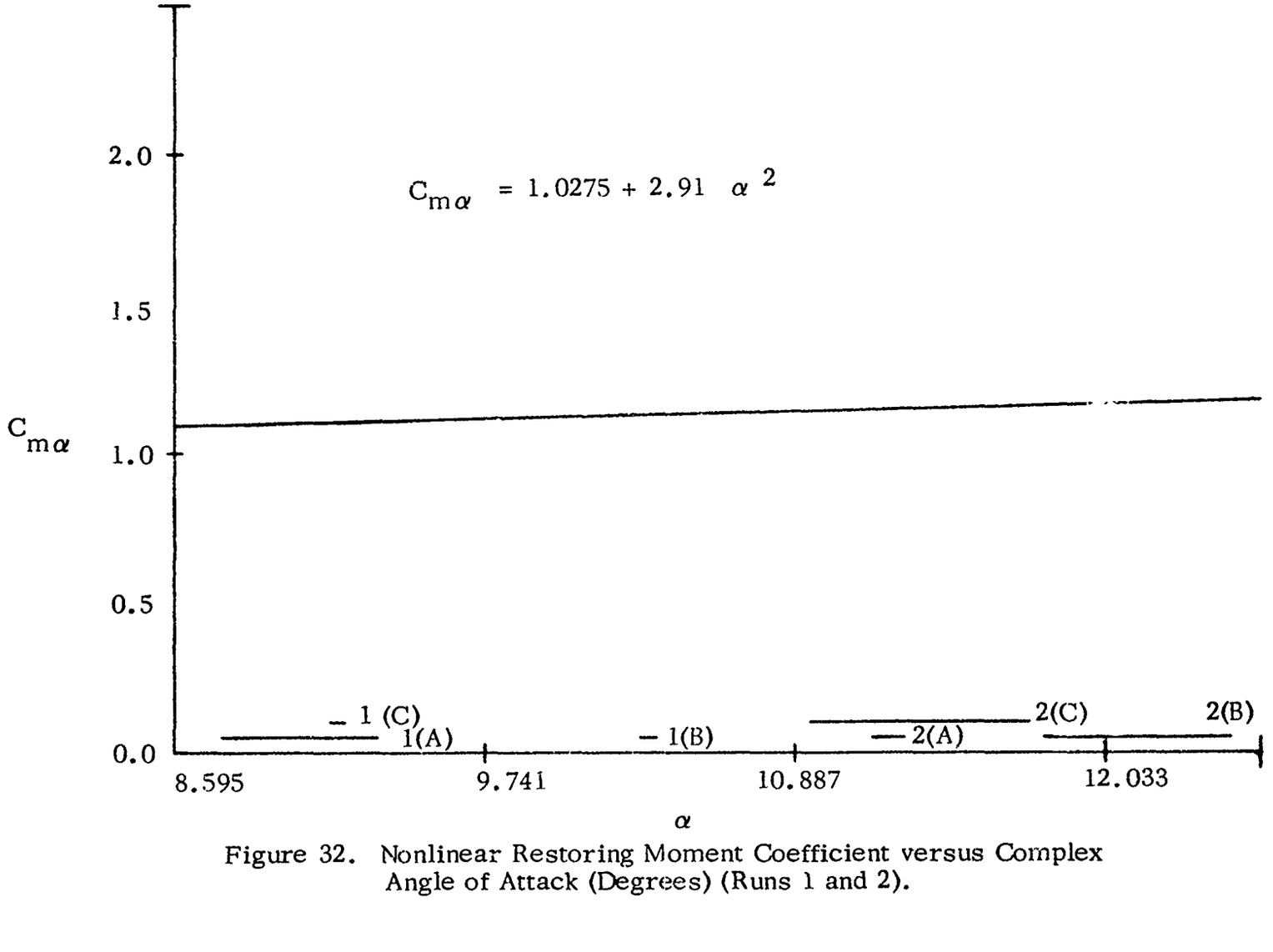

Figure 32. Nonlinear Restoring Moment Coefficient versus Complex Angle of Attack (Degrees) (Runs 1 and 2).

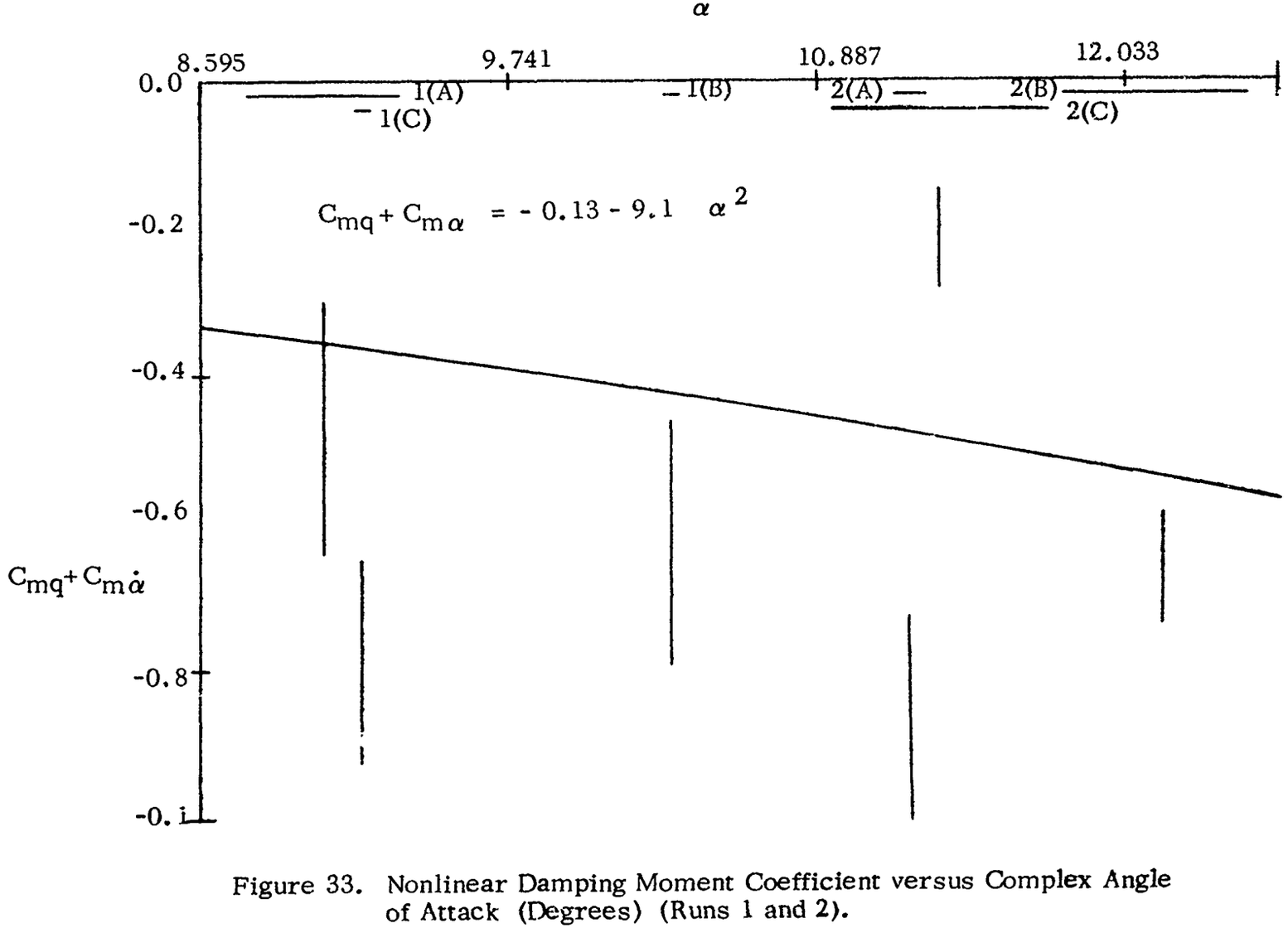

Figure 33. Nonlinear Damping Moment Coefficient versus Complex Angle of Attack (Degrees) (Runs 1 and 2).

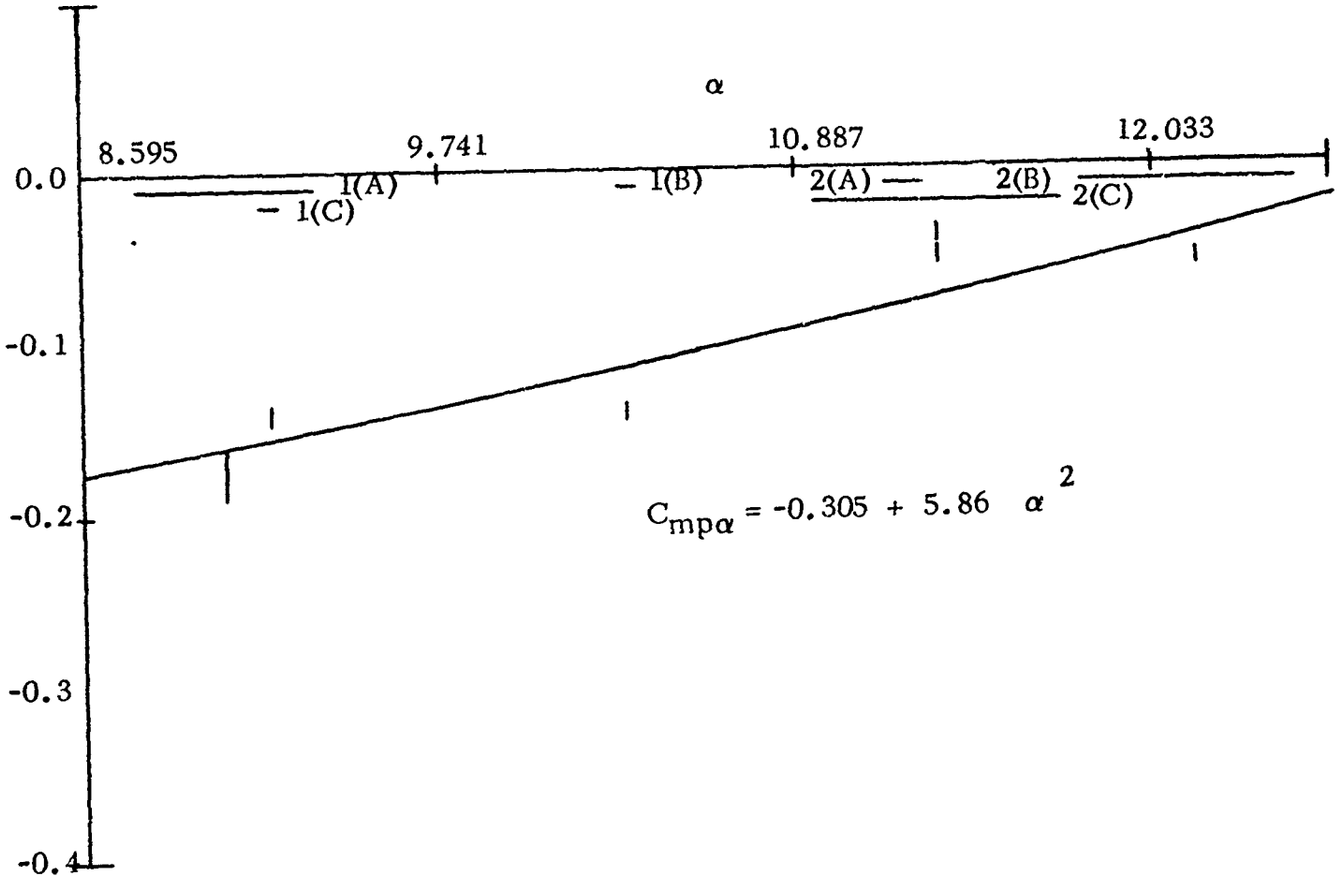

Figure 34. Nonlinear Magnus Moment Coefficient versus Complex Angle of Attack (Degree) (Runs 1 and 2).

On the other hand, the nonlinear Magnus moment coefficient has an opposite effect. As the angle of attack increases, the value of the coefficient will become positive, having a stabilizing effect on the precession arm and a destabilizing effect on the nutation arm. These effects were observed in the qualitative tests.

Due to the nonlinear effects of $C_{mp\alpha}$ and $C_{mq} + C_{m\dot{\alpha}}$, it is possible for the model to possess dynamic stability at higher angles of attack. However, a critical balance must be attained between the two moments along with a suitable roll rate. The roll rate would have to be high to reduce the effects of $C_{mq} + C_{m\dot{\alpha}}$ on the precession arm.

7.5-Degree Boattail Analysis

Qualitative tests conducted on the 7.5-degree boattail model disclosed that the aerodynamic characteristics for that model were quite different from those of the zero-degree boattail model.

For comparison sake, the initial roll rate was about 900 rpm. Low angle excitation of the model resulted in a motion comprised of a small precession arm of decreasing amplitude and a small nutation arm of increasing amplitude.

The nutation arm undamped rapidly to a point where the motion was so violent that the model would separate itself from the sting. In some cases, the nutation amplitude would build up from near zero to a value appearing to be twice as large as the precession amplitude (approximately 2.5 degrees). In some cases this would occur before the completion of two precession cycles.

A large angle disturbance resulted in stability in both the nutation and precession modes. A precession amplitude of approximately eleven degrees damped at about the same rate as at a low angle disturbance. The nutation mode was extremely stable. It was impossible to create a nutation disturbance that would last for any more than one-third of a precession cycle.

If the model was disturbed at a high angle, the nutation mode would damp quickly along with a moderately damped precession mode. The total motion would then finally reach the small angle range where the nutation amplitude would begin to increase wildly. It was then concluded from the Linear Theory that for the angle of attack range observed, the nutation instability stemmed from an improper balance between a positive damping moment and a positive Magnus moment.

Quantitative tests dealt only with the small angle of attack range only because a suitable nutation mode could not be attained at the higher angles.

TABLE III. NONLINEAR COEFFICIENTS FOR ZERO-DEGREE AND 7.5-DEGREE BOATTAIL MODELS.

	$C_{m\alpha_o}$(1/Rad)	$C_{m\alpha_2}$(1/Rad^3)	C_{mq_o}(1/Rad)	C_{mq_2}(1/Rad^3)	$C_{mp\alpha_o}$(1/Rad^3)	$C_{mp\alpha_2}$(1/Rad^4)
Zero-degree Boattail	1.0275	2.910	-0.130	-9.100	-0.3051	5.860
7.5-degree Boattail	1.096	2.500	1.918	-95.010	0.050	32.500

A larger nutation disturbance may have been possible at a slower roll rate, but the need for like conditions to compare the two models prevented study in this area. Four test runs [3(A), 3(B), 3(C) and 3(D)] were conducted on the 7.5-degree boattail model, and the stability parameters were obtained by analyzing the data with the "Wobble" program. The stability parameters are plotted as a function of time in Figures 35 through 41. The dynamic damping factors were corrected for varying frequencies due to the decaying roll rate and then for friction as with the zero-degree boattail model before plotting.

Run 3(C) was the only run in which the friction damping factor was greater in magnitude than the dynamic precession damping factor. This condition only persisted through about half the duration of the test. The total motion was smaller for run 3(B) than for the other runs and may have been a contributing factor.

Linear aerodynamic coefficients were calculated for the 7.5-degree boattail model from the stability parameters obtained from the "Wobble" program. The coefficients are plotted in Figures 42 through 44 and the average values are listed in Table II.

As with the zero-degree boattail model, $C_{m\alpha}$ remained fairly constant with time for a given run. Therefore, Equation (5) could again be used to compute the roll rate for the nonlinear analysis.

The average Magnus moment coefficients are all greater than zero. From the Linear Theory, a positive Magnus moment will have a destabilizing effect on the nutation arm and a stabilizing effect on the precession arm.

The damping moment coefficients are also greater than zero. Positive values will destabilize the nutation arm and stabilize the precession arm. Added together, the effects of $C_{mp\alpha}$ and $C_{mq} + C_{m\dot{\alpha}}$ predict a highly unstable nutation arm and a stable precession arm.

From the large angle qualitative tests, the possibility of highly nonlinear Magnus and damping moment coefficients exists.

Nonlinear coefficients were obtained by evaluating together the stability parameters from all the test runs; however, the angle-of-attack range was limited so a possibility of error exists. The nonlinear coefficients are plotted versus angle of attack in Figures 45 through 47 and are listed in Table III. A comparison between the nonlinear and linear results is also shown on the figures.

The nonlinear results support the qualitative observations; the restoring and Magnus moment possessed hard spring characteristics while the damping moment was of the soft spring type.

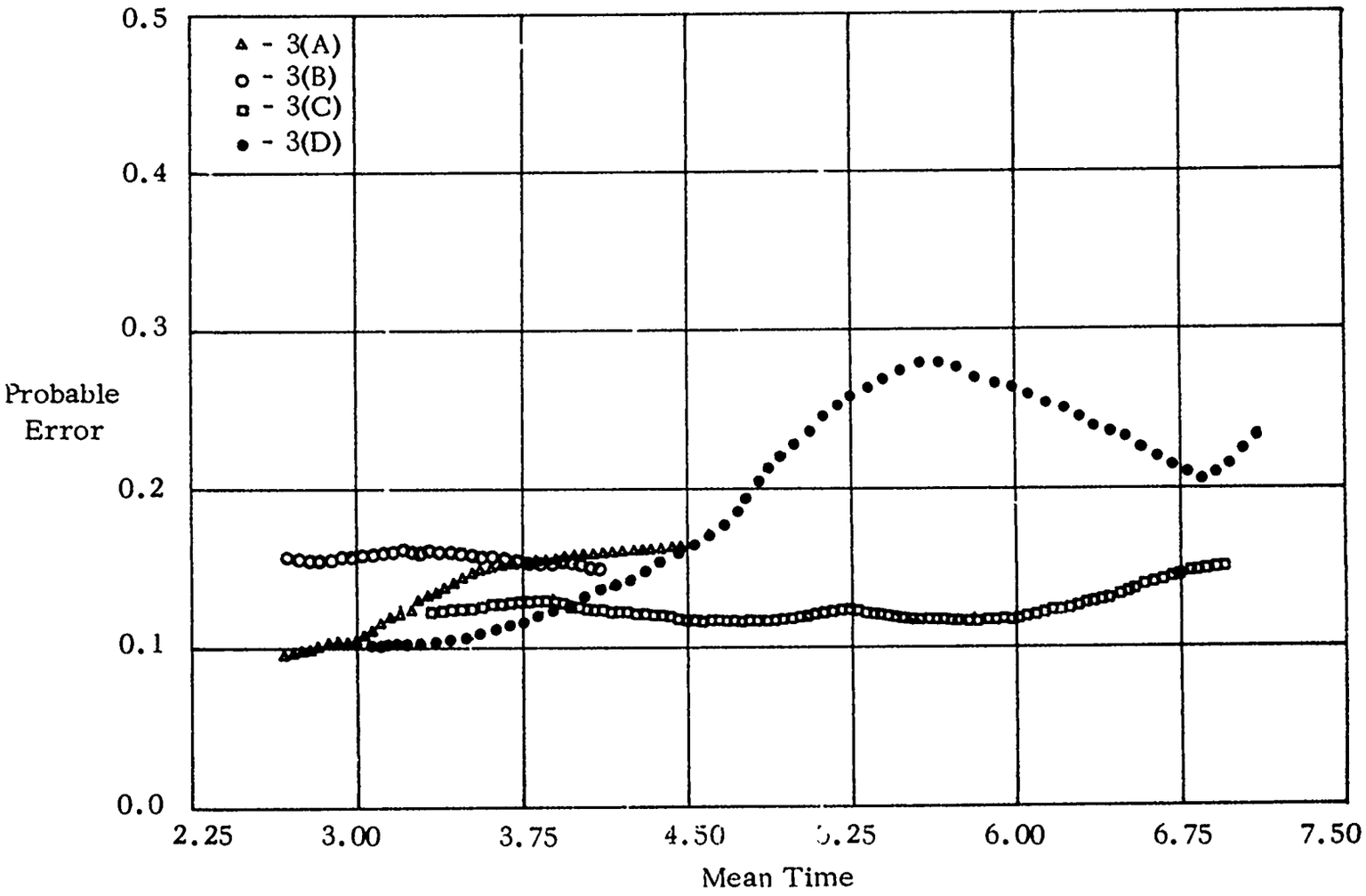

Figure 35. Probable Error-of-Fit (Degree) versus Mean Time (Seconds)[Runs 3(A), 3(B), 3(C), 3(D)] .

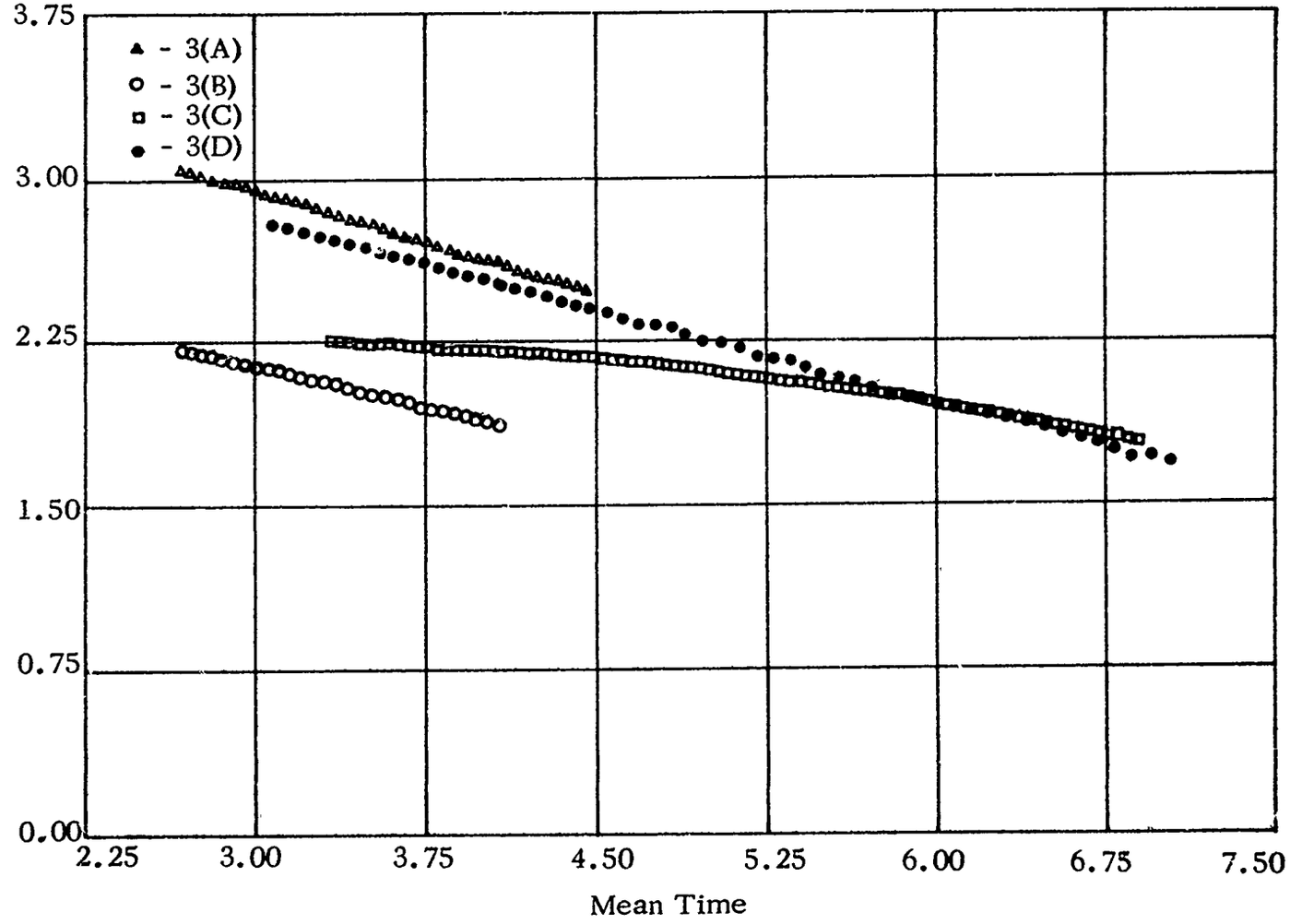

Figure 36. Precession Arm (Degrees) versus Mean Time (Second) [Runs 3(A), 3(B), 3(C), 3(D)].

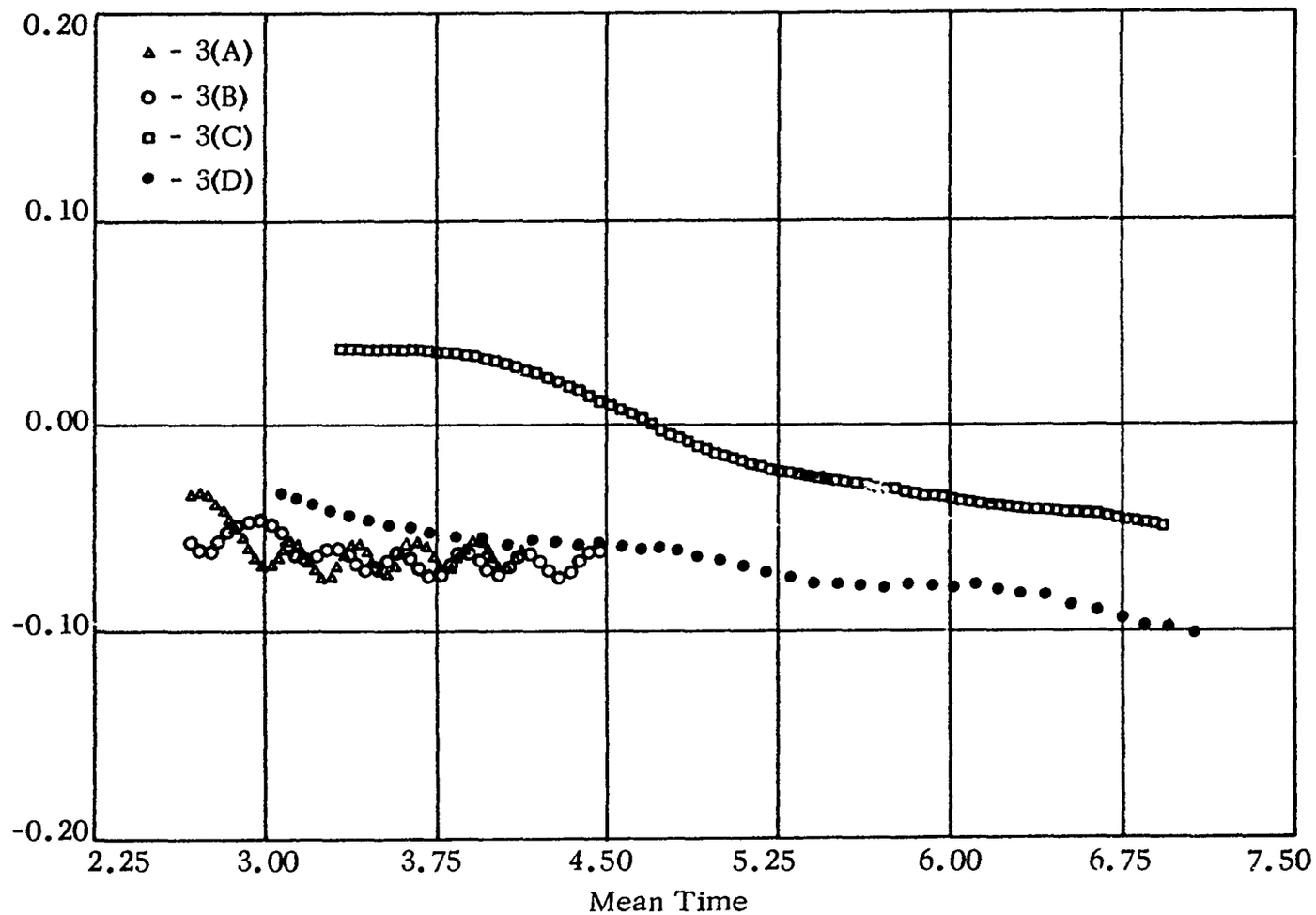

Figure 37. Dynamic Precession Damping Factor (One/Second) versus Mean Time (Second) [Runs 3(A), 3(B), 3(C), 3(D)] .

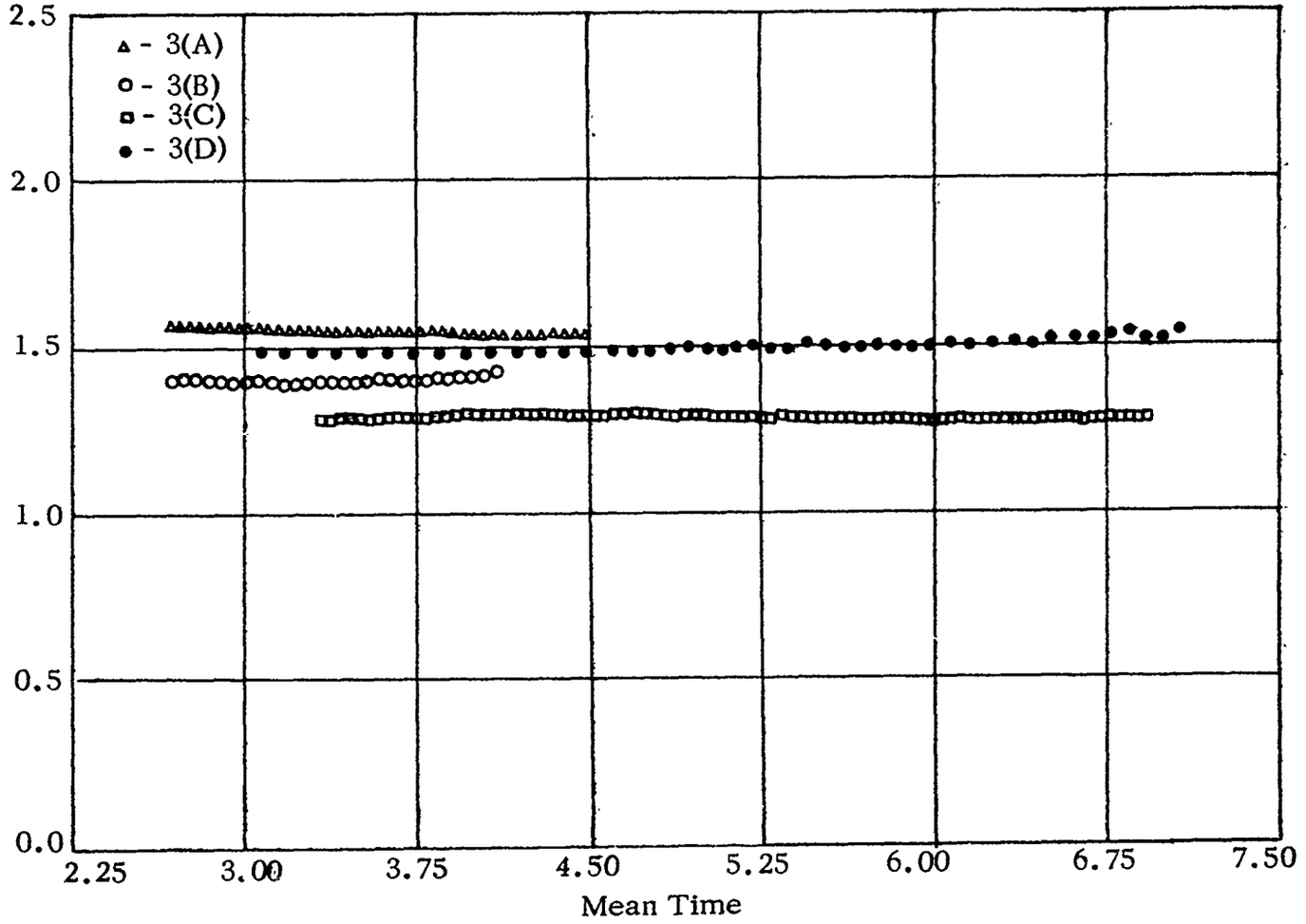

Figure 38. Precession Frequency (Radians/Second) versus Mean Time (Second) [Runs 3(A), 3(B), 3(C), 3(D)].

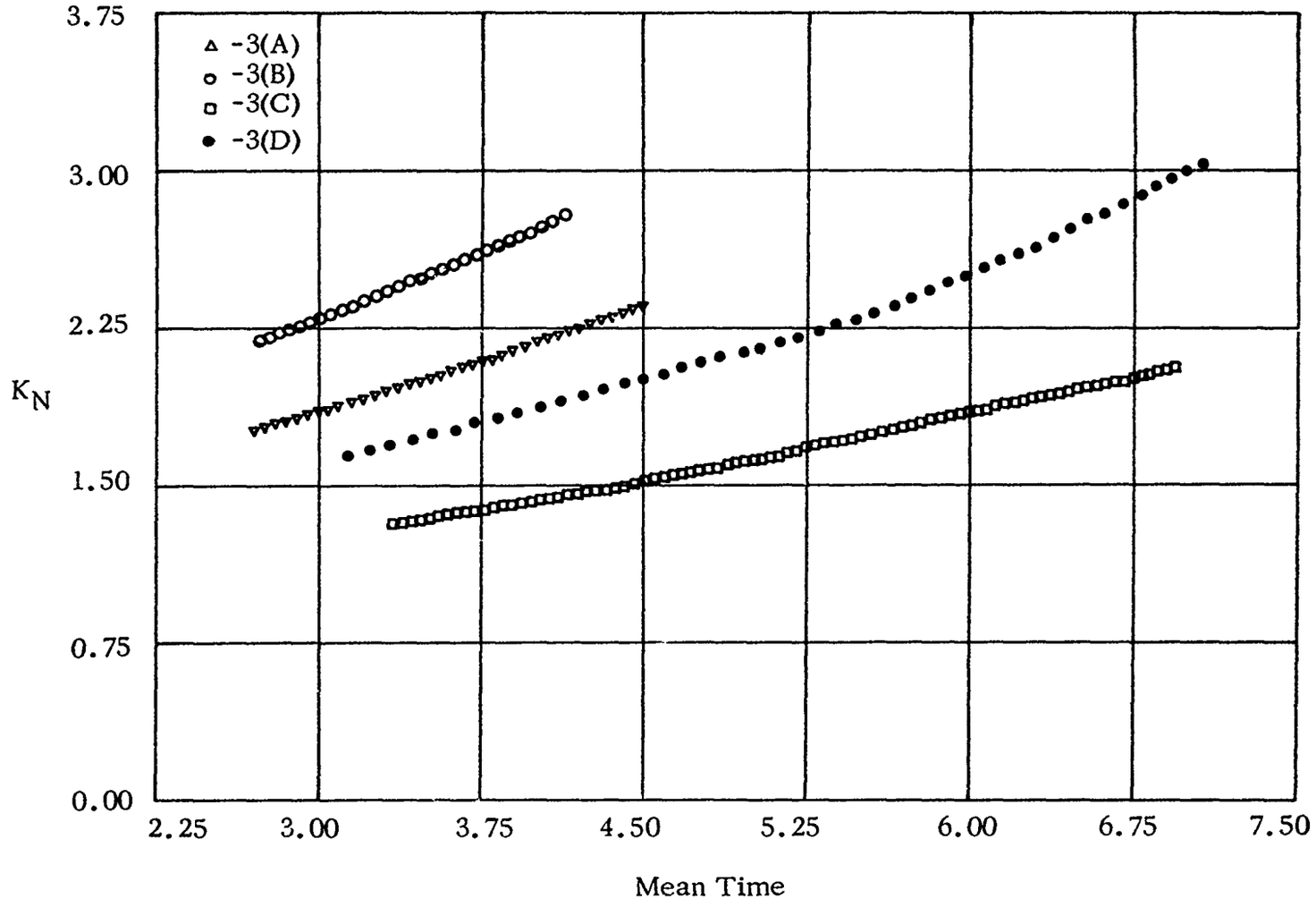

Figure 39. Nutation Arm (Degree) versus Mean Time (Second)[Runs 3(A), 3(B), 3(C), 3(D)].

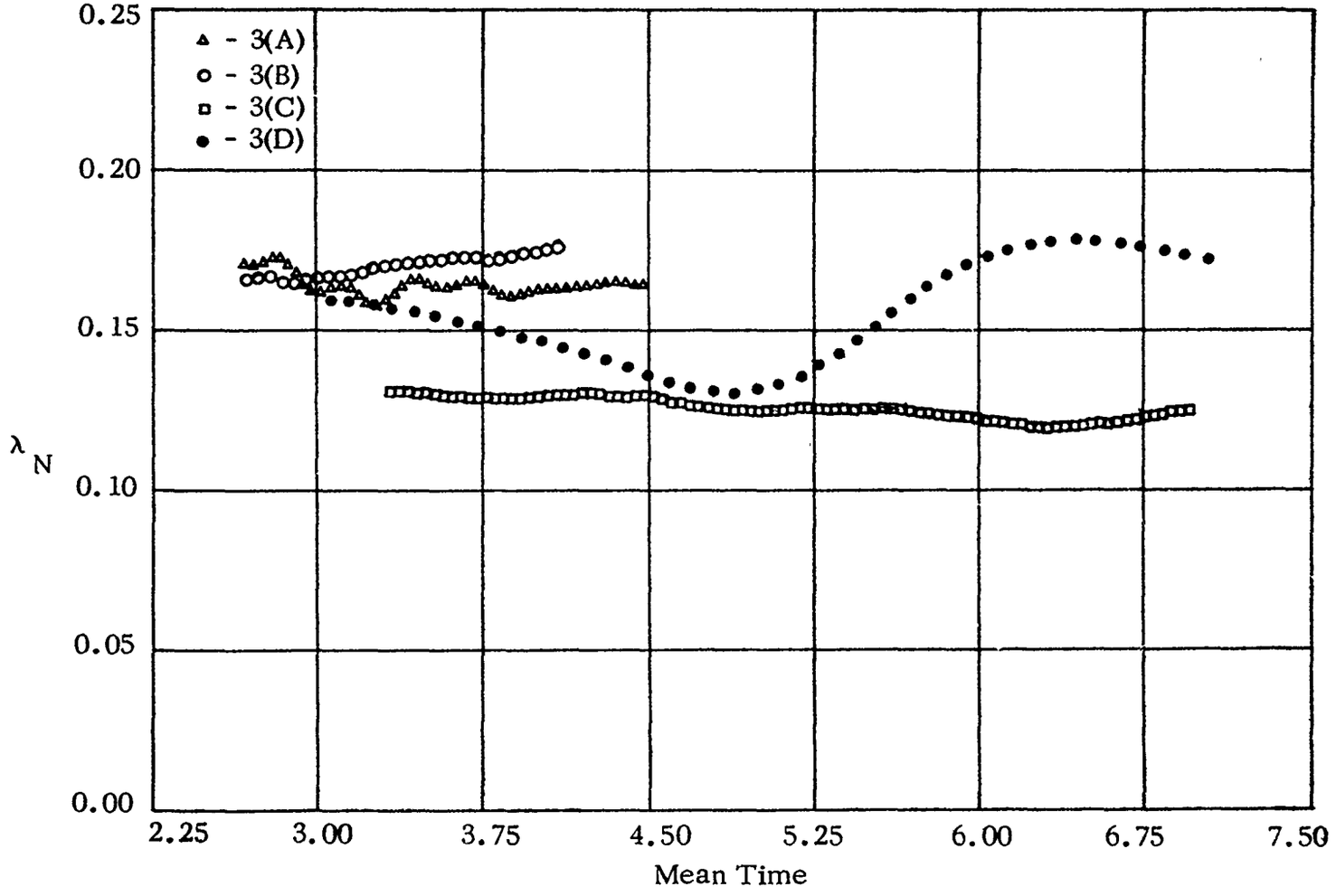

Figure 40. Dynamic Nutation Damping Factor (One/Second) versus Mean Time (Second) [Runs 3(A), 3(B), 3(C), 3(D)].

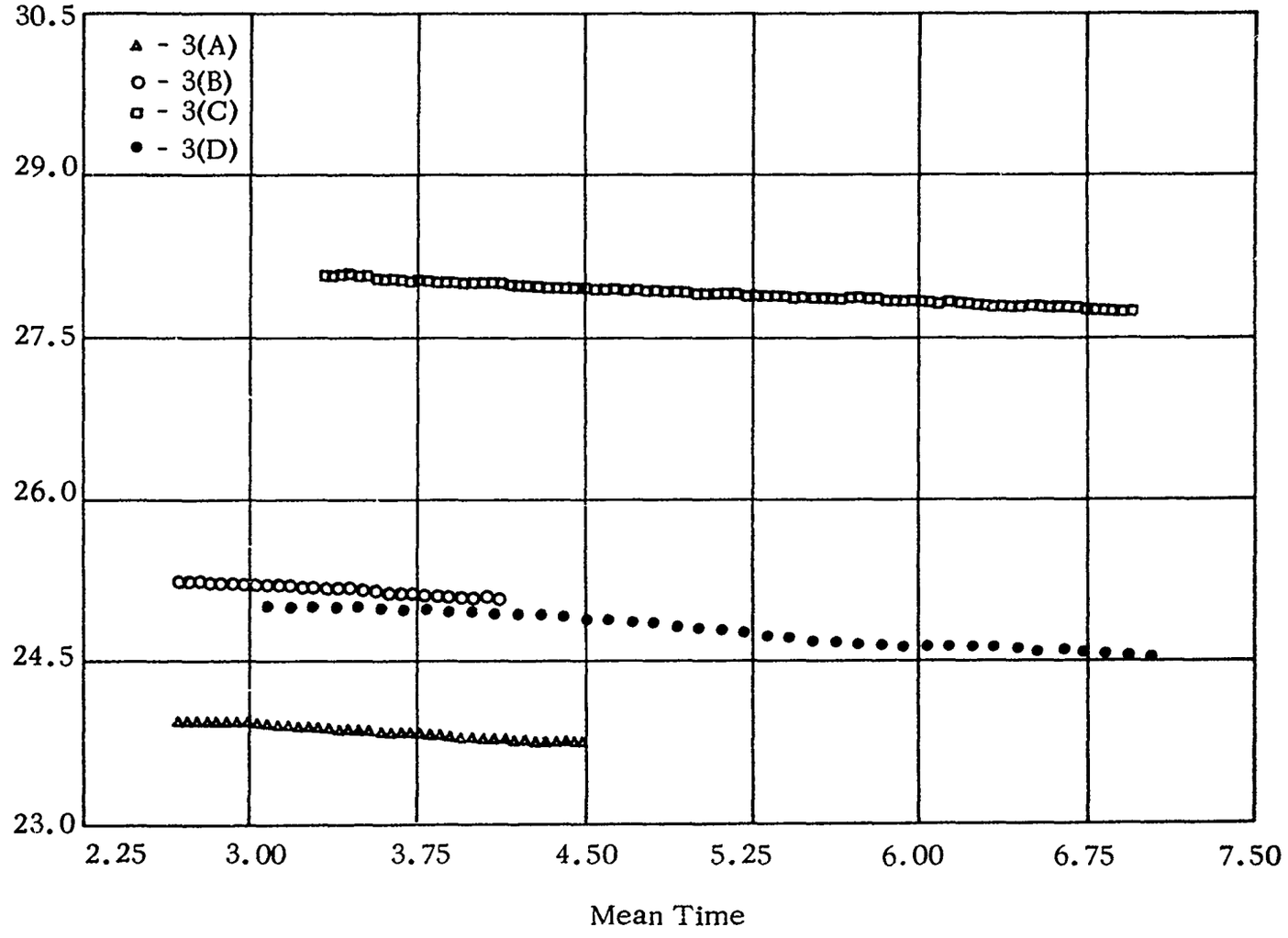

Figure 41. Nutation Frequency (Radian/Second) versus Mean Time (Second) [Runs 3(A), 3(B), 3(C), 3(D)].

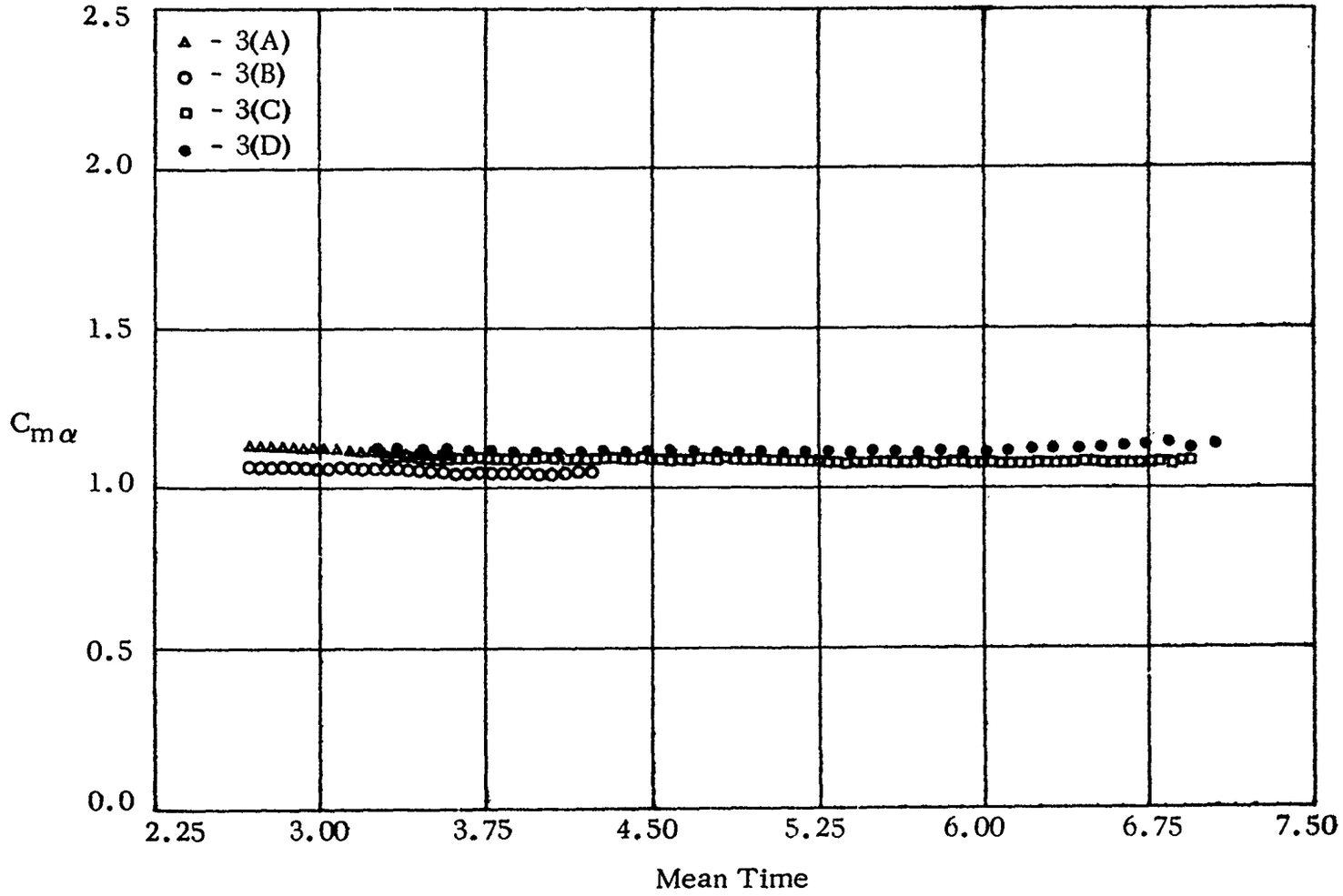

Figure 42. Restoring Moment Coefficient (One/Radian) versus Mean Time (Second) [Runs 3(A), 3(B), 3(C), 3(D)].

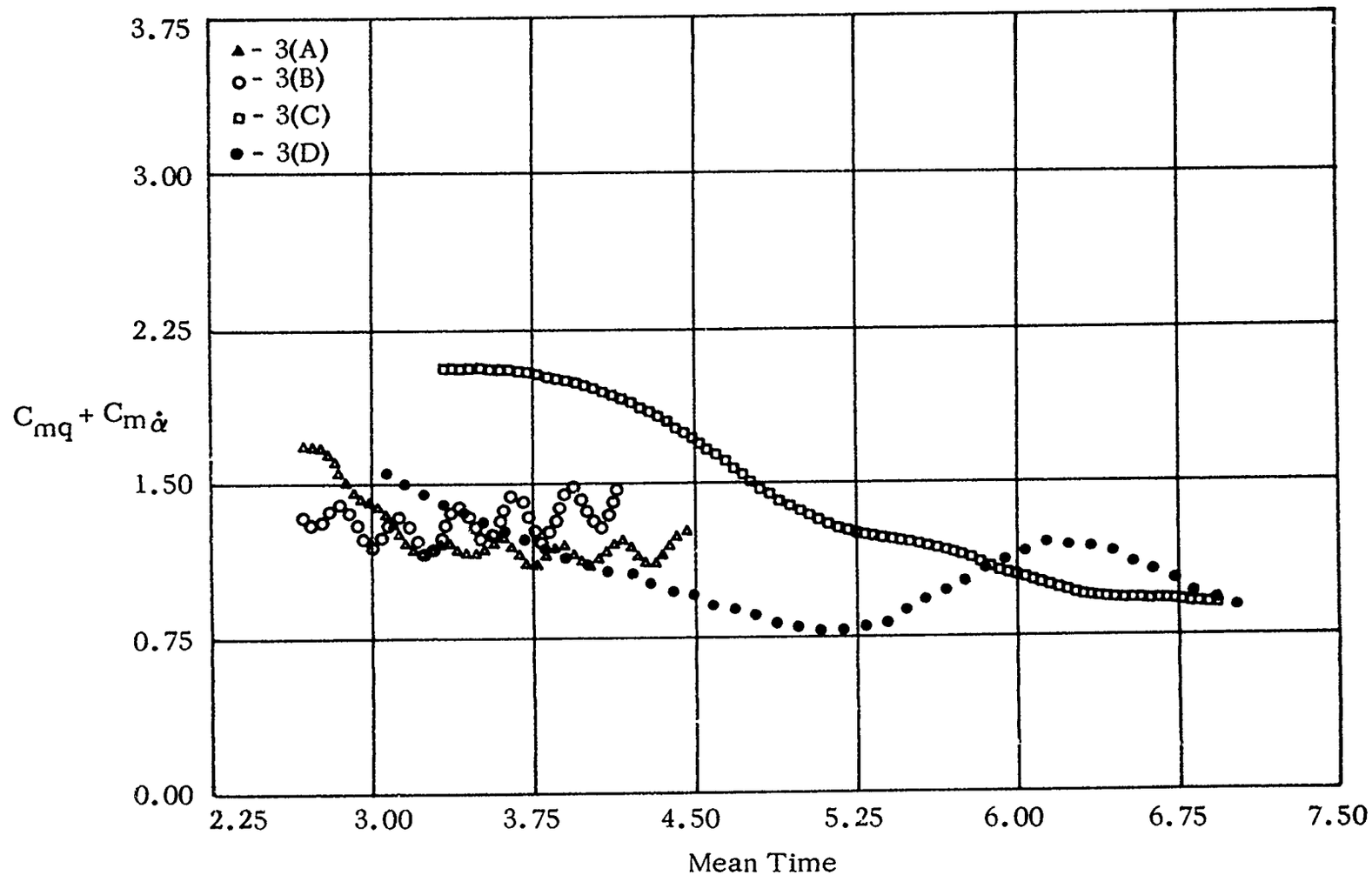

Figure 43. Damping Moment Coefficient (One/Radian) versus Mean Time (Second) [Runs 3(A), 3(B), 3(C), 3(D)].

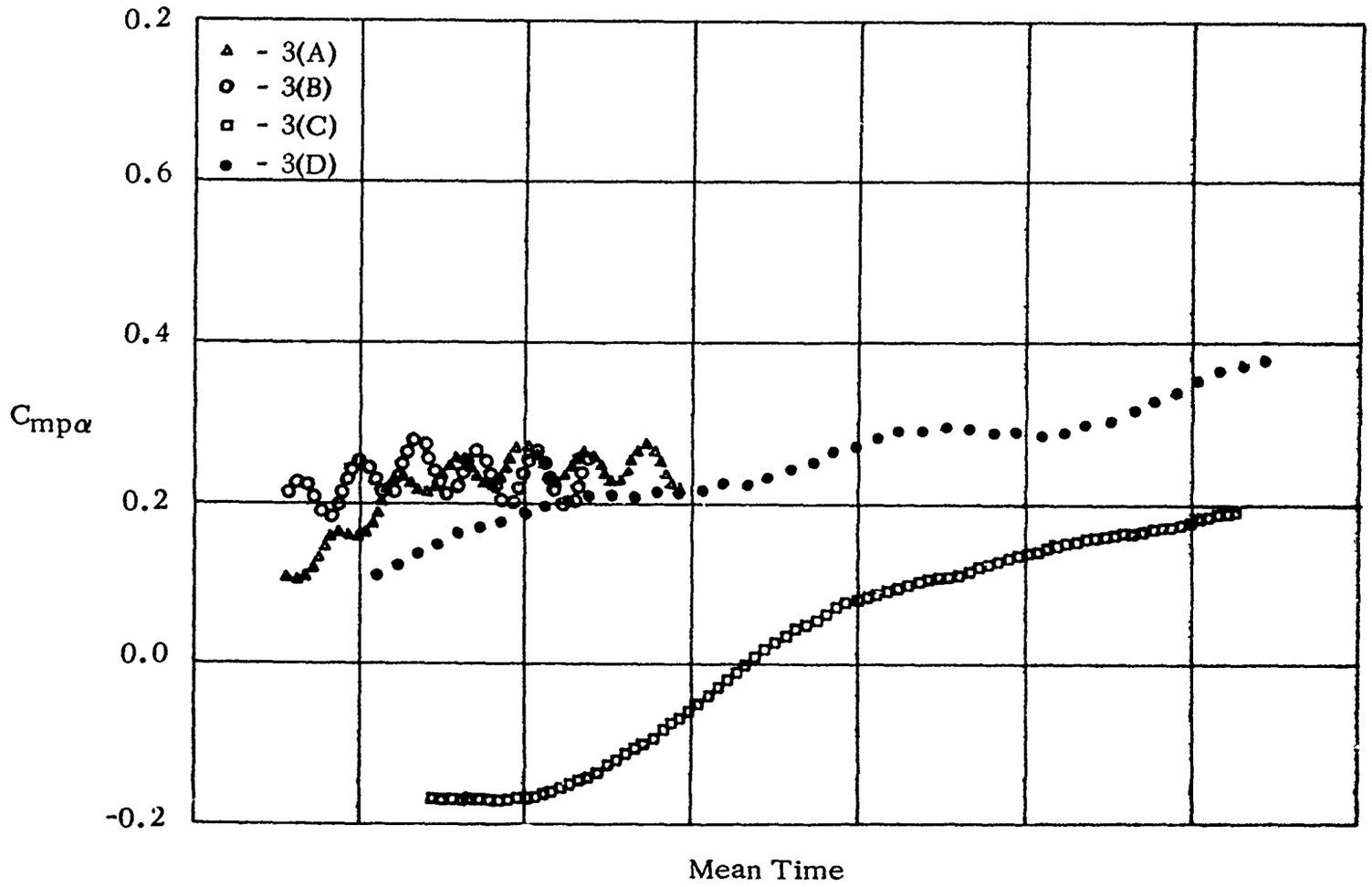

Figure 44. Magnus Moment Coefficient (One/Radian^2) versus Mean Time (Seconds) [Runs 3(A), 3(B), 3(C), 3(D)].

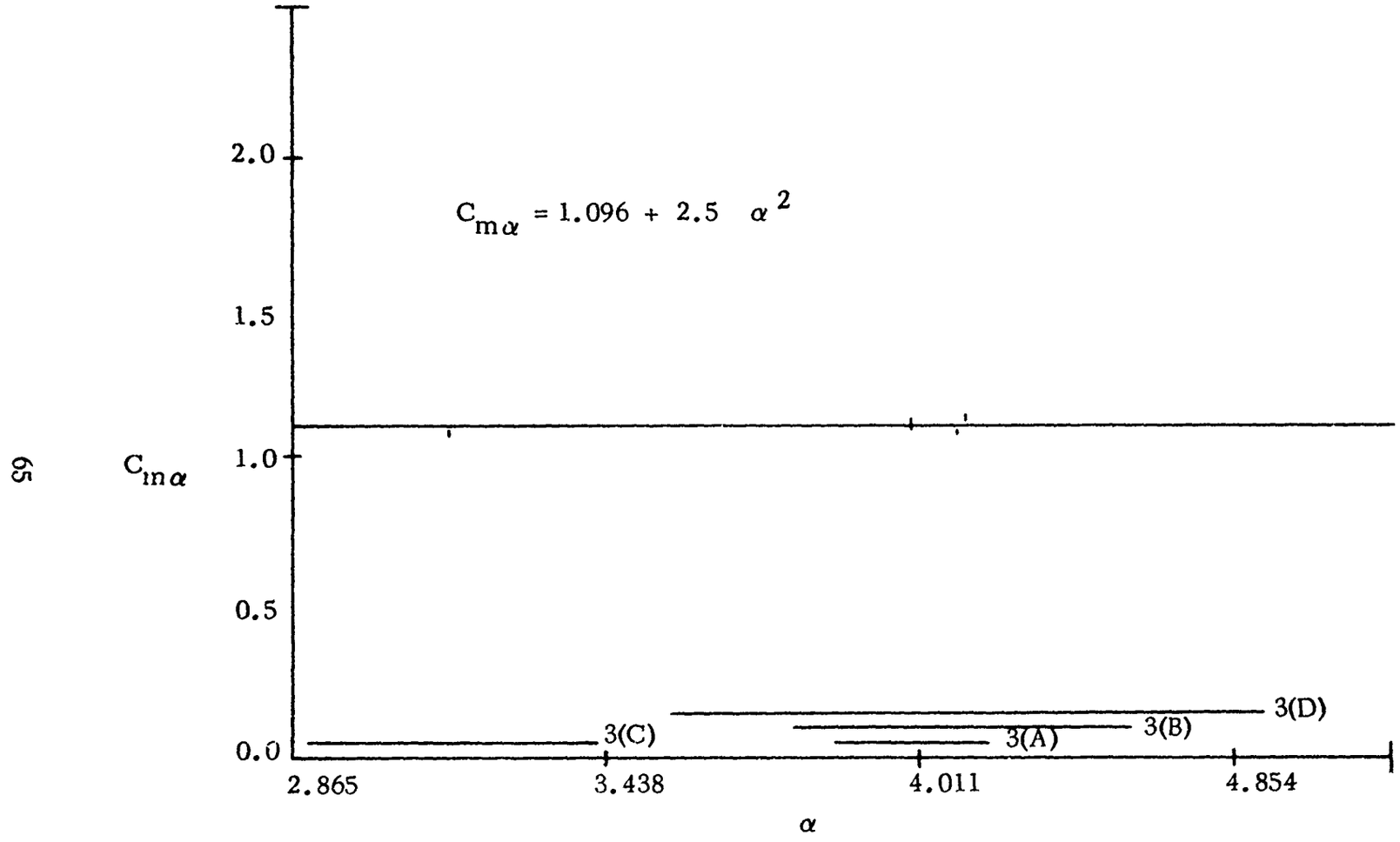

Figure 45. Nonlinear Restoring Moment Coefficient Cone/Radian versus Complex Angle of Attack (Degree) (Runs 3).

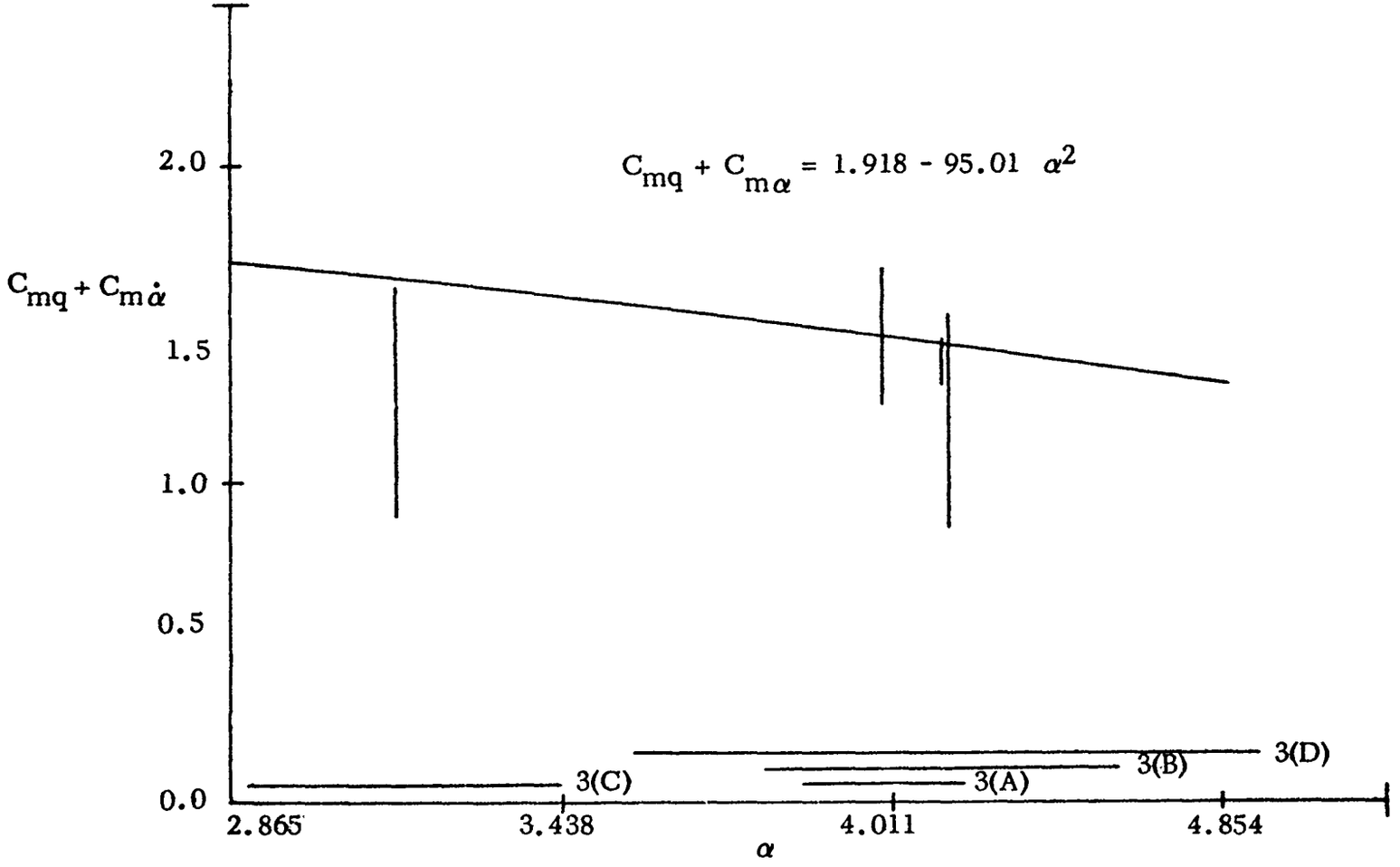

Figure 46. Nonlinear Damping Moment Coefficient (One/Rad) versus Complex Angle of Attack (Degrees) (Run 3).

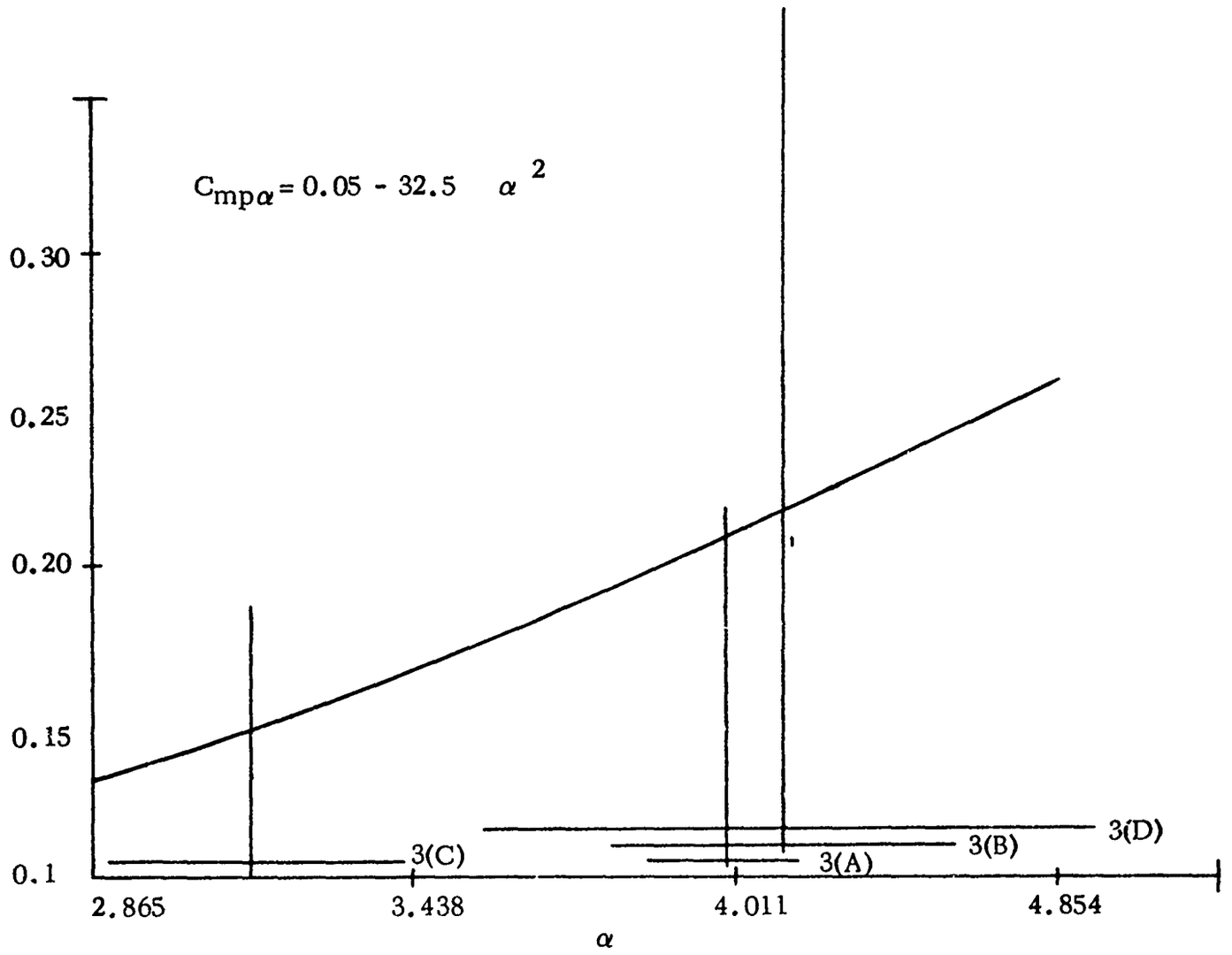

Figure 47. Nonlinear Magnus Moment Coefficient (One/Radian^2) versus Complex Angle of Attack (Degree) (Runs 3).

The variation in C_{m_α} with angle of attack was again found to be small. The smaller angle-of-attack range reduced the nonlinear effects even more.

$C_{m_q} + C_{m_{\dot{\alpha}}}$ was highly nonlinear, changing sign from positive to negative at around 8.5 degrees. It was this that caused the nutation arm to become stable at the higher angles of attack.

The Magnus moment was also very nonlinear and a stabilizer to the precession arm; however, its destabilizing effects on the nutation arm are overshadowed by the strong damping moment. At small angles, the Magnus and damping moments both contribute to the instability of the nutation arm and the stability of the precession mode.

SECTION VI

CONCLUSIONS

The three-degrees-of-freedom dynamic wind tunnel tests of the three-caliber Army-Navy basic spinner projectile model demonstrated the feasibility and reliability of obtaining nonlinear aerodynamic stability coefficients from vertical wind tunnel testing. As a result of these tests on the zero-degree boattail model, it is concluded that:

- The model exhibits a precession instability at low angles of attack due primarily to a negative Magnus moment.
- Dynamic stability is possible at high angles of attack.
- Due to the nonlinear characteristics of the Magnus and damping moments the model has a stable nutation mode at all angles of attack (assuming gyroscopic stability).
- The effect of the nonlinearity exhibited by $C_{m\alpha}$ was small.

For the 7.5 - degree boattail model the tests indicated that:

- The model has a nutation instability at low angles of attack due to positive Magnus and damping moments.
- The model is stable in both nutation and precession modes at higher angles of attack due to the nonlinear characteristics of the Magnus and damping moments.
- The effect of the nonlinearity exhibited by $C_{m\alpha}$ was small.

It is, therefore, concluded that addition of a 7.5-degree boattail to the three-caliber Army-Navy basic spinner (c.g. positioned two calibers from nose) destabilizes an otherwise stable nutation arm and stabilizes an otherwise unstable precession arm at low angles of attack. At higher angles of attack little effect is noted on the stable nutation arm but the precession mode becomes stable.

SECTION VII

RECOMMENDATIONS

Because of the complex relations existing between the damping and Magnus moments of the projectile, additional dynamic tunnel tests should be conducted to:

- Determine the fluid flow properties affecting the damping and Magnus moments.
- Establish the damping and Magnus characteristics for a wide range of boattail angles and sizes.
- Correlate the measured damping and Magnus coefficients with the flow field properties.

REFERENCES

1. Nicolaides, J.D., Free Flight Dynamics, Text, Aerospace Engineering Department, University of Notre Dame, 1961.

2. Chin, S.S., Missile Configuration Design, McGraw-Hill Book Company, Inc., New York, 1961.

3. Murphy, C.H., Free Flight Motion of Symmetric Missiles, Ballistic Research Laboratories Report No. 1216, Ballistic Research Laboratories, Aberdeen Proving Ground, Maryland, July 1963.

4. Murphy, C.H., The Measurement of Nonlinear Forces and Moments by Means of Free-Flight Tests, Ballistic Research Laboratories Report No. 974, Aberdeen Proving Ground, Maryland, 1956.

5. Ingram, C.W., On Obtaining the Nonlinear Aerodynamic Stability Coefficients from the Free Angular Motion of Rigid Bodies, Ph.D. Dissertation, Aerospace Engineering Department, University of Notre Dame, June 1969.

6. Eikenberry, R., Analysis of Angular Motions of Missiles, Aerospace Engineering Department, University of Notre Dame. Published by the Sandia Corporation Report, No. SC-CR-70-1970 - SC-CR-70-6051, Sandia Laboratories, Albuquerque, New Mexico.

7. Cormier, D.R., and Noethen, T.H., A Three-Dimensional Dynamic Wind Tunnel Testing Technique, Department Report, Aerospace Engineering Department, University of Notre Dame, September 1969.

8. Cormier, D.R., and Noethen, T.H., Experimental Study of Jewel Bearings in Dynamic Testing, Departmental Report, Aerospace Engineering Department, University of Notre Dame, June 1970.

(The reverse of this page is blank)

INITIAL DISTRIBUTION

NAVSHIP R&D, AERO LAB (CODE 046, 651)	2
LANGLEY RES CTR	1
NAVWPNS CTR, CODE 403	1
NAVWPNS CTR, CODE 50704	1
PICATINNY ARS, ATTN: A.LOEB	2
AFFDL(FDCC/C.MAYHEW)	1
ASD (TECH LIB)	1
USNOL, AERO DEPT/S HASTINGS	1
USNOL, AERO DEPT/DR LYONS	1
AERO RSCH GP/A. FLATAU	1
FMC, DEF TECH LAB	1
AUL (AUL/LSE-70-239)	1
BRL	2
DEPT OF ARMY, CH R&D	1
USA RES OFF (CRD-AA-IP	1
REDSTONE SCI INFO CTR	2
AMES RSCH CTR	1
BATTELLE MEM INST	1
NAVWPNS LAB	1
DDC	2
HARRY DIAMOND LAB	1
HONEYWELL, INC	3
SANDIA CORP	1
ALPHA RSCH, IND	1
AEROSPACE CORP	1
AEROJET GEN CORP	1
CHAMBERLAIN CORP	2
GOODYEAR AEROSPACE CORP	2
NORTH AMER AVIATION INC	1
ARMAMENT SYSTEMS INC	1
MARTIN-MARIETTA CORP	1
BOEING CO	2
NORTHRUP-NORTRONICS	2
AVCO CORP	1
LITTON IND	2
U OF NOTRE DAME	5
LOUISIANA STATE U	1
CORNELL AERO LAB	1
U OF FLA	2
NAVSHIP R&D LAB	1
ASD (ENYS)	1
ADTC (WX-10)	1
TAWC (DT)	1

AFATL	
DL	1
DLD	1
DLF	1
DLO	1
DLI	1
DLW	1
DLY	1
DLK	1
DLG	1
DLU	1
DLB	1
DLR	1
DLGC	20
DLOSL	2
DLU (CDCLNO)	2

(The reverse of this page is blank)

UNCLASSIFIED
Security Classification

DOCUMENT CONTROL DATA - R & D

(Security classification of title, body of abstract and indexing annotation must be entered when the overall report is classified)

1. ORIGINATING ACTIVITY (Corporate author)
Department of Aerospace & Mechanical Engineering
University of Notre Dame
Notre Dame, Indiana 46556

2a. REPORT SECURITY CLASSIFICATION
UNCLASSIFIED

2b. GROUP
---

3. REPORT TITLE
(6) BOATTAIL EFFECTS ON THE DYNAMIC STABILITY OF THE THREE-CALIBER ARMY-NAVY BASIC SPINNER PROJECTILE.

4. DESCRIPTIVE NOTES (Type of report and inclusive dates)
(9) Final Report, 15 Jan [redacted]70 - 14 Jan [redacted]71

5. AUTHOR(S) (First name, middle initial, last name)
(10) John D./Nicolaides
Charles W./Ingram
Thomas H./Noethen

6. REPORT DATE
(11) Feb [redacted]71

(12) 85 p.

7a. TOTAL NO. OF PAGES
~~88~~

7b. NO. OF REFS
8

8a. CONTRACT OR GRANT NO.
(15) F08635-70-C-0033

b. PROJECT NO.
(16) AF-670A

c. Task No. (17) 34

d. Work Unit No. 002

9a. ORIGINATOR'S REPORT NUMBER(S)

9b. OTHER REPORT NO(S) (Any other numbers that may be assigned this report)
(18) AFATL-TR-71-28 (19)

10 DISTRIBUTION STATEMENT Distribution limited to U.S. Government agencies only; this report documents tests and evaluation of a military munition; distribution limitation applied February 1971. Other requests for this document must be referred to the Air Force Armament Laboratory (DLGC), Eglin Air Force Base, Florida 32542.

11. SUPPLEMENTARY NOTES
Available in DDC

12. SPONSORING MILITARY ACTIVITY
Air Force Armament Laboratory
Air Force Systems Command
Eglin Air Force Base, Florida 32542

13. ABSTRACT

Wind tunnel tests were conducted to study the effects of a boattail on the dynamic stability of the three-caliber Army-Navy basic spinner projectile. Three-degrees-of-freedom angular data was obtained in vertical subsonic wind tunnel tests on one model with no boattail and on one model with a 7.5-degree boattail. Data reduction yielded the restoring, damping, and Magnus moments as functions of time and nonlinear functions of angle of attack for eacn model. The testing technique employed a low friction jewel bearing model mount and a means for obtaining two-axis data.

MBD

DD FORM 1 NOV 65 1473

UNCLASSIFIED
Security Classification

401 877

UNCLASSIFIED

Security Classification

14 KEY WORDS	LINK A		LINK B		LINK C	
	ROLE	WT	ROLE	WT	ROLE	WT
Wind Tunnel Tests						
Dynamic Stability						
Three-Degrees-of-Freedom						
Linear Coefficients						
Nonlinear Coefficients						
Moment of Inertia						
Zero-Degree Boattail						
7.5-Degree Boattail						
Error-of-Fit						
Precession Arm						
Precession Frequency						
Nutation Arm						
Nutation Frequency						

UNCLASSIFIED

Security Classification